

# 40èmes Journées des Actinides & 2nd Workshop on Actinide Targets

Saturday 27 March 2010 - Thursday 01 April 2010

CERN



## Book of Abstracts



# Contents

Production and Characterization of Highly Porous Carbides for the SPES Target . . . . .	1
Synthesis and Characterization of Carbide Foams for the SPES target . . . . .	1
The Features of Luminol Chemiluminescence in Detection of Trace Amounts of Actinides in Solutions . . . . .	2
The SPES project at LNL . . . . .	2
Actinide Target Use at ATLAS . . . . .	3
CACAO, a laboratory for the production and the characterization fo radioactive thin layers . . . . .	3
Magnetic anisotropy of a UFe <sub>5</sub> Al <sub>7</sub> single crystal . . . . .	4
Pressure effect on the crystal lattice of unconventional superconductor UCoGe. . . . .	4
Field-Induced Phase Transitions in UIrGe Probed by Ultrasound Measurements . . . . .	6
Investigation of uranium-colloid interactions in soil by dual Capillary Electrophoresis / Field-Flow Fractionation hyphenated with Inductively Coupled Plasma-Mass Spectrom- etry. . . . .	6
High-pressure hydrogen doping into the UTGe compounds. . . . .	7
Quadrupolar interactions in UPd <sub>3</sub> observed by inelastic neutron scattering . . . . .	8
Electrical properties of (Pu,Lu)Pd <sub>3</sub> . . . . .	9
On the existence of cerium (IV) orthophosphate, 'Ce <sub>3</sub> (PO <sub>4</sub> ) <sub>4</sub> ' . . . . .	9
Thermodynamic study of the molten salt fast reactor fuel . . . . .	10
Electronic structure theory of Pu-based alloys and compounds: Pu-Am, Pu-Ce-alloys and PuCoGa <sub>5</sub> . . . . .	10
Electronic structure and ionicity of actinide oxides from first principles . . . . .	11
Bulk properties of the ζ-U-Pu phase . . . . .	11
Study of Thorium-Uranium (IV) oxalate dihydrate phase transition through coupled XRD / Raman . . . . .	12
Specific heat of the antiferro / ferro-magnet NpGa <sub>3</sub> . . . . .	13

Study of $CeIV_{1-x}LnIII_xO_{2-x/2}$ dissolution . . . . .	14
Resonant inelastic X-ray scattering probe of inter- and intra-atomic interactions in uranium systems . . . . .	15
Influence of crystallization state and microstructure over chemical durability of mixed dioxides . . . . .	16
First-principles study of uranium dioxide and oxygen self-diffusion in uranium dioxide . . . . .	17
Synthesis and characterization of $MIVSiO_4$ compounds . . . . .	18
The Schrieffer-Wolff transformation for the $S=1$ Underscreened Kondo Lattice model : Application to Uranium compounds . . . . .	19
Synthesis of nanocrystalline oxide fuel . . . . .	20
Uranium Carbide Target for SPIRAL2: fission products effusion optimization studies . . . . .	21
$^{237}Np$ Mössbauer effect study of $NpPdSn$ . . . . .	22
Oxidative corrosion of carbide inclusions at the surface of uranium metal during exposure to water vapour. . . . .	23
Initial electron back-scattered diffraction observations of Ce-La alloy . . . . .	24
Distribution of soil-to-plant transfer factors for the natural uranium isotopes in the vegetation in zones affected by uranium mines . . . . .	25
$^{234}U/^{238}U$ disequilibrium studies in soil and vegetation samples from tailing dumps . . . . .	26
Uranyl behaviour at the gibbsite-water interface: a Car Parrinello molecular dynamics study . . . . .	27
Investigation of Uranium Materials for a Two-Step Target . . . . .	28
Isothermal section of the U-Fe-Ge ternary system at $900^\circ C$ . . . . .	28
High-field metamagnetism in $UCo_2Si_2$ . . . . .	29
Crystallographic study of new phases from the U-Zn-Al ternary system . . . . .	30
Magnetic ordering in the heavy-fermion compound $UZn_{12}$ . . . . .	31
Considerations on the U-Fe-B ternary system . . . . .	33
Long-term behavior of thorium-plutonium phosphate-diphosphate solid solutions . . . . .	34
Electrical transport properties of single crystalline $U_2Cu_4As_5$ . . . . .	34
Ferromagnetic ordering in novel ternary germanides: $URu_{1-x}Ge_2$ and $U_{34}Ru_{4-x}Ge_{33}$ . . . . .	35
Synthesis and first tests at CERN-ISOLDE of $UC_x$ targets produced with carbon nanotubes . . . . .	36
Low temperature properties of $AnFe_2Si_2$ systems ( $An = Th, Np, Pu$ ) . . . . .	36
Techniques elaborated for the R&D on fission targets for SPIRAL2 . . . . .	37

Study on the U-Co-Ge ternary system at 973K . . . . .	38
Development of an actinide target and laser ion-source test-bed at iThemba LABS, South Africa . . . . .	39
Design concerns for future RIB production facilities at TRIUMF . . . . .	40
Recent progress in the synthesis and characterization of uranium carbide compounds . . . . .	40
Crystal structure and physical properties of NpRh <sub>2</sub> Sn, a new Np-based ternary compound . . . . .	41
Synthesis and magnetic properties of a new ferromagnetic Kondo-lattice system Np <sub>2</sub> PdGa <sub>3</sub> . . . . .	42
Electronic structure and magnetic properties of UNi <sub>1/2</sub> Sb <sub>2</sub> compound . . . . .	43
Transport and thermodynamic properties of UFe <sub>2</sub> Zn <sub>20</sub> . . . . .	44
X-ray absorption and emission spectroscopic study at O K-edges of light actinide oxides . . . . .	45
Kondo effect in the presence of ferromagnetism in U <sub>1-x</sub> Th <sub>x</sub> NiSi <sub>2</sub> . . . . .	46
White line of actinide x-ray absorption spectra as a tool for their atomic environment description . . . . .	47
Concepts for high power targets of thorium and uranium . . . . .	48
Synthesis of <sup>244</sup> Bk by <sup>11</sup> B + <sup>238</sup> U reaction for spectroscopic investigations . . . . .	49
Solid state physics at ISOLDE: using radioactive ion beams to study materials . . . . .	50
High temperature drop calorimetry for actinide samples . . . . .	50
Dose coefficients for radiation protection at present and future RIB facilities . . . . .	51
use of actinide targets at the HRIBF . . . . .	51
Review on UC targets (Invited talk) . . . . .	52
Invited talk (TBC) . . . . .	52
Measurements of neutron capture and fission cross-sections on actinides at n_TOF . . . . .	52
NTOF 2 . . . . .	52
Remote and optimized inspection, measurement and handling for radiation areas at CERN. . . . .	52
Summary and Closure . . . . .	52
Opening of conference . . . . .	52
Fuels & targets talk I TBC . . . . .	53
Fuels & targets talk II (TBC) . . . . .	53
Fuels & targets talk III (TBC) . . . . .	53

Fuels & targets Invited talk (TBC) . . . . .	53
Keith Kershaw: Development of equipment and optimized procedures for remote inspection, measurement and handling in radiation areas at CERN . . . . .	53
Plans For the Production Building at the future Radioactive Ion Beam production laboratory SPIRAL 2 at GANIL and handling of the targets . . . . .	53
Details of poster session . . . . .	53

WAT-II / 0

## Production and Characterization of Highly Porous Carbides for the SPES Target

**Author:** Lisa Biasetto<sup>1</sup>

**Co-authors:** Alberto Andrichetto<sup>1</sup>; Gianfranco Prete<sup>1</sup>; Pierluigi Zanonato<sup>2</sup>; SaraMaria Carturan<sup>1</sup>

<sup>1</sup> LNL-INFN

<sup>2</sup> UNIPD

**Corresponding Author:** lisa.biasetto@lnl.infn.it

The development of targets for RIBs production is a challenging field for material scientists, who are asked to develop materials possessing tailored properties in order to:

- 1) produce the isotopes requested by the specific experiment
- 2) grant for high release efficiency of the produced isotopes
- 3) long life of the target during bombardment

In addition, the severe operating conditions in terms of high temperature, thermal stresses, nuclear reactions that occur in the material, make the choice of the appropriate material very tricky.

Within the SPES Project the research in this field is very active and the production of lanthanide, actinide and metal transition carbides has been driven towards the development of materials capable of satisfying the above mentioned requests.

Main attention has been directed to the production of carbides with controlled:

- 1) composition and grain size
- 2) specific surface area
- 3) porosity in terms of amount of free volume, available for isotopes effusion.

Different processing routes will be analyzed, so as the their effects on material properties.

**Introductions to Posters / 1**

## Synthesis and Characterization of Carbide Foams for the SPES target

**Author:** Stefano Corradetti<sup>1</sup>

**Co-authors:** Alberto Andrichetto<sup>1</sup>; Lisa Biasetto<sup>1</sup>; Piero Zanonato<sup>2</sup>; Sara Carturan<sup>1</sup>

<sup>1</sup> INFN-LNL

<sup>2</sup> Università di Padova

**Corresponding Author:** stefano.corradetti@lnl.infn.it

Materials used in targets for RIBs production have to satisfy several requirements, related to their capability both to produce specific isotopes with high efficiencies and to withstand harsh operating conditions.

Within the SPES group, new carbides with tailored properties are currently studied and developed in order to maximize isotopes production at extreme conditions.

In particular, lanthanide and transition metal carbide foams possessing a large amount (up to 90%) of open interconnected porosity have been produced.

Characterization of these foams is made by evaluation of different aspects:

- 1) Quantity and size of the pores created during the foaming process
- 2) Type of porosity obtained
- 3) Effect of porosity on physical properties such as thermal emissivity and gas permeability.

**Chemistry I / 2****The Features of Luminol Chemiluminescence in Detection of Trace Amounts of Actinides in Solutions****Author:** Igor Izosimov<sup>1</sup>**Co-authors:** Nikolai Firsin<sup>1</sup>; Nikolai Gorshkov<sup>1</sup>; Vladimir Mikhalev<sup>1</sup><sup>1</sup> *Khlopin Radium Institute***Corresponding Author:** izing@mail.ru

A widespread application of tunable lasers to analytical problems gave impetus to development of new procedures for detection of trace amounts of a substance in various media. A capability to vary the wavelength of laser radiation allows selective action on atoms and molecules and also their selective detection. From the practical standpoint, liquids are the most suitable for analysis since atoms and molecules in liquids are in the area of interaction with laser radiation at all times. The analytical procedures based on laser spectroscopy as applied to liquids allow determination of valent states of the element and type of molecule [1].

Plutonium, neptunium and some uranium compounds do not exhibit direct luminescence in solutions and, hence, conventional procedure with time resolution (TR) of analytical luminescent signal (TRLIF) cannot be used for their detection in solutions. However, for detection of plutonium, neptunium and uranium the TR procedure can be used with registration of chemiluminescence of luminol (5-amino-1,2,3,4-tetrahydro-1,4-phthalazinedione), which arises under the action of OH radicals generated in solutions by light-excited actinide ions. We used this procedure for detection of actinides in solutions containing AnO<sub>2</sub>(2+) ions (An = U, Np, Pu) [2]. In this case, the chemiluminescence kinetics is characterized by burning up for three microseconds and decay of chemiluminescence with a characteristic time of approximately two microseconds.

Selective two-step excitation of actinyl-containing complexes by tunable lasers allows detection of actinide elements from the chemiluminescence of luminol.

For detection of small amounts of actinides it is necessary to exclude a possibility of registration of luminol luminescence having nature different from chemiluminescence. Therefore, we studied luminol luminescence in aqueous-alcoholic solutions with various water contents. It was found that with decreasing water content the intensity of luminescence having chemiluminescence nature decreases; in addition we observed a luminescence with red-shifted spectrum and kinetics having no burning-up stage typical for chemiluminescence. It should be noted that this luminescence different from chemiluminescence arises in single-quantum UV excitation of luminol molecule and can be significantly depressed in two-quantum excitation induced by radiation with longer wavelength since luminol has no absorption bands in visible region.

The results of the study allows conclusion that the presence of a burning-up stage with duration of several microseconds is typical for chemiluminescence in aqueous or aqueous-alcoholic solutions. Luminol luminescence in alcoholic solutions with a high degree of dehydration is not of chemiluminescence nature and can be significantly suppressed in two-quantum excitation.

The features of chemiluminescence kinetics in detection of actinides in solutions are discussed.

This work was financially supported by the ISTC (project no. 3694).

**References**

[1] I.N. Izosimov, Phys. Prt. Nucl., 38, 177 (2007).

[2] I.N. Izosimov et al, Proc. Int. Conf. Actinides 2005, Manchester, UK, 2005, p. 779.

**JDA-WAT I / 3****The SPES project at LNL****Author:** Alberto Andrighetto<sup>1</sup>



<sup>1</sup> INFN - Laboratori di Legnaro

**Corresponding Author:** andrighetto@lnl.infn.it

The SPES project at Laboratori di Legnaro of INFN (Italy) is concentrating on the production of neutron-rich radioactive nuclei by the Uranium fission at a rate of  $10^{13}$  fission/s. The emphasis to neutron-rich isotopes is justified by the fact that this vast territory has been little explored, at exceptions of some decay and in-beam spectroscopy following fission. The Rare Ion Beam (RIB) will be produced by ISOL technique using the proton induced fission on a Direct Target of UCx.

The most critical element of the SPES project is the Multi-Foil Direct Target. Up to day the proposed target represents an innovation in term of capability to sustain the primary beam power. The design is carefully oriented to optimise the radiative cooling taking advantage of the high operating temperature of 2000°C.

The main goal of the proposed facility is to provide an accelerator system to perform forefront research in nuclear physics by studying nuclei far from stability. The SPES project is concentrating on the production of neutron-rich radioactive nuclei with mass in the range 80-160. The final energy of the radioactive beams on target will range from few MeV/u up to 10 MeV/u for A=130 using the exiting ALPI linac as RIB post-accelerator.

WAT-III / 4

## Actinide Target Use at ATLAS

**Author:** John Greene<sup>1</sup>

**Co-authors:** Irshad Ahmad<sup>1</sup>; Robert Janssens<sup>1</sup>

<sup>1</sup> Argonne National Laboratory

**Corresponding Author:** greene@anl.gov

Molecular plating provides an efficient method to prepare sources and targets of actinide elements on thick and thin backings. These are required for experiments at the Argonne Tandem Linac Accelerator System (ATLAS) heavy-ion accelerator. Although the technique is simple and fairly reproducible, because of the radioactive nature of the targets, it is vital to record the various parameters employed during the preparation process. At Argonne National Laboratory, 200-500  $\mu\text{g}/\text{cm}^2$  thick actinide targets were required for Coulomb Excitation (COULEX) studies involving GAMMASPHERE. These targets were plated on 50  $\text{mg}/\text{cm}^2$  Au backings and were subsequently covered by a 200  $\mu\text{g}/\text{cm}^2$  Au foil in order to capture any material lost by sputtering. Targets of  $^{230}\text{Th}$ ,  $^{237}\text{Np}$ ,  $^{239, 240, 242, 244}\text{Pu}$ ,  $^{241}\text{Am}$ ,  $^{248}\text{Cm}$ , and  $^{249}\text{Cf}$  were prepared by dissolving the material in isopropyl alcohol and electroplating the actinide ions by applying a potential of 600 V. The amount of material in the target was determined by alpha particle counting and gamma-ray spectroscopy. Many laboratories routinely prepare these targets on thick backings using this technique. However, it becomes more difficult when employing thin backings (i.e. less than 1  $\text{mg}/\text{cm}^2$ ). In recent years, we have plated targets on, for example, thin Ni and carbon backings. The Ni foils, evaporated on a copper substrate, are purchased commercially. We used these foils to plate  $^{234}\text{U}$ . Afterwards we removed the copper by acid dissolution. In this way 400  $\mu\text{g}/\text{cm}^2$   $^{234}\text{U}$  targets were prepared on a 200  $\mu\text{g}/\text{cm}^2$  Ni backing. Another application involved preparation of a 100  $\mu\text{g}/\text{cm}^2$   $^{243}\text{Am}$  target by plating onto a commercially available 75  $\mu\text{g}/\text{cm}^2$  carbon film left on its glass substrate for subsequent floating. A column made of Delrin™ was used which did not produce any scratches on the carbon film surface. Details of the technique as well as future prospects will be presented.

(Delrin™ is a registered trademark of E. I. du Pont de Nemours and Company)

This work was supported by the U.S. Department of Energy, Office of Nuclear Physics, under Contract No. DE-AC02-06CH11357

JDA-WAT I / 5

## CACAO, a laboratory for the production and the characterization of radioactive thin layers

**Author:** Charles-Olivier Bacri<sup>1</sup>

<sup>1</sup> CNRS/IN2P3 Institut de Physique Nucléaire

**Corresponding Author:** bacri@ipno.in2p3.fr

CACAO, Chimie des Actinides et Cibles radioActives à Orsay, is a project of laboratory for the production and characterization of thin radioactive layers. The project is now launched and almost financed. It should be fully operational by the end 2010.

Besides the production of targets, CACAO aims to be a node of a kind of network of laboratories dedicated to find isotopes, but also to strengthen the know-how for the fabrication, and eventually to share installations.

### Summary:

Motivations of a new laboratory dedicated to production and characterization of thin radioactive layers is 2-fold. The first one is of course the needs of physics programs: nuclear fuel cycle studies, but also astrophysics and studies related to super-heavy elements need radioactive targets (and especially actinide ones) to be done. The second one is related to the relative loss of skills, at least in Europe, in the production of thin radioactive layers. This is the reason why CACAO project aims to be a node in a network of installations and specialists of thin layers producers, and actinide chemists.

After presenting these motivations, the CACAO project of new laboratory for radioactive targets will be presented. Difficulties related to preparation of such layers will be presented, as well as the constraints we had to face during the elaboration of the project, and their consequences. To conclude, the planning of the project will be presented.

### Introductions to Posters / 6

## Magnetic anisotropy of a UFe<sub>5</sub>Al<sub>7</sub> single crystal

**Author:** Alexander Andreev<sup>1</sup>

<sup>1</sup> Institute of Physics AVCR, Prague

**Corresponding Author:** a.andreev@seznam.cz

See the andreev\_jda10.doc and andreev\_jda10.pdf files sent by e-mail.

### Strongly Correlated Systems II / 7

## Pressure effect on the crystal lattice of unconventional superconductor UCoGe.

**Author:** Anna Maria Adamska<sup>1</sup>

**Co-authors:** Jiří Pospíšil<sup>2</sup>; Ladislav Havela<sup>2</sup>; N.-T.H. Kim-Ngan<sup>3</sup>; Stanislav Daniš<sup>2</sup>; Stephen Heathman<sup>4</sup>; Suzy Surblé<sup>4</sup>

<sup>1</sup> AGH University of Science and Technology

<sup>2</sup> Charles University

<sup>3</sup> Pedagogical University

<sup>4</sup> European Commission, Joint Research Center, Institute for Transuranium Elements

**Corresponding Author:** anna@mag.mff.cuni.cz

Several unconventional superconductors, i.e. those where non-phonon mediated superconductivity is considered, can be found among U-based compounds. Such materials occur at the onset of magnetic order, and magnetic fluctuations have to be considered as a key ingredient of a pairing mechanism. A recently investigated example of such an unconventional compound is UCoGe, reported to be a weak ferromagnet ( $T_C = 2.8$  K) and superconductor ( $T_c = 0.8$  K) [1]. High-pressure experiments are a useful tool to provide information about the relationship of magnetism and superconductivity (SC). UCoGe was found to be easily tunable by hydrostatic pressure whereby ferromagnetism is suppressed and vanishes near  $p_c = 1.4$  GPa but superconductivity is enhanced and survives in the paramagnetic phase up to at least 2.2 GPa [2,3]. In other superconducting ferromagnets such as UGe<sub>2</sub> or URhGe, SC exist only in a ferromagnetic phase under pressure, close to the critical point, and then both ferromagnetism and SC disappear continuously at the critical pressure  $p_c$  [4,5].

The sensitivity of magnetic properties to interatomic spacing is also demonstrated in the case of lattice expansion stimulated by hydrogen absorption. This expansion, partly controlled by the hydrogen pressure, can simulate to some extent a negative pressure. The studies performed on UCoGe indicated a stabilization of ferromagnetism with  $T_C$  shifted up to the vicinity of 50 K for the dihydride UCoGeH<sub>2</sub>. In this context it was surprising to detect the fully reproducible loss of the weak ferromagnetism in UCoGe for the  $\delta$ -hydride (roughly UCoGeH<sub>0.1</sub>) with a small but non-negligible volume expansion of 0.25% [6]. As volume contraction has to be generally expected for high-pressure experiments, we face the peculiar situation with magnetism disappearing with both volume contraction and expansion. Such a paradox brings about the necessity to determine the real lattice reaction to applied hydrostatic pressure.

The structural behaviour of UCoGe with pressure was studied using a diamond anvil cell (DAC) and a modified Bruker D8 diffractometer (Mo-K $\alpha$  radiation). Experimental data were collected at room temperature and pressure increasing gradually up to  $p = 30$  GPa. UCoGe crystallizes in the orthorhombic structure of the TiNiSi type (space group Pnma). High-pressure XRD data showed that the TiNiSi type of structure was preserved up to the highest applied pressure. A Le Bail analysis of the high pressure diffraction patterns yielded data about the pressure variation of the lattice parameters. The quality of the diffraction data was insufficient for full Rietveld analysis however, the attempted refinement gave information about interatomic uranium distances (dU-U), which decrease under applied pressure. The most apparent fact deduced is that the pressure variations of  $b$  and  $c$  are much weaker than for  $a$ . The observed anisotropy of compressibility with the  $a$ -axis as the soft direction obeys the same rule as in the compounds with the ZrNiAl structure type [7], pointing to a profound unifying underlying mechanism for the anisotropy of compressibility. This work also illustrates the fact that the hydrogenation-induced volume expansion cannot be mechanically taken as the equivalent of “negative” pressure, because the geometry of the expansion can be dramatically different than the geometry of compression under hydrostatic pressure. The equilibrium bulk modulus was estimated both from the fit of the Birch and Murnaghan equation of state to the relative volume changes  $V/V_0$  calculated at each pressure  $-B_0 = 1/k_V$ , where  $k_V$  is the volume compressibility (Figure 1) and the sum of individual compressibilities along given lattice directions  $-B_0 = 1/(k_a + k_b + k_c)$  (Figure 2). Individual compressibilities were obtained from a linear fit of the pressure variations of each individual lattice. The equilibrium bulk modulus is relatively high ( $B_0 \sim 340$  GPa) when compared to the UTX compounds with the ZrNiAl structure type [7], but it is in line with results obtained on UTSi-H compounds which form in a structure similar to TiNiSi type ( $B_0 = 257$  GPa for UPdSiH<sub>1.0</sub> [8]).

Fig. 1. Relative volume as a function of pressure for UCoGe. The line represents the fit of the Birch and Murnaghan equation.

Fig. 2. Pressure dependence of lattice parameters  $a$ ,  $b$  and  $c$  for UCoGe. The lines represent the fits mentioned in the text.

Participation in the European Commission JRC-ITU Actinide User Laboratory program through the support of the European Community-Access to Research Infrastructures action of the Improving Human Potential Programme (IHP), contract RITA-CT-2006-026176, is acknowledged.

#### References

- [1] N. T. Huy et al., Phys. Rev. Lett. 99, 067006 (2007).
- [2] E. Hassinger et al., J. Phys. Soc. Jpn. 77, 073703 (2008).
- [3] E. Sloote et al., Phys. Rev. Letters 103, 097003 (2009).
- [4] S. S. Saxena et al., Nature (London) 406, 587 (2000).

- [5] D. Aoki et al., *Nature (London)* 413, 613 (2001).
- [6] A. Adamska et al., *Int. J. Mat. Res.*, 100, 9 (2009).
- [7] L. Havela et al., *J. Alloys Compds.* 322, 7-13 (2001).
- [8] A.V. Kolomiets et al., *J. Magn. Magn. Mater.* 272-276, e343-e344 (2004).

## Introductions to Posters / 8

# Field-Induced Phase Transitions in UIrGe Probed by Ultrasound Measurements

**Author:** Shadi Yasin<sup>1</sup>

**Co-authors:** Alexander V. Andreev<sup>2</sup>; Joachim Wosnitza<sup>1</sup>; Sergei Zherlitsyn<sup>1</sup>

<sup>1</sup> *Hochfeld-Magnetlabor Dresden, Forschungszentrum Dresden-Rossendorf, Germany*

<sup>2</sup> *Institute of Physics ASCR, Na Slovance 2, 182 21 Prague 8, The Czech Republic*

**Corresponding Author:** yasin@fzd.de

The Uranium ternary intermetallic material UIrGe belongs to the large family of UTX compounds (T = transition metal and X = Si or Ge) and crystallizes in the orthorhombic TiNiSi-type structure (space group Pnma) [1]. Its isoelectronic analogs URhGe and UCoGe have recently attracted much attention due to exotic coexistence of ferromagnetism and super-conductivity [2,3]. Previous high-field magnetization, specific-heat, and neutron-diffraction studies on a single crystal of UIrGe reveal antiferromagnetic (AF) ordering below  $T_N = 16$  K [4-7]. The AF structure of the U magnetic moments in UIrGe is non-collinear and commensurate with the crystallographic unit cell. The four ordered U moments in the unit cell are strongly reduced ( $0.36 \mu_B/U$  at 1.8 K) compared to the U<sup>3+</sup> or U<sup>4+</sup> single-ion moment. UIrGe exhibits a large magnetic anisotropy with the hard magnetization direction along the a axis. For magnetic fields applied along the b and the c axis, a metamagnetic transition (MT) towards a field-induced ferromagnetic (FIF) phase is observed. At 2 K, the critical fields  $B_c$  of the MTs along the b and the c axis are 21 and 14 T, respectively.

In the present work, we report results on the sound velocity  $v$  and sound attenuation  $\alpha$  as a function of temperature and magnetic field in UIrGe. The UIrGe single crystal (grown in a tri-arc furnace by use of the Czochralski method) studied in the present experiment is the same crystal used previously for magnetic measurements [5,6]. The ultrasound measurements were performed using the pulse-echo technique [8] at a frequency of 62 MHz. A pair of piezoelectric film transducers were glued to prepolished flat and parallel faces normal to the b axis. The absolute value of the sound velocity in zero magnetic field was extracted from the “echo train” of the ultrasonic signal and is found to be equal to 4250 m/s at 4.2 K. The temperature and magnetic field dependences of the acoustic characteristics were measured in static field (up to 18 T) applied along the c axis. Since the transition field along the b axis exceeds the available steady-field value, the field dependence in this direction was measured in pulsed fields up to 32 T at 4.2 K.

The field- and temperature-dependent changes of the acoustic properties normalized to the values at 4.2 K and zero magnetic field are presented in Figs. 1-4. Figure 1 shows the temperature dependence of the longitudinal sound velocity along the b axis  $v_{bb}$  in zero field and 12 T applied along the c axis (both the wave vector  $k$  and the sound-polarization vector  $u$  are parallel to the b axis). The sound velocity in zero field displays a step-like anomaly of the order of  $10^{-4}$  at  $T_N = 16$  K. At 12 T, an anomaly, that is by more than one order larger, appears at lower temperatures (10.4 K). This is caused by the transition to the FIF state above the metamagnetic transition. As seen in Fig. 2, the metamagnetic transition for fields applied along the c-axis is accompanied by a lattice softening with a sound-velocity change of about  $1.5 \times 10^{-3}$ . A similar effect is observed at the metamagnetic transition for fields applied along the b axis as well (Fig. 3). Thus, the metamagnetic transitions affect the sound velocity much stronger than the spontaneous antiferromagnetic ordering. Regarding the sound attenuation, the metamagnetic transition manifests itself by a strong additional dissipation (Fig. 4; a similar effect is observed for fields applied along the c axis).

We will discuss the observed magnetoelastic effects in conjunction with magnetization and specific-heat results reported earlier [5,6].

**Chemistry I / 9****Investigation of uranium-colloid interactions in soil by dual Capillary Electrophoresis / Field-Flow Fractionation hyphenated with Inductively Coupled Plasma-Mass Spectrometry.****Author:** Céline Claveranne-Lamolère<sup>1</sup>**Co-authors:** Eric Pili<sup>2</sup>; Fabien Pointurier<sup>2</sup>; Gaëtane Lespes<sup>3</sup>; Jean Aupiais<sup>2</sup>; Martine Potin-Gautier<sup>3</sup><sup>1</sup> *IPREM/LCABIE and CEA-DAM-DIF*<sup>2</sup> *CEA-DAM-DIF*<sup>3</sup> *IPREM/LCABIE***Corresponding Author:** celine.claveranne-lamolere@etud.univ-pau.fr

Uranium is an actinide which naturally occurs in the environment. Its applications (civilian nuclear industry, agriculture, military applications, etc...) have induced an anthropogenic contamination, particularly in soils. So it is essential to know conditions and understand mechanisms of its transport. According to IUPAC, colloids refer to molecules or polymolecular particles which have in one direction a dimension roughly between 1 nm and 1 µm. In some cases, colloids are assumed to be responsible for the actinide transport thanks to a strong chelating capacity and an important specific surface [(1), (2)]. Despite a great deal of scientific interest [(3), (4), (5), (6), (7)], much information remains unknown.

The aim of this work was to investigate uranium-colloid interactions thanks to CE-ICP-MS coupling. For this, the more mobile fraction of a soil obtained after leaching experiments was studied. In the different samples analysed, colloids were in balance with uranium. By varying the pH and media, the variations of affinity with surface sites were studied. The specific objective was to observe what could be the influence of these factors on the present uranium colloidal species. Indeed, on the site studied site, pH variation is expected between slightly acidic rain water and alkaline chalk soil. To complete the colloidal characterization (nature and size), Asymmetrical Flow Field-Flow Fractionation (As-Fl-FFF)-multi-detection (UV, Multi-Angle Laser-Light Scattering (MALLS) and ICP-MS) was used.

**References**

- [1] K.V. Ticknor et al., *Applied Geochemistry* 11 (1996) 555-565
- [2] V. Moulin and C. Moulin, *Applied Geochemistry* 10 (1995) 573-580
- [3] A.B. Kersting et al., *Nature* 39717 (1999) 56-59
- [4] M. Dai et al., *Environmental Science and Technology* 36 (2002) 3690-3699
- [5] M. Dai et al., *Journal of Environmental Radioactivity* 53 (2001) 9-25
- [6] L. Chunli et al., *Radiochimica Acta* 89 (2001) 387-391
- [7] T. Matsunaga et al., *Applied Geochemistry* 19 (2004) 1581-1599

**Introductions to Posters / 10****High-pressure hydrogen doping into the UTGe compounds.****Author:** Anna Maria Adamska<sup>1</sup>**Co-authors:** Jiří Pospíšil<sup>2</sup>; Ladislav Havela<sup>2</sup>; N.-T.H. Kim-Ngan<sup>3</sup><sup>1</sup> *AGH University of Science and Technology*<sup>2</sup> *Charles University*<sup>3</sup> *Pedagogical University***Corresponding Author:** anna@mag.mff.cuni.cz

Hydrogenation is a powerful tool capable of changing both crystal structure and magnetic properties of intermetallic compounds. The hydrogen absorption of UT<sub>2</sub>Si compounds (T = Co, Pd, Ni) compounds obtained by direct synthesis from intermetallic precursors at high H<sub>2</sub> pressure (pH<sub>2</sub> > 100 bar) leads to a notable lattice expansion and an increase of respective magnetic ordering temperatures [1,2]. This opens even better possibility for fine tuning of magnetism by H doping in UT<sub>2</sub>Ge compounds, replacing Si by larger Ge. The effect of hydrogenation is already known for U(Fe,Rh)Ge compounds [3]. In the present work, the hydrogenation was performed for UT<sub>2</sub>Ge series with T = Rh, Pd, Ir and Ni by applying the highest hydrogen pressure (pH<sub>2</sub> ~ 60 bar) and temperature cycling up to T = 773 K. Most of the UT<sub>2</sub>Ge compounds crystallize in the orthorhombic TiNiSi-type of structure (space group Pnma). In the case of a-hydride of URhGe obtained at slightly lower pressure, the crystal structure remains orthorhombic with the volume expansion of 1.0 %. The value of TC was difficult to determine due to apparent inhomogeneity of the system. However, one can say that TC extends to substantially higher values than for URhGe (9 K) [3]. By applying the highest pH<sub>2</sub> we obtained another a-hydride of URhGe with 0.3 H/f.u. and the volume expansion of 1.3 %. Unlike URhGeH<sub>0.1</sub>, URhGeH<sub>0.3</sub> is magnetically homogeneous, the value of TC of 17 K was determined from the Arrott plot (Fig. 1). The spontaneous magnetization increases from 0.14 mB/U-atom for the parent compound to 0.34 mB/U-atom for the hydride (both fixed powder data) at T = 2 K.

Fig. 1. Arrott plot for URhGeH<sub>0.3</sub>.

The hydrogenation of UPdGe and UIrGe at pH<sub>2</sub> ~ 160 bar causes the volume expansion of 0.5 % and 0.7 %, respectively, preserving the TiNiSi type of structure. The pure UPdGe undergoes two phase transitions FM–AFM–PM with the phase transitions at TC ~ 30 K and TN ~ 50 K. Hydrogen absorption in UPdGe does not change TN, but it leads to a suppression of TC down to 26 K (Fig. 2.). In the case of UIrGe, we observe the antiferromagnetic ground state (TN ~ 16 K) [4] transformed into ferromagnetic one in the a-hydride (UIrGeH<sub>0.1</sub>). Such a transition was revealed by a well-pronounced but broad peak of ac susceptibility with maximum around 30 K (Fig. 2.). The spontaneous magnetization corresponds to 0.29 mB/U-atom. The onset of ferromagnetism can be assumed around 40 K, but the system looks magnetically inhomogeneous. A single-phase hydride of UNiGe with high H occupancy (1.2 H atoms per formula unit) was synthesized at the highest H<sub>2</sub> pressure. After hydrogenation the orthorhombic symmetry of the parent compound is lifted to hexagonal (ZrBeSi-type) and the unit cell volume expands by 7.6 %. UNiGe exhibits two antiferromagnetic phase transition, one below TN ~ 42-44 K and the second one just below 50 K [4], whereas UNiGeH<sub>1.2</sub> is a ferromagnet with TC below 100 K (Fig. 3.) and the spontaneous magnetization around 0.40 mB/U-atom. The results of the crystal structure refinement and the fitting parameters of the modified Curie-Weiss law for UT<sub>2</sub>Ge and its hydrides are given in Table 1.

Fig. 2. ac susceptibility- ac(T) (real and imaginary part) for UPdGe, UPdGeH<sub>0.1</sub> and UIrGeH<sub>0.1</sub>.

Fig. 3. Temperature dependence of the magnetic susceptibility for UNiGe and its hydride measured in mOe = 2 T.

Table 1. Comparison of crystal structure and magnetic susceptibility parameters of UT<sub>2</sub>Ge and its hydrides.

It gives lattice parameters a, b, and c, volume per formula unit, relative increase of volume with respect to UT<sub>2</sub>Ge (DV/V), inter-uranium spacing dU-U, the ordering Curie temperature TC and parameters of the fit of the susceptibility in the modified Curie-Weiss regime (high T): effective moments meff, paramagnetic Curie temperature Op, and the T-independent term . \*- data from Ref. [4].

#### References

- [1] K. Miliyanchuk et al., J. Alloys Comp. 383, 103-107 (2004).
- [2] A. V. Kolomiets et al., Phys. Rev. B 66, 144423 (2002).
- [3] A. M. Adamska et al., Magnetism in hydrogenated UT<sub>2</sub>Ge compounds, IOP Conf. Proc 2010, in press.
- [4] R. Troc, V.H. Tran, J. Magn. Mater. 73, 389-397 (1988).

## Quadrupolar interactions in UPd3 observed by inelastic neutron scattering

**Author:** Manh Duc Le<sup>1</sup>

**Co-authors:** Keith A McEwen<sup>2</sup>; Robert I Bewley<sup>3</sup>; Tatiana Guidi<sup>3</sup>

<sup>1</sup> *Helmholtz Zentrum Berlin für Materialien und Energie*

<sup>2</sup> *University College London*

<sup>3</sup> *ISIS Facility, STFC Rutherford Appleton Laboratory*

**Corresponding Author:** duc.le@helmholtz-berlin.de

UPd3 is a rare example of a compound where the low temperature ordered phase involves the alignment of electric quadrupoles of the f-electrons on neighbouring ionic sites, rather than their magnetic dipole moments. We show inelastic neutron spectra of the dispersion of crystal field excitations in UPd3, which are consistent with RPA calculations assuming quadrupolar exchange interactions between the f-electrons on the hexagonal U4+ sites.

### Introductions to Posters / 12

## Electrical properties of (Pu,Lu)Pd3

**Author:** Manh Duc Le<sup>1</sup>

**Co-authors:** Eric Colineau<sup>2</sup>; Jean-Christophe Griveau<sup>2</sup>; Keith A McEwen<sup>3</sup>; Rachel Eloirdi<sup>2</sup>

<sup>1</sup> *Helmholtz Zentrum Berlin für Materialien und Energie*

<sup>2</sup> *European Commission, JRC, Institute for Transuranium Elements*

<sup>3</sup> *University College London*

**Corresponding Author:** duc.le@helmholtz-berlin.de

We present the resistivity and Hall coefficient of the heavy fermion compound PuPd3 and its solid solution with LuPd3. A simple crystal field model of conduction s-electrons scattering off local f-electron moment was found to describe the low temperature behavior of the resistivity. This model suggests that the s-f exchange interaction as well as the inter f-electron interactions decrease with increasing Lu doping. The high temperature resistivity shows Kondo behaviour up to 50% doping.

### Introductions to Posters / 13

## On the existence of cerium (IV) orthophosphate, 'Ce3(PO4)4'

**Authors:** Adrian Borhan<sup>1</sup>; Bogdan Apetrachioaiei<sup>1</sup>

**Co-author:** Karin Popa<sup>1</sup>

<sup>1</sup> *"A.I. Cuza" University, Faculty of Chemistry, 11 - Carol I Blvd., 700506 - Iași, Romania*

**Corresponding Author:** kpopa@uaic.ro

The present study is aimed to elucidate the existence of the ceric orthophosphate by synthesis and characterization of 'Ce3(PO4)4' and CePO4. The results obtained indicate a mixed valence in both phosphates obtained, corresponding to nonstoichiometric compounds of cerium in an intermediate oxidation state (molar ratios P/Ce of 1.06 to 1.18). Based on the results obtained, the existence of other ceric phosphates synthesized at high temperatures is discussed.

JDA-WAT I / 14

## Thermodynamic study of the molten salt fast reactor fuel

**Author:** Ondrej Benes<sup>1</sup>

**Co-authors:** Marcus Beilmann<sup>1</sup>; Rudy Konings<sup>2</sup>

<sup>1</sup> EC-JRC-ITU

<sup>2</sup> EC\_JRC\_ITU

**Corresponding Author:** [ondrej.benes@ec.europa.eu](mailto:ondrej.benes@ec.europa.eu)

The Molten Salt Reactor (MSR) is one of the six reactor concepts of the Generation IV (GenIV) initiative. In this concept the fissile material (<sup>233</sup>U, <sup>235</sup>U and <sup>239</sup>Pu) is dissolved in the molten fluoride matrix circulating in the primary circuit from the reactor core to the heat exchanger and back. Compared to solid fuel reactors, the advantage of the MSR is the possibility of fuel purification during the operation. Since the salt is in the liquid form it can be extracted, either online or in batches, and cleaned from the fission products in chemical re-processing plant. This process increases the effectiveness of the reactor because most of the fission products cause parasitic neutron capture and their accumulation would slow down the chain reaction.

Currently there are two main approaches of the MSR. The first are moderated and non-moderated breeder reactors based on the <sup>232</sup>Th/<sup>233</sup>U cycle, for which respectively 7LiF–BeF<sub>2</sub> and 7LiF are considered as an ideal matrix due to the very low parasitic neutron capture cross section of given cations. When designed as an actinide burner the fuel will be most likely PuF<sub>3</sub> with possibly small addition of minor actinide tri- or tetra-fluorides (AmF<sub>3</sub>, NpF<sub>4</sub>, ...). To achieve a favourable melting temperature of the fuel, the matrix based on the 7LiF–NaF–BeF<sub>2</sub> system is the prime candidate.

In this study we perform a thermodynamic investigation of the LiF–NaF–UF<sub>4</sub>–ThF<sub>4</sub> system in order to optimize the fuel composition of the molten salt fast reactor (MSFR) concept [1]. First the binary sub-systems are assessed based on the available experimental data and based on these results the higher order systems are extrapolated according to the developed mathematical formalisms. This approach was shown as a very strong tool of predicting the fuel behaviour as demonstrated in previous studies [2,3,4]. Furthermore once the thermodynamic database is developed properties such as melting temperature, vapour pressure or solubility of actinide fluorides in the fuel matrix can be calculated. All of these properties are very important quantities for the nuclear reactor design; hence the knowledge of the thermodynamic database is of importance.

The initial matrix of the molten salt fast reactor is based only on the pure 7LiF compound, however as shown in this study the melting temperature of the fuel based only on a single component solvent is rather high, around 840 K. This is also the main reason that the designed inlet temperature of this reactor concept is set relatively high at 903 K. One of the possible solutions to decrease the melting temperature of the fuel is to add another matrix component. Therefore one of the objectives of this work was to investigate the effect of the NaF addition as another possible component in the fuel solvent. It has been found that such addition has significant influence on the melting behaviour decreasing the melting point of the fuel by more than 50 K. This is reported in Figure 1 which shows a liquidus projection of the LiF–NaF–ThF<sub>4</sub> pseudoternary system with a concentration of UF<sub>4</sub> fixed at 2 mol% which corresponds to the initial concentration of this fissile material in the MSFR. The calculated lowest melting temperature was found at 772.6 K and ThF<sub>4</sub> concentration of 22 mol%. This value is in agreement with the proposed concentration of this fertile material in the MSFR.

Theory and Spectroscopy II / 15

## Electronic structure theory of Pu-based alloys and compounds: Pu-Am, Pu-Ce-alloys and PuCoGa5

**Author:** Alexander Shick<sup>1</sup>

**Co-authors:** Jindrich Kolorenc<sup>2</sup>; Ladislav Havela<sup>3</sup>

<sup>1</sup> Institute of Physics ASCR, Prague

<sup>2</sup> Institute of Physics ASCR, Prague and University of Hamburg



<sup>3</sup> Charles University, Prague

**Corresponding Author:** shick@fzu.cz

In the present work, we study the electron correlation effects in the electronic structure and spectra of Pu-Am, Pu-Ce alloys and PuCoGa5. We make use of the “local density matrix” approximation (LDMA) to DMFT, that combines the Hubbard-I approximation with the full-potential linearized augmented plane wave (FP-LAPW) method, including self-consistency over the charge density. Calculated PE spectra and electronic specific heat coefficient are in good agreement with available experimental data.

## Theory and Spectroscopy I / 16

### Electronic structure and ionicity of actinide oxides from first principles

**Author:** Leon Petit<sup>1</sup>

**Co-authors:** Axel Svane<sup>2</sup>; Malcolm Stocks<sup>3</sup>; Walter Temmerman<sup>1</sup>; Zdzislawa Szotek<sup>1</sup>

<sup>1</sup> Daresbury Laboratory

<sup>2</sup> Aarhus University

<sup>3</sup> Oak Ridge National Laboratory

**Corresponding Author:** leon.petit@stfc.ac.uk

The ground-state electronic structures of the actinide oxides AO, A<sub>2</sub>O<sub>3</sub>, and AO<sub>2</sub>

## Theory and Spectroscopy II / 17

### Bulk properties of the ζ-U-Pu phase

**Author:** Ladislav Havela<sup>1</sup>

**Co-authors:** Alexander Shick<sup>2</sup>; Daniel Bouexiere<sup>3</sup>; Eric Colineau<sup>3</sup>; Jean-Christophe Griveau<sup>3</sup>; Rachel Eloirdi<sup>3</sup>

<sup>1</sup> Charles University Prague

<sup>2</sup> Institute of Physics, Prague

<sup>3</sup> ITU Karlsruhe

**Corresponding Author:** havela@mag.mff.cuni.cz

In the U-Pu phase diagram a mysterious ζ-U-Pu phase exists over a large composition range (35-70 % U). This cubic (rhombohedrally distorted) phase has 10 different crystallographic positions, randomly occupied by U and Pu. When compared with other Pu allotropic phases, its volume density of 18.55 g/cm<sup>3</sup> fits about half way between a-(19.92 g/cm<sup>3</sup>) and b-Pu (17.70 g/cm<sup>3</sup>). This value is much smaller than the d-Pu and presents clear interesting features. Indeed recent theoretical analyses suggest that this is not the volume density but the 5f occupancy, which decides about the type of ground state in Pu system. Besides fundamental purposes, related mostly to a realistic description of Pu-based systems, the ζ-phase is an important part of potential future metal nuclear fuels.

Here we report on basic properties at low temperature of samples presenting ζ-U-Pu phase. Two samples with concentrations U<sub>59</sub>Pu<sub>41</sub> and U<sub>41</sub>Pu<sub>59</sub> were synthesized by arc melting and annealing. XRD revealed the proper cubic structure with space group Pm-3m (the small rhombohedral distortion with angle  $\alpha$  89.7 deg was not considered during the refinement) with a small trace of UO<sub>2</sub>. The lattice parameters U<sub>41</sub>Pu<sub>59</sub>:  $a = 10.664(2)$  Å, U<sub>59</sub>Pu<sub>41</sub>:  $a = 10.661(1)$  Å are close to values reported

in literature.

The samples have been studied by magnetic and specific heat studies using a SQUID magnetometer (MPMS-7) and a PPMS-9 T. Both concentrations turned out to be weak paramagnets. In this case the correction for the sample holder becomes important, representing more than 10 % of the samples susceptibility. The obtained data exhibit only a very weak T-dependence that could not be analysed in terms of a modified Curie-Weiss law. The examination of absolute values reveals, that compared to the values of Pu phases or a-U, both U-Pu samples present higher susceptibility. At room temperature, one obtains  $8.0 \times 10^{-9}$  m<sup>3</sup>/mol for U<sub>0.41</sub>Pu<sub>0.59</sub> and  $7.3 \times 10^{-9}$  m<sup>3</sup>/mol for U<sub>0.59</sub>Pu<sub>0.41</sub> while one gets  $8.5 \times 10^{-8}$  m<sup>3</sup>/mol and  $7.7 \times 10^{-8}$  m<sup>3</sup>/mol respectively in a broad weak maximum below T = 50 K. This is clearly higher than for a-U ( $4.8 \times 10^{-9}$  m<sup>3</sup>/mol) or for a-Pu ( $6.7 \times 10^{-9}$  m<sup>3</sup>/mol). Nevertheless, this enhancement can not be assimilated to magnetism. A tentative analysis of the contribution of Pu to susceptibility leads to assume that the contribution to susceptibility of U corresponds to that of a respective fraction U in the sample. It has been shown that in PES spectra, the character of Pu-5f states does not change significantly from the situation of a-U. Assuming that the U contribution corresponds to that of the same amount of a-U, we obtain  $1.02 \times 10^{-8}$  m<sup>3</sup>/mol Pu for U<sub>0.59</sub>Pu<sub>0.41</sub> and  $1.09 \times 10^{-8}$  m<sup>3</sup>/mol Pu for U<sub>0.59</sub>Pu<sub>0.41</sub>. These results suggest that the relative contribution of Pu may in fact increase if Pu is more diluted. One should notice that such susceptibility values per Pu are in the ζ-U-Pu phase higher than e.g. in d-Pu stabilized by various dopants or even substantially expanded by Am doping.

The heat capacity measurements reveal that the Debye temperatures are slightly higher than for d-Pu alloys (100 K) while the Sommerfeld coefficient of electronic specific heat g is lower than that for d-Pu. Comparing the two U-Pu alloys, the higher Pu concentration has the higher g-value and lower Debye temperature. The actual g-values amount to 23 mJ/mol K<sup>2</sup> for U<sub>0.59</sub>Pu<sub>0.41</sub> and 35 mJ/mol K<sup>2</sup> for U<sub>0.59</sub>Pu<sub>0.41</sub>. The respective values of Debye T (153 K and 142 K) are close to the value given for a-Pu. Estimating the contribution of Pu into the g-value of the alloy, we can follow the same procedure used for susceptibility, i.e. assuming the fictitious U contribution equal to appropriate amount of a-U (g taken as 9 mJ/mol K<sup>2</sup> for a-U). The values obtained by this way (42 mJ/mol Pu K<sup>2</sup> for U<sub>0.59</sub>Pu<sub>0.41</sub> and 53 mJ/mol Pu K<sup>2</sup> for U<sub>0.59</sub>Pu<sub>0.41</sub>) are in the range of the values reported for d-Pu, i.e. much enhanced comparing to 17 mJ/mol K<sup>2</sup> for a-Pu. The results will be discussed in the framework of LDA+U and LDA+Hubbard I calculations.

Neither hint of superconductivity nor any phase transition has been observed on U<sub>0.59</sub>Pu<sub>0.41</sub> by heat capacity. Despite the use of a <sup>3</sup>He insert and the very small mass of our sample (350 mg), self heating power of <sup>239</sup>Pu has prevented us to cool our material below 2K.

## Chemistry II / 18

### Study of Thorium-Uranium (IV) oxalate dihydrate phase transition through coupled XRD / Raman

**Author:** Nicolas Clavier<sup>1</sup>

**Co-authors:** Francis Abraham<sup>2</sup>; Murielle Rivenet<sup>2</sup>; Nicolas Dacheux<sup>1</sup>

<sup>1</sup> ICSM

<sup>2</sup> UCCS

**Corresponding Author:** nicolas.clavier@icsm.fr

The co-precipitation of tetravalent actinides as an oxalate single phase is currently considered as a promising option to improve the homogeneity as well as the sinterability of mixed oxides fuels envisaged in several concepts of Gen-IV nuclear reactors [1]. Even if actinides oxalates are studied since several decades in this purpose, some uncertainties remain about the associated crystallographic data. In this frame, the crystal structure of Th<sub>1-x</sub>U<sub>x</sub>(C<sub>2</sub>O<sub>4</sub>)<sub>2</sub> · 2H<sub>2</sub>O solid solutions was first elucidated at room temperature. While these compounds are usually reported as orthorhombic [2], all the samples studied during this study were found to crystallize at ambient temperature with a monoclinic (pseudo-orthorhombic) lattice (space group C 2/c). The structure determined from twinned single crystals consists in a two-dimensional metal organic framework formed by metallic centers connected through bis-bidentate oxalate ions (fig. 1a). The stability is then ensured through two kinds of hydrogen bonds achieved with the coordinated water molecules (fig. 1b).

Fig. 1. Projection along a axis  $\text{Th}_{1-x}\text{U}_x(\text{C}_2\text{O}_4)_2 \cdot 2\text{H}_2\text{O}$  metal-organic framework (a) and scheme of hydrogen bonding between the layers (b).

The variation of unit cell parameters versus the thorium substitution rate showed that only the  $c$  axis was significantly modified while the  $\beta$  angle was found to tend to  $90^\circ$  when increasing the uranium amount in the sample. This slight structural variation observed between thorium and uranium(IV) end-members was also evidenced through  $\mu\text{S}$ -Raman spectroscopy analysis since the double band associated to the  $\mu\text{S}(\text{C-O})$  vibration (around  $1470\text{-}1490\text{ cm}^{-1}$ ) was found to be highly sensitive to the cationic environment.

In a second step, in situ HT-XRD and HT-Raman experiments allowed to point out a phase transition leading to an orthorhombic variety of  $\text{Th}_{1-x}\text{U}_x(\text{C}_2\text{O}_4)_2 \cdot 2\text{H}_2\text{O}$  solid solutions. The structure was solved for  $x = 0.5$  from single crystal data collected at  $90^\circ\text{C}$  in the space group  $Ccca$ . The transformation mainly consists in a rearrangement of the oxalate entities leading to a unique carbon site and a reduction from 4 to 2 oxygen atomic positions. In this form, all the hydrogen bonds became equivalent. Moreover, the ferroelastic-paraelastic type transition between the monoclinic and orthorhombic forms is accompanied by few differences in the structural arrangement and the reverse transition led to systematically twinned crystals. Finally,  $\mu\text{S}$ -Raman spectrometry allowed to point out the phase transition through the observation of the  $\mu\text{S}(\text{C-O})$  vibration bands, that turned as a single band due to the symmetrisation of the oxalate group (fig. 2). This study also led to determine the temperature of transition which was found to decrease linearly with the increase of uranium amount in the solid, leading to a strong difference between thorium (around  $116^\circ\text{C}$ ) and uranium (IV) ( $42^\circ\text{C}$ ) end-members.

Fig. 2. Variation of the in situ HT-Raman spectrum through the monoclinic  $\rightarrow$  orthorhombic transition of  $\text{Th}_{1-x}\text{U}_x(\text{C}_2\text{O}_4)_2 \cdot 2\text{H}_2\text{O}$  solid solutions.

References

## Strongly Correlated Systems II / 19

### Specific heat of the antiferro / ferro-magnet $\text{NpGa}_3$

Author: eric colineau<sup>1</sup>

<sup>1</sup> European Commission

Corresponding Author: eric.colineau@ec.europa.eu

The actinide compounds  $\text{AnX}_3$ , where  $X$  is an element from Group IIIA or IVA, crystallize in the cubic  $\text{AuCu}_3$  structure. They are characterized by an actinide-actinide interatomic distance far above the Hill limit, therefore  $5f$ -ligand hybridization is the main mechanism responsible for the delocalization of the  $5f$  electrons. The systematic of this hybridization has been well demonstrated for the  $\text{UX}_3$  compounds, which either do not order magnetically ( $X=\text{Al, Si, Ge, Sn}$ ) or exhibit antiferromagnetism ( $X=\text{Ga, In, Tl, Pb}$ ). It was concluded that the  $5f$ -ligand hybridization increases as one moves up a column of the Periodic Table or moves from a Group IIIA element to a Group IVA element [1,2]. Although data on corresponding  $\text{Np}$  intermetallics are much less documented, a similar trend was noticed. However, it is clear that the  $\text{Np}$ -based compounds are more "magnetic" than their uranium analogues, which is consistent with the general picture that the hybridization decreases as one substitutes a heavier actinide. Indeed, all  $\text{NpX}_3$  compounds ( $X=\text{Al, Ga, In, Sn}$ ) order magnetically at the exception of  $\text{NpGe}_3$  and  $\text{NpSi}_3$  [3,4,5].

Several  $\text{UX}_3$  systems ( $X=\text{Al, Ga, In, Sn, Pb}$ ) present enhanced specific heat at low temperature, in particular  $\text{USn}_3$  ( $\chi = 170\text{ mJ mol}^{-1}\text{ K}^{-2}$ ) and  $\text{UPb}_3$  ( $\chi = 110\text{ mJ mol}^{-1}\text{ K}^{-2}$ ). In the neptunium analogues, only  $\text{NpSn}_3$  ( $\chi = 88\text{ mJ mol}^{-1}\text{ K}^{-2}$ ),  $\text{NpIn}_3$  ( $\chi = 72\text{ mJ mol}^{-1}\text{ K}^{-2}$ ) and  $\text{NpGe}_3$  ( $\chi = 34\text{ mJ mol}^{-1}\text{ K}^{-2}$ ) have been investigated [6].

In the present study, we focus on the specific heat properties of  $\text{NpGa}_3$ . It is worth noticing that  $\text{UGa}_3$  is the only  $\text{UX}_3$  compound considered to be itinerant that displays magnetic order [2].  $\text{NpGa}_3$  exhibits antiferromagnetic ordering ( $k = (\frac{1}{2}\ \frac{1}{2}\ \frac{1}{2})$ ) below  $T_N \approx 65\text{K}$ , but ferromagnetic order with an

ordered moment  $\approx 1.5 \mu_B$  is stabilized below TC  $\approx 50$  K [7]. The high pressure behavior of NpGa<sub>3</sub> indicates a weak delocalization of the 5f electrons [8].

Figure 1 shows the temperature dependence of the specific heat in NpGa<sub>3</sub>. The room-temperature value corresponds to the Dulong-Petit limit ( $\approx 100$  J mol<sup>-1</sup> K<sup>-2</sup>). Going down in temperature, we observe a lambda-type anomaly at 66 K that corresponds to the onset of antiferromagnetic ordering. At 51 K, an intense and narrow peak emerges from the curve, indicating the magnetic phase transition from antiferromagnetism to ferromagnetism. This sharp peak reveals the first-order nature of the transition, as previously pointed out by the thermal variation of the magnetic moment measured by Mössbauer spectroscopy and neutron diffraction [7]. At low-temperature, the extraction of the electronic specific heat is delicate, due to the magnetic contribution and the presence of an upturn, but the Sommerfeld coefficient can be roughly estimated to  $\sim 40$  mJ mol<sup>-1</sup> K<sup>-2</sup>, which is smaller than the  $\gamma$  values reported for the other ordered NpX<sub>3</sub> compounds and for UGa<sub>3</sub>. This observation is consistent with the narrow-band picture suggested by high-pressure experiments [8].

Experiments in magnetic fields up to 14 T have also been performed and will be presented. The antiferromagnetic phase is destroyed above 4 T. The magnetic phase diagram was precisely rebuilt and essentially confirms the previously established one.

#### Acknowledgements

The high-purity Np metal required for the fabrication of NpGa<sub>3</sub> was made available in the framework of a collaboration with the Lawrence Livermore and Los Alamos National Laboratories and the U.S. Department of Energy.

#### References

- [1] D.D. Koelling, B.D. Dunlap, G.W. Crabtree, Phys. Rev. B 31, 4966 (1985).
- [2] A. L. Cornelius, A. J. Arko, J. L. Sarrao, J. D. Thompson, M. F. Hundley, C. H. Booth, N. Harrison and P. M. Oppeneer, Phys. Rev. B 59, 14473 (1999).
- [3] J. Gal, I. Yaar, S. Fredo, I. Halevy, W. Potzel, S. Zwirner and G.M. Kalvius, Phys. Rev. B 46, 5351 (1992).
- [4] J.P. Sanchez, M.N. Bouillet, E. Colineau, A. Blaise, M. Amanowicz, P. Burlet, J.M. Fournier, Physica B 186–188, 675 (1993).
- [5] J.P. Sanchez, E. Colineau, P. Vulliet, K. Tomala, J. Alloys and Comp. 275–277, 154 (1998).
- [6] D. Aoki, Y. Homma, H. Sakai, S. Ikeda, Y. Shiokawa, E. Yamamoto, A. Nakamura, Y. Haga, R. Settai and Y. Onuki, J. Phys. Soc. Japan 75, 084710 (2006) and references therein.
- [7] E. Colineau, F. Bourdarot, P. Burlet, J.P. Sanchez, J. Larroque, Physica B 230–232, 773 (1997).
- [8] S. Zwirner, V. Ichas, D. Braithwaite, J.C. Warenborgh, S. Heathman, W. Potzel, G.M. Kalvius, J.C. Spirlet, J. Rebizant, Phys. Rev. B 54, 12283 (1996).

## Chemistry II / 20

### Study of CeIV<sub>1-x</sub>LnIII<sub>x</sub>O<sub>2-x/2</sub> dissolution

**Author:** Denis Horlait<sup>1</sup>

**Co-authors:** Nicolas Clavier<sup>1</sup>; Nicolas Dacheux<sup>1</sup>

<sup>1</sup> ICSM/LIME

**Corresponding Author:** denis.horlait@cea.fr

The understanding of dissolution processes of actinides dioxides has become essential for the optimization of reprocessing operations associated to the back-end of nuclear fuel cycle. As several GenIV reactor concepts plan to operate the simultaneous reprocessing of majors and minors actinides (such as AmIII and CmIII) in new fuel elements, we focused a study on the influence of the incorporation of a trivalent lanthanide cation (NdIII or ErIII) in fluorite-type matrix CeIVO<sub>2</sub>, as model compounds before forthcoming work based on AnIV-LnIII oxides.

In this aim, several mixed-oxides were synthesized using an initial oxalic co-precipitation of the cations in order to maximize the homogeneity of the final compounds, obtained after heat treatment

at 1000°C. From a structural point of view, the substitution of CeIV by LnIII appears to be accompanied by the formation of oxygen vacancies, in good agreement with literature data [1]. From XRD study of CeIV<sub>1-x</sub>Ln<sub>x</sub>III<sub>2</sub>O<sub>7</sub> mixed dioxides, fluorite structure (Fm3m) remains stable up to about  $x = 0.4$ . For higher  $x$  values a cubic superstructure (Ia-3) appeared, resulting of rearrangement of oxygen vacancies. Finally, for CeIV<sub>0.25</sub>NdIII<sub>0.75</sub>O<sub>1.625</sub> and upper  $x$  values, formation of additional hexagonal Ln<sub>2</sub>O<sub>3</sub> (space group P3mm) was observed.

Dissolution experiments of dioxides compounds were then undertaken in 4M HNO<sub>3</sub>. Small amounts of solution were regularly uptaken and cations concentrations were measured by ICP-AES. Fig. 1 reports the evolution of normalized weight loss of Cerium (NL,Ce) for several CeIV<sub>1-x</sub>Nd<sub>x</sub>III<sub>2</sub>O<sub>7</sub> samples. The associated initial dissolution rates (RL<sub>i</sub>) determined from this results and reported in fig. 2 clearly showed that the trivalent cations fraction (and therefore the oxygen vacancies) strongly enhance the dissolution rate. Conversely, the crystalline structure-type does not seem to have any significant influence on the dissolution rate.

Environmental SEM and BET studies were then undertaken on several samples to follow the variation of the samples morphology throughout the dissolution process. We observed in the first times of the dissolution a strong increase of the specific surface area, correlated to the breakaway of nanometric crystalites (fig. 3, 3days). For longer leaching times, the formation of a gelatinous layer was systematically observed and could be linked to the decrease of dissolution rate after few hours.

Similar experiments were carried on sintered pellets ( $t = 10$  hours,  $T = 1400^\circ\text{C}$ ) (fig. 4). The material appeared preferentially altered 1) through the creation of corrosion pits randomly dispersed onto grains surface, 2) along grain boundaries, which also causes surface grains break away, and 3) by an alteration of the grains surface only observable after 60 hours for this example. Thereby, it seems that there is not only one preferential site or mechanism of dissolution in sintered compounds since the material is more rapidly dissolved from the alteration of grain boundaries and surface local defects.

## Theory and Spectroscopy I / 21

### Resonant inelastic X-ray scattering probe of inter- and intra-atomic interactions in uranium systems

**Author:** Kristina Kvashnina<sup>1</sup>

**Co-authors:** Pieter Glatzel<sup>1</sup>; Sergei Butorin<sup>2</sup>

<sup>1</sup> ESRF

<sup>2</sup> Uppsala University

**Corresponding Author:** kvashnin@esrf.fr

A central issue in the investigation of various properties of actinide systems is the nature of the 5f electrons in different systems. Many of the unusual properties found specifically in uranium (U) compounds are thought to be related to the delocalization of the partially filled U 5f electron states and their hybridization with the U 6d-7s states. However, due to the complexity of the physics involved, a complete understanding of the electronic structure of actinides has not yet been achieved. An element-selective probe of the electronic structure is provided by inner-shell X-ray spectroscopy. Especially, hard X-ray spectroscopy is the ideal candidate for the actinide systems, since it does not require the high-vacuum environment around the sample. For the moment, the X-ray absorption near edge spectroscopy (XANES) at the L3 edge of U (~17.166 keV) has been the most commonly reported. Nevertheless, the large lifetime broadening at the 2p level (~7.4 eV for U) renders the technique little sensitive to the electronic structure. Hämäläinen and co-workers [1-2] showed that the L3 edge of lanthanides can be studied in considerably more details as compared to standard absorption spectroscopy by employing an X-ray emission spectrometer with an instrumental energy resolution similar to the core hole lifetime broadening.

We have studied the electronic structure of U systems in different oxidation states by means of resonant inelastic X-ray scattering (RIXS) via transitions between core levels and between core and valence levels at U L3 edge. The pre-edge structure near the main L3 edge is clearly resolved in U

L3 XANES spectra with a help of X-ray emission spectrometer. The general model for interpreting pre-edges of lanthanides is to consider them as quadrupole transitions into the empty f states. In order to analyze the possible existence of quadrupole transitions of U compounds we carried out FDMNES [3] calculations for the different U systems. Crystal field splitting of the U 6d states were observed in valence band RIXS spectra for UO<sub>2</sub> system and reproduced theoretically using LDA+ U [4] approximation.

On the other hand, the f shell can be directly probed via dipole transitions from 3d core levels (U M<sub>4,5</sub> absorption edge). RIXS spectroscopy has also been used to record changes of the oxidation state in the U systems, by directly observing f-f interactions at U M<sub>5</sub> edge. The experimental results are supported by the atomic multiplet calculations[5]. The f-f transitions uniquely identify the ground state configuration of the uranium ion and can therefore provide an indication of the valence state of U in different complex materials.

Reference:

- [1] K. Hamalainen et al., Phys Rev Lett 67, 2850 (1991).
- [2] P. Carra, M. Fabrizio, and B. T. Thole, Phys Rev Lett 74, 3700 (1995).
- [3] Y. Joly, Phys Rev B 63, art. no. (2001).
- [4] V. I. Anisimov, J. Zaanen, and O. K. Andersen, Phys Rev B 44, 943 (1991).
- [5] R. D. Cowan, University of California Press, Berkeley (1981).

## Chemistry II / 22

### Influence of crystallization state and microstructure over chemical durability of mixed dioxides

**Author:** laurent CLAPAREDE<sup>1</sup>

**Co-authors:** Nicolas CLAVIER<sup>2</sup>; Nicolas DACHEUX<sup>2</sup>

<sup>1</sup> CEA/DEN/DRCP/SCPS/LC2A

<sup>2</sup> ICSM/LIME

**Corresponding Author:** laurent.claparede@cea.fr

Influence of crystallization state and microstructure over chemical durability of mixed dioxides  
L. Claparède 1,2, N. Clavier 2, N. Dacheux 2, R. Podor2, J. Ravaux2  
P. Moisy 1 and J. Dauby 1

1 CEA/DEN/DRCP/SCPS/LCA, Site de Marcoule, BP 17171, 30207 Bagnols / Cèze, France, e-mail: Laurent.claparede@cea.fr

2 ICSM, Site de Marcoule, BP 17171, 30207 Bagnols / Cèze, France

The reprocessing of actinides from nuclear spent fuel into new fuel elements has emerged to economise uranium resources, reduce long-term radiotoxicity of waste and increase resistance of plutonium to proliferation. Such a strategy, initiated with the recycling of uranium and plutonium into MOX fuel obtained through dry chemistry processes, could be improved by the initial co-precipitation of cations into low-temperature precursors such as oxalates. The final compounds are then expected to present a greater homogeneity in term of cations repartition as well as an improved microstructure. In this context, it appears important to evaluate the consequences of these changes over dissolution processes.

Particularly, this study aims to highlight the relationships between the crystallization state and the microstructure of dioxide materials and their ability to dissolve since several studies already shown that parameters such as density, porosity, grain size or density of grain boundaries could have a significant impact on dissolution rates [ , ]. As a first approach before the preparation of actinides mixed dioxides, model compounds with general formula Ce<sub>1-x</sub>NdxO<sub>2</sub> were synthesized from oxalic co-precipitation then fired to obtain the corresponding oxides (300°C < T < 1100°C)

Fig 1: XRD patterns of CeO<sub>2</sub> versus temperature of heat treatment in air.

Fig 2: Variation of the FWHM versus the temperature

Above 300°C, the XRD patterns show the characteristic diffraction lines of the face-centered cubic structure of fluorite-type CeO<sub>2</sub> (space group Fm3m). The variation of the crystallization state of cerium dioxide with the heat treatment was evidenced through the average full width at half maximum (Fig 2).

In a first step, average FWHM decreases strongly between 300°C to 700°C, and then stabilized up to 1100°C. The crystallization of the cerium dioxide seems optimal from 700°C.

The dissolution of these solids was then studied in 2M HNO<sub>3</sub> at 60°C. Whatever the temperature of the heat treatment, the variation of the normalized weight loss (NL) show two distinct tendencies. On the one hand, the evolution of the normalized mass loss is linear during the first days. On the other hand, after about 8 days of leaching, the normalized dissolution rate,  $R_t$ , decreases by an order of magnitude over  $R_0$ . This result could be explained by the formation of a amorphous gelatinous layer at the surface of the solid. The variation of normalized dissolution rates  $R_0$  and  $R_t$  was then studied versus the temperature of the heat treatment (fig 3).

a) b)

Fig 3: Variation of  $R_0$  (a) and  $R_t$  (b), versus heat treatment

The initial dissolution rate decreases inversely with temperature. This result is in good agreement with the variation of the full width at half maximum of diffraction peaks. Moreover the ratio and appear nearly equal, which tends to indicate that FWHM is a good indicator to evaluate the influence of crystallization state. Conversely, the  $R_t$  value was not found to be sensitive to crystallisation state. This result could be correlated to the presence of the gel which annihilates the influence of crystallization state.

Studies are now currently underway on sintered pellets to highlight the relationships between the microstructure of dioxide materials and their dissolution.

## Theory and Spectroscopy I / 23

# First-principles study of uranium dioxide and oxygen self-diffusion in uranium dioxide

Author: BORIS DORADO<sup>1</sup>

Co-authors: MARJORIE BERTOLUS<sup>1</sup>; MICHEL FREYSS<sup>1</sup>

<sup>1</sup> CEA CADARACHE

Corresponding Author: boris.dorado@cea.fr

Uranium dioxide UO<sub>2</sub> is the standard nuclear fuel used in current pressurized water reactors. The description of this oxide by first-principles calculations remains challenging because of the peculiar properties of the uranium 5f electrons which do not allow the standard LDA or GGA functionals to accurately reproduce its electronic properties.

In this study, we use the DFT+U approximation to take into account the strong correlations among 5f electrons and we first investigate the stability of the Jahn-Teller distortion in UO<sub>2</sub> seen experimentally at low temperature. We also study the relative stability of the collinear (1k) and the noncollinear (3k) antiferromagnetic orders, taking into account the spin-orbit coupling.

Second, in order to better understand the behavior of uranium dioxide under irradiation, we investigate the stability and migration mechanisms of point defects, in particular oxygen defects, whose excess governs radiation tolerance, as well as fission product accommodation and release. Activation energies for oxygen self-diffusion have already been measured and reported in the literature, but still little is known about migration mechanisms. We therefore determine the formation energies of the oxygen single interstitial and vacancy in UO<sub>2</sub>, and we compare the results obtained in the fluorite structure with those in the Jahn-Teller distorted structure. We finally calculate migration energies for these defects using the Nudged Elastic Band method. We investigate simple migration pathways, such as the interstitialcy mechanism for the single interstitial, as well as diffusion along

the [100] and [110] directions for the single vacancy.

Using formation and migration energies calculated, we determine the activation energies for oxygen diffusion in UO<sub>2</sub> and compare our results with recent DFT+U results, as well as with new experimental values determined by electrical conductivity measurements.

In order to prevent the system from reaching metastable states created by the DFT+U approximation, all calculations are carried out using an efficient scheme based on the control of uranium 5f occupation matrices.

## Introductions to Posters / 24

# Synthesis and characterization of MIVSiO<sub>4</sub> compounds

**Author:** Dan Tiberiu Costin<sup>1</sup>

<sup>1</sup> CEA

**Corresponding Author:** dan.costin@cea.fr

Actinides silicates, including coffinite (USiO<sub>4</sub>), and derived mineral phases obtained either by cationic or anionic substitutions have been widely studied from various points of view (chemistry, geology, radioecotoxicology). Even if some recent studies led to a reproducible method of preparation for synthetic coffinite samples, this family of compounds remains poorly described in terms of crystal structure. Moreover, in the way of an underground radwaste repository, the degradation of the confining barriers during an accidental situation could induce alteration phenomena. In such conditions, the interaction between actinides and the environment could lead to thermodynamic equilibrium controlling the concentration of actinides in solution, especially through the precipitation of neoformed phases such as coffinite and associated solid solutions. This study thus aims to investigate the formation of actinides bearing silicates, then to collect associated thermodynamic data, including solubility constants.

Several silicates of the zircon group MIVSiO<sub>4</sub> (MIV = Zr, Hf, Ce, Si, Th, U) were then synthesized by both dry and wet chemistry methods. On the one hand, ZrSiO<sub>4</sub> and HfSiO<sub>4</sub> were obtained by mixing stoichiometric quantities of respectively ZrO<sub>2</sub> and HfO<sub>2</sub> with amorphous SiO<sub>2</sub> (silica gel). The powdered mixtures were shaped into pellets and heated up to 1400° C for 24 hours. The pellets were then ground and analyzed by XRD (Fig. 1). The diffraction patterns revealed the formation of the silicate phases, respectively zircon and hafnon at 1400° C. Nevertheless, weak XRD lines of cubic MO<sub>2</sub> were systematically observed and confirmed the formation of additional secondary phase.

Fig. 1 XRD powder pattern for the ZrSiO<sub>4</sub> (left) and HfSiO<sub>4</sub> (right) samples.

On the other hand, the main protocol for wet syntheses of the silicates deals with the hydrothermal route developed by V. Pointeau et al. [1] after the method used by L.H. Fuchs and H.R. Hoetkstra in 1959, based on the principle that an insoluble metal silicate is usually precipitated as a gelatinous amorphous medium when a solution of a polyvalent metal salt is added to a solution of a soluble alkali metal silicate [2]. ThSiO<sub>4</sub> was then prepared by adding drop wise thorium nitrate solution to sodium silicate solution in the expected stoichiometry and adjusting the pH value to 10 using concentrated sodium hydroxide solution. The resulting gel was heated at 200° C for 20h. After cooling, the solution was centrifuged and the precipitate was separated, washed, dried then analyzed by XRD, SEM as well as IR and Raman spectroscopies. The XRD powder pattern (Fig.2) clearly evidences the formation of ThSiO<sub>4</sub> while SEM micrographs show a homogeneous phase composed by nanocrystals 20 nm in length. (Fig.2)

Fig. 2 XRD diagram and SEM observation of ThSiO<sub>4</sub> obtained through hydrothermal synthesis.

Complementary studies are now performed to obtain USiO<sub>4</sub> following the same protocol, with the exception that all the reactants will be outgassed and the synthesis will take place in inert atmosphere (glove box) to avoid the oxidation of tetravalent uranium into uranyl.

References



1. V. Pointeau, A.P Deditius: Synthesis and characterization of coffinite: Journal of Nuclear Materials 393 ( 2009) 449-458
2. L.H. Fuchs, H. R. Hoekstra: The preparation and properties of uranium(IV) silicate: The American Mineralogist 44 1057-1063 1959

## Theory and Spectroscopy II / 27

# The Schrieffer-Wolff transformation for the S=1 Underscreened Kondo Lattice model : Application to Uranium compounds

**Author:** Bernard COQBLIN<sup>1</sup>

**Co-authors:** Acirete DA ROSA SIMOES<sup>2</sup>; Christopher THOMAS<sup>2</sup>; Claudine LACROIX<sup>3</sup>; J. Roberto IGLESIAS<sup>2</sup>; Natasha PERKINS<sup>4</sup>

<sup>1</sup> CNRS-Univ. Paris-Sud, 91405-Orsay, France

<sup>2</sup> UFRGS, 91501-970-Porto Alegre, Brazil

<sup>3</sup> Inst. Neel, CNRS-UJF, 38042 Grenoble, France

<sup>4</sup> Univ. Wisconsin-Madison, Madison, WI53706, USA

**Corresponding Author:** coqblin@lps.u-psud.fr

The Schrieffer-Wolff transformation for the S=1 Underscreened Kondo Lattice model : Application to Uranium compounds

Christopher Thomas<sup>1</sup>, Acirete S. da Rosa Simoes<sup>1</sup>, J. R. Iglesias<sup>1</sup>, C. Lacroix<sup>2</sup>, N. B. Perkins<sup>3</sup>, B. Coqblin<sup>4</sup>

<sup>1</sup> Instituto de Física, Universidade Federal do Rio Grande do Sul, 91501-970 Porto Alegre, Brazil.

<sup>2</sup> Institut Néel, CNRS-UJF, 38042 Grenoble Cedex 9, France.

<sup>3</sup>Department of Physics, University of Wisconsin-Madison, Madison, WI 53706, USA.

<sup>4</sup> L. P. S., Université Paris-Sud, UMR-8502 CNRS, 91405 Orsay, France, coqblin@lps.u-psud.fr

It is well known that the interplay between the Kondo effect and magnetism plays a very important role in Cerium, Ytterbium, Uranium or other anomalous rare-earth and actinide systems. Both effects depend strongly on the hybridization between the f and conduction electrons, which in turn significantly depends on the level of localization of the f electrons. In the case of Cerium compounds, 4f-electrons are usually well localized, while in the case of Uranium and other actinide compounds, 5f-electrons can be either localized or itinerant or in between, depending on the studied system. The difference between 4f- and 5f-electrons can lead to very different magnetic properties of rare-earth and actinide compounds.

It is now established that some actinide compounds exhibit a co-existence between magnetic order and Kondo effect. This phenomenon was observed in several Uranium compounds, like UTe, UCu<sub>0.9</sub>Sb<sub>2</sub>, UCo<sub>0.5</sub>Sb<sub>2</sub> or UNiSi<sub>2</sub>, in which a ferromagnetic order with large Curie temperatures (equal respectively to T<sub>c</sub> = 102K, 113K, 64.5K and 95K) and a logarithmic Kondo-type decrease of the resistivity above T<sub>c</sub> have been experimentally observed [1] [2]. Moreover, the Curie temperature of UTe is passing through a maximum and is then decreasing with applied pressure, which is interpreted as a weak delocalization of the 5f electrons under pressure [3] [4]. A similar observation has been done in the Neptunium compound NpNiSi<sub>2</sub> with a Curie temperature equal to 51.5K [5]. This behaviour is very different from that of Cerium compounds, in which there is a competition between the Kondo effect and the magnetic ordering of the Ce moments, leading to rather low ordering temperatures, typically of order 5 to 10 K.

The first attempt to describe the coexistence of ferromagnetism and Kondo effect in Uranium compounds has been performed within an underscreened Kondo lattice (UKL) model which considers localized f-spins S<sub>f</sub> = 1 to describe a 5f<sub>2</sub> configuration of Uranium ions with 2 f-electrons [6]. This model describes the interaction between the localized spins and s=1/2 spins of conduction electrons through the local Kondo interaction, JK, and the inter-site exchange interaction between the f-spins,

JH. The UKL model gives a new diagram for the Curie  $T_c$  and the Kondo  $T_K$  temperatures versus  $JK$ : at a critical value of  $JK$ , there is a steep increase of  $T_K$ , while  $T_c$  increases smoothly above this critical value of  $JK$ . This diagram, which is different from the Doniach diagram used for Cerium compounds, can account for the coexistence of ferromagnetism and Kondo effect and for the increase of  $T_c$  with pressure at low pressures in UTe. However, this model is based on the assumption of localized 5f-electrons, which does not reflect the situation of several Uranium compounds. Thus, it is necessary to include in the UKL model the possibility of describing the 5f electron delocalization and this will be done here by considering a finite f-band width.

Here we start with an underscreened Anderson Lattice (UAL) Hamiltonian and transform it to an effective Kondo-type spin Hamiltonian by use of a generalized Schrieffer-Wolff (SW) transformation [7]. Namely, the SW transformation yields the usual exchange Kondo-type term for  $S_f = 1$  spins with an exchange interaction proportional to the square of the hybridization parameter  $V_{kf}$  between conduction and f-electrons, and a new scheme for the bands, giving two hybridized bands and one f-band which has a spin-dependent width given by  $W = -JKA\bar{n}/2$ , with  $A\bar{n} = [(n_{f\uparrow})^2 - (1/2)n_{f\uparrow}n_{f\downarrow} - (1/4)(n_{f\downarrow})^2]$ , where  $n_{f\sigma}$  is the average number of f-electrons per site  $i$  in one of the orbitals 1 or 2 and spin  $\sigma$ .

We discuss now the results obtained by this improved UKL model. In the joint Figure 1, we plot  $T_c$  and  $T_K$  temperatures versus the Kondo interaction parameter  $JK$ , obtained for the two following cases: in case (a), the f-band width is proportional to  $JK$ ,  $W = QJK$  with  $Q=0.12$  and in case (b), the relation between  $W$  and  $JK$  is that previously derived by the SW transformation and is spin-dependent,  $W = PJKA\bar{n}$ , with here  $P = -2$ .

Figure 1. Plots of the Curie temperature,  $T_c$ , and the Kondo temperature,  $T_K$ , versus  $JK$ , in the two cases explained in the text. The parameters are:  $JH = -0.01$ , a total number of 5f electrons equal to 2, a number of conduction electrons  $\langle n_c \rangle = 0.8$ ,  $U' = J = 0$  and  $U$  infinite.

In the case (a), we obtain a maximum at the crossing point between  $T_c$  and  $T_K$  and finally  $T_c$  is tending to zero. Since  $JK$  increases with pressure, this dependence can provide a possible explanation for the pressure dependence of  $T_c$  in UTe compound. In the case (b) the behaviour  $T_c$  with  $JK$  is qualitatively similar. Thus, for low values of  $JK$ , there are no Kondo effect and only a ferromagnetic order, as resulting from the exchange interaction  $JH$ . On the other hand, at a sufficiently large  $JK$ , there is a very steep increase of the Kondo temperature, indicating that the Kondo screening takes place and, at large  $JK$ , a ferromagnetic-Kondo regime is realized. However, as expected, the Kondo effect tends to suppress the ferromagnetic order and as a result, the Curie temperature  $T_c$  is passing through a maximum and decreasing with  $JK$ .

In conclusion, taking into account a f-band width, derived correctly from the SW transformation for  $S_f = 1$  spins, improves considerably the description of the Kondo-ferromagnetism coexistence and presents a first approach for describing the decrease of the localization of the 5f electrons when the Kondo effect arises or when pressure increases.

#### References

- [1] J. Schoenes, O. Vogt, J. Lohle, F. Hulliger and K. Mattenberger, Phys. Rev. B 53, 14987 (1996).
- [2] V. H. Tran, R. Troc, Z. Bukowski, D. Badurski and C. Silkowski, Phys. Rev. B 71, 094428 (2005).
- [3] P. Link, U. Benedict, J. Wittig and H. Wuhl, J. Phys. Condens. Matter 4, 5585 (1992)
- [4] Q. G. Sheng and B. R. Cooper, J. Mag. Mag. Mater. 164, 335 (1996)
- [5] E. Colineau, F. Wastin, J. P. Sanchez and J. Rebizant, J. Phys. Condens. Matter 20, 075207 (2008)
- [6] N. B. Perkins, M. D. Nunez-Regueiro, B. Coqblin and J. R. Iglesias, Phys. Rev. B 76, 125101 (2007).
- [7] J. R. Schrieffer and P. A. Wolff, Phys. Rev. 149, 491 (1966).

## Introductions to Posters / 28

### Synthesis of nanocrystalline oxide fuel

**Author:** Raquel Jovaní Abril<sup>1</sup>

**Co-authors:** Jose Luis Spino<sup>1</sup>; Rikard Malmbeck<sup>1</sup>

<sup>1</sup> Institute for Transuranium Elements

High-performance ceramics with nanosized microstructures and functionalized porosities provide the technical base for a large variety of applications in many technologies. This type of microstructure of interest in the nuclear field is due to its appearance at the periphery of Light Water Reactor (LWR) UO<sub>2</sub> fuel at high burn-up. As shown in the past, the fuel spontaneously transforms to a closed porous nanocrystalline structure during irradiation [1,2]. The mechanical properties of this newly formed material are far superior to the original due to the nanostructure.

The aim of these studies is the development of a fuel consisting of nc-UO<sub>2</sub>, which, besides the advantages of enhanced plasticity and faster creep characteristic of the nc-state, diminish the pellet-cladding-interaction (PCI)-stresses and cladding failure risks. In addition, the potentiality has to maintain closed porosity under irradiation to safely retain fission gases. The latter is supported by observations of the in-pile behaviour of the nanoscale High-Burnup Structure (HBS) formed in LWR-fuels after prolonged irradiation [3], and by experimental simulation studies with nc-ZrO<sub>2</sub> [4].

First studies at the JRC-ITU were performed to determine the critical ranges of U-concentration and acidity (pH) for nanophase UO<sub>2+x</sub> precipitation from U(IV)-sulphate solutions [5]. It was shown that the precipitation of UO<sub>2+x</sub> nanoparticles aggregates occurred at very low U-concentrations (<10<sup>-6</sup> M), but the formation of complex U-sulphate compounds overwhelmed the formation of oxide nanoparticles at higher U-concentrations. Thus, the sulphate route for large-yield production of nanoscale UO<sub>2+x</sub> material [6] was excluded.

An alternative route also based on the precipitation of colloidal U(IV)-oxide from slightly oversaturated (near equilibrium), electrolytically reduced U(IV)-solutions, has been explored using U-chloride solutions. Positive results yielding 3 to 5 nm UO<sub>2+x</sub> crystals with the typical fcc structure (see Fig.1) were obtained for the whole range of U-concentrations, especially for the industrial relevant range [U] ≈ 10<sup>-2</sup> M (pH ~1.8 to 2.8).

High-temperature X-ray diffraction investigations of the material indicate that the crystal size remains <10 nm for temperatures below 700° C, followed by a sharp increase, culminating with sizes around 80 nm at 1200° C (see Fig. 2,3). Furthermore, an important shift in the lattice parameter has been observed as a function of temperature (Fig. 2), indicating a lattice expansion that extends beyond that caused by thermal effects. The origin of this abnormal (size-dependent) lattice expansion could be the reduction of the material during thermal treatment or the relaxation of binding-forces at the crystal surface. Detailed investigations are in course to elucidate these trends.

WAT-II / 29

## Uranium Carbide Target for SPIRAL2: fission products effusion optimization studies

**Author:** AHMET OZGUMUS<sup>1</sup>

**Co-authors:** Botoum Hy<sup>1</sup>; Brigitte Roussière<sup>1</sup>; Christophe Lau<sup>1</sup>; Evelyne Cottureau<sup>1</sup>; Henri Noël<sup>2</sup>; Maher Cheikh Mhamed<sup>1</sup>; Mathieu Pasturel<sup>2</sup>; Nicole Barré-Boscher<sup>1</sup>; Olivier Tougait<sup>2</sup>; Said Essabaa<sup>1</sup>

<sup>1</sup> Institut de Physique Nucléaire d'Orsay, UMR 8608 CNRS, Université Paris-Sud 11, Orsay

<sup>2</sup> Sciences Chimiques de Rennes, UMR CNRS 6226, Université de Rennes 1, 263 Avenue de Général Leclerc, Rennes F-35042, France

**Corresponding Author:** ozgumus@in2p3.fr

Very recently studies have been started at IPNO within the framework of the SPIRAL2 project to optimize the properties of uranium carbide used as a fission target. The required characteristics of this target are both the high fission production yield and the capability to release the fission products outside the material as fast as possible. The method of production of this material must be safe and reproducible. The method must allow to control various properties such as the stoichiometry, the density, the size of the pore and their connectivity, the mechanical resistance to swelling during irradiation and the thermal stability. Through the studies we are undertaking, the objective is to get an in depth understanding of the properties of the uranium compounds as a function of the synthesis parameters and also of their behaviour under operating conditions: high temperature and

high irradiation dose. Our studies concern three ways of synthesis: the first two methods are the carbo-thermic reductions of a mixture of uranium oxide and uranium oxalate and graphite at high temperature [1-4]. The third way is the synthesis by fusing a stoichiometric mixture of metallic uranium and graphite into an electrical arc [5]. Most of the important characteristics detailed above are controlled by dependant parameters like synthesis and sintering temperatures and durations. Because of the drastic conditions of use, all these characteristics could change. High temperature and high irradiation dose will modify considerably the initial properties of the material and could lead to the collapse of the material by swelling, polygonization or amorphization [6-11].

Our first studies show that we are able to well-control the stoichiometry of the material (monocarbide UC or dicarbide UC<sub>2</sub>) determined by the X-Ray diffraction measurements. We can also control the density ranging from 3.5 g.cm<sup>-3</sup> to 13.2 g.cm<sup>-3</sup> (25% to 97% of the theoretical density of UC). The density is determined by helium pycnometry. The control of the grain size ranging from 1 to 30 μm (measured by Scanning Electron Microscope) and also the control of the size and the distribution of the pore size (measured by mercury porosimetry) are in progress. The target release properties will be performed by comparing the quantity of radio-nuclides present in irradiated pellets before and after heating by gamma-spectrometry. The behaviour of the most interesting targets obtained will be studied under high temperature and high irradiation dose. The kinetic of the closing of the pores and the evolution of the mechanical strength of the pellet during long term operation will also be studied.

### Strongly Correlated Systems III / 30

## 237Np Mössbauer effect study of NpPdSn

**Author:** Piotr Gaczyński<sup>1</sup>

**Co-authors:** Eric Colineau<sup>1</sup>; Franck Wastin<sup>1</sup>; J. Rebizant<sup>1</sup>; Jean-Christophe Griveau<sup>1</sup>; Krzysztof Gofryk<sup>2</sup>; R. Jardin<sup>1</sup>; Roberto Caciuffo<sup>1</sup>

<sup>1</sup> JRC Institut for Transuranium Elements

<sup>2</sup> Los Alamos National Laboratory, Los Alamos

**Corresponding Author:** piotr.gaczynski@ec.europa.eu

During the past decades ternary actinide-based compounds containing d- and p-electron elements have attracted much attention for their large variety of physical behaviors arising mostly from the hybridization of actinide 5f electrons with s, p and /or d states on neighboring sites. An example of a system with promising physical behavior is the ATX composition where A stands for actinide atoms, T for d-element metals and X for p-electron elements.

Among this family, the uranium stannite UPdSn exhibits an antiferromagnetic phase transition at 37 K leading to a magnetic structure with orthorhombic symmetry. A second transition occurs at 25 K and the magnetic structure becomes of monoclinic symmetry [1]. The plutonium analogue PuPdSn undergoes two successive antiferromagnetic transitions at 21 K and 9.6 K [2]. In contrast, the neptunium analogue NpPdSn exhibits only one antiferromagnetic transition at 19 K [3]. An effective magnetic moment  $\mu_{\text{eff}} = 2.66 \mu_B$ , close to the Np<sup>3+</sup> free ion value, was inferred from magnetization measurements but the ordered moment was not determined in previous studies. Here, we present a 237Np Mössbauer investigation of the NpPdSn compound.

The ATX compounds crystallize in various crystal structures, like the hexagonal ZrNiAl- and GaGeLi-types, the orthorhombic TiNiSi- type and the cubic MgAgAs-type.

NpPdSn crystallizes into the hexagonal ZrNiAl-type structure with space group P-62m. A Rietveld analysis of the x-ray powder diffraction profile measured at room temperature has been performed to refine the lattice parameters and the internal atomic coordinates. The diffraction pattern is shown in Figure 1, together with the calculated profile and the residual line. The results show that the investigated sample is single-phase, with lattice parameters  $a = 7.5075 \text{ \AA}$  and  $c = 4.0954 \text{ \AA}$ , in agreement with previous investigations [3]. The Np atoms occupy the 3f site ( $x=0.5875$ ), the Pd atoms are located on the 1a and 2c sites and the Sn atoms fill the 3g site ( $x=0.2487$ ).

237Np Mössbauer spectra were recorded between 4 K and 25 K in a transmission geometry spectrometer with a ~100mCi 241Am source kept at a temperature of about 4 K. The absorber was prepared

by grinding the sample to a fine powder to ensure a constant surface density with an optimal thickness of 140mg Np/cm<sup>2</sup>. The velocity scale was calibrated using the NpAl<sub>2</sub> standard compound. The isomer shift, IS, is given relative to NpAl<sub>2</sub>. The spectra were analyzed using Lorentzian lines. The position and relative intensities of the absorption lines of Np nuclei were calculated by solving the complete Hamiltonian for the hyperfine interaction in both the excited and ground nuclear state of <sup>237</sup>Np.

Mössbauer spectra of NpPdSn at 25 K and 4.2 K are presented on the Figure 2.

Following the value of IS = 14.4 mm/s (vs NpAl<sub>2</sub>) we assigned a formal 3+ oxidation state to Np atoms [4], which is in agreement with the magnetization data.

In the paramagnetic region, the spectrum consists in only one a small quadrupolar splitting (QS), reflecting the fact that Np occupies a unique crystallographic site.

At 4K, the spectrum is split by the magnetic hyperfine interaction caused by the ordering of the magnetic moments. However, several subspectra - with equal IS and QS parameters but different magnetic hyperfine field Bhf - are required to reproduce the experimental pattern. In our fit, we used three different values of Bhf, corresponding to three different magnetic moments carried by the neptunium atoms. Two of the measured moments have a similar value ( $\mu_{\text{Np}} = 1.53(5) \mu\text{B}$  and  $1.44(5) \mu\text{B}$ ), the third one is almost vanishing ( $\mu_{\text{Np}} = 0.05(5)\mu\text{B}$ ). The latter is indeed visible on the central line of the 4 K spectrum.

The higher number of subspectra than expected from the crystallographic structure may be due to different orientations of the principal axis (*V*<sub>zz</sub>) of electric field gradient of Np atoms at 3f site vs. crystallographic axis, as observed in FeSn, crystallizing also into an hexagonal crystal structure [5]. The existence of several subspectra with different magnetic moments could also originate from a complex magnetic structure, like e.g. in NpIn<sub>3</sub> where a modulated antiferromagnetic order, including vanishing moments, was observed by Mössbauer spectroscopy and neutron diffraction [6].

#### Acknowledgements

PG acknowledges the European Commission for support in the frame of the “Training and Mobility of Researchers” programme. The high purity Np metals required for the fabrication of the compound were made available through a loan agreement between Lawrence Livermore National Laboratory and ITU, in the frame of a collaboration involving LLNL, Los Alamos National Laboratory and the US Department of Energy.

#### References

- [1] H. Nakotte, R.A. Robinson, A. Purwanto, Z. Tun, K Prokeš, E. Brück, F.R. de Boer, Phys Rev. B 58 9269 (1998)
- [2] K. Gofryk, J.-Ch. Griveau, E. Colineau, R. Jardin, J. Rebizant, F. Wastin, R. Caciuffo, Journal of Nuclear Materials, 385, 220 (2009).
- [3] K. Gofryk, J.-C. Griveau, R. Jardin, E. Colineau, J. Rebizant, F. Wastin, R. Caciuffo; Acta Phys Pol. A 115 7 (2009)
- [4] G.M. Kalvius, J. Gal, L. Ash, W. Potzel; Hyp. Inter. 72 77 (1992)
- [5] L. Häggström, T. Ericsson, R. Wäppling, K. Chandra, Phys Sripta. 11 47 (1975)
- [6] E. Colineau, A. Blaise, P. Burlet, J. P. Sanchez and J. Larroque, Physica B: Cond. Matter 206-207, 528 (1995)

JDA-WAT I / 31

## Oxidative corrosion of carbide inclusions at the surface of uranium metal during exposure to water vapour.

**Author:** Thomas Scott<sup>1</sup>

**Co-authors:** Geoffrey Allen <sup>1</sup>; James Petherbridge <sup>2</sup>; Joe Glascott <sup>2</sup>; Nicholas Harker <sup>1</sup>; Richard Ball <sup>1</sup>

<sup>1</sup> University of Bristol

<sup>2</sup> AWE Aldermaston, UK

**Corresponding Author:** t.b.scott@bristol.ac.uk

The interaction between metallic uranium surfaces and water vapour is considered to be most important in regard to the environmental corrosion of the metal. Numerous studies have examined the initial stages of these interactions. However, there have been discrepancies in the published data describing kinetic laws, pressure dependence of the reaction rate constant and activation energies. The precise mechanism for uranium corrosion is not entirely clear. Existing discrepancies in the published data may, in part, be related to differences in the provenance and purity of the metal used by different groups, with the reactivity of impurity species such as carbide precipitates, affecting recorded data.

To provide data for an improved understanding of the role of impurity phases in the uranium-water reaction, samples of uranium containing 600 ppm carbon were analysed during and after controlled exposure to water vapour at 19 mbar pressure in an environmental secondary electron microscope (ESEM).

The oxidative corrosion of carbide (UC) inclusions at the surface of uranium metal was readily observed, forming voluminous secondary precipitates determined to be nominally  $\text{UO}_3 \cdot \text{H}_2\text{O}$  by X-ray diffraction techniques. A focused ion beam (FIB) system was used to produce sections that were cut through the reacted carbides for subsequent analysis by electron microscopy. Over the period of a week the precipitates were observed to grow in size, consuming only the carbide particles and not the surrounding metal. In some cases complete decomposition of the surface carbides was observed.

From the results of the current work it is apparent that the carbide particles reacted readily with the water vapour. Resultantly it is suggested that disparities between previous studies of the uranium-water reaction may be partly attributable to differential purities of uranium metal used by different research groups, with resultantly different populations of carbide particles.

## Introductions to Posters / 32

### Initial electron back-scattered diffraction observations of Ce-La alloy

**Author:** Thomas Scott<sup>1</sup>

**Co-authors:** Charles Younes<sup>1</sup>; Chris Jones<sup>1</sup>; Michael Ling<sup>2</sup>; Roderick Jenkins<sup>2</sup>

<sup>1</sup> *University of Bristol*

<sup>2</sup> *AWE, Aldermaston, UK*

**Corresponding Author:** t.b.scott@bristol.ac.uk

Experimental surrogates for Plutonium may provide an effective means to help understand and model some of the many complex metallurgical issues concerning material. Cerium, located in the lanthanide family of the periodic table, is considered to be a non-radioactive surrogate of Pu because of the several similarities between the two metals including similar crystal structures (fcc), multiple allotropic forms, large volume changes associated with phase transformations, pressure–melting temperature dependence, unusually low melting temperatures (Ce = 798°C, Pu = 640°C), formation of asymmetric crystal structures, similarity in electronic configurations and the itinerancy of f electrons, and their alloys exhibit solid-state microsegregation (Ce–La and Pu–Ga). This connection defines a foundation for the use of Ce as a surrogate for Pu.

Electron back-scattered diffraction (EBSD) orientation mapping has proven to be a valuable microstructural characterization technique for understanding phase transformations, texture, orientation relationships, grain-boundary character distribution, phase identification, etc., for pure metals and alloys (Schwartz et al. 2000). However, owing to its extreme surface reactivity, EBSD analysis of pure Cerium has only been reported on one occasion (Farr et al 2003). This current work represents the first successful attempt to obtain EBSD patterns and orientation maps of Ce-La5 alloy. Initial data were generated using a combined ion-electron beam system, where ion milling and EBSD mapping were performed EBSD in situ. For subsequent samples surface preparation by ion milling was performed in a focused ion beam (FIB) system and the sample was briefly transferred through

air for analysis in a separate secondary electron microscope (SEM) fitted with EBSD instrumentation.

### Introductions to Posters / 33

## Distribution of soil-to-plant transfer factors for the natural uranium isotopes in the vegetation in zones affected by uranium mines

**Author:** Carmen Ileana Cristache<sup>1</sup>

**Co-authors:** Laura Aldave de las Heras<sup>2</sup>; Mihaela Bragea<sup>3</sup>; Ramon Carlos Marquez<sup>2</sup>; Toro Laszlo<sup>3</sup>

<sup>1</sup> IFIN-HH

<sup>2</sup> European Commission, Joint Research Centre, Institute for Transuranium Elements, P.O. Box 2340, 76125, Karlsruhe, Germany

<sup>3</sup> Institute of Public Health, V. Babeş 16, 300226, Timisoara, Romania

**Corresponding Author:** ocarmen@ifin.nipne.ro

Gamma ray spectrometry and ICP-MS methods were investigated in vegetation samples, collected from the surface tailing, near a uranium mine, located in the Baita region, West part of Romania. The main goal of this investigation was to determine distribution of soil-to-plant transfer factors for the natural uranium isotopes and to compare the experimental results obtained between these methods. The results will be presented in this paper.

### Summary:

High levels of radionuclides are usually found in the surface soil and vegetation of areas affected by uranium mining and milling. It is also important to understand the behavior of natural uranium in the environment (e.g., mobility, transfers, translocation), because such information can be used to develop, to test models and to obtain the associated parameter values appropriate for radiological assessments [1]. Accurate measurements of the total radionuclide concentration in contaminated soils are required to assess their potential risk. Migration and accumulation of contaminants (including radionuclides) in the soil-plant system is complex, involving processes such as leaching, capillary rise, runoff, sorption, root uptake and re-suspension into the atmosphere. Assessment models commonly utilize a soil-plant concentration ratio, referred to as a transfer factor (TF), to estimate the transport of radionuclides through the food chain [2]. This ratio describes the amount of radionuclide expected to enter in a plant from the soil. Factors such as soil characteristics, climatic conditions, type of plants, part of the plant concerned, physico-chemical form of the radionuclides and the interfering elements can all influence the TF values [3]. In the present study, centered on the around disused uranium mine located in the Baita region in the West of Romania, two compartments are being considered: soil and vegetation. The aim is to investigate the association of the natural uranium (<sup>234</sup>U, <sup>235</sup>U and <sup>238</sup>U) with each compartment and the possible transfer between them. The vegetation samples at each point were collected from the surface tailing near a uranium mine at which the soil sample had to be removed. In all cases, only the aerial fraction was sampled. The samples were carefully washed in the laboratory in order to remove all the adhered soil particles. Ten sampling campaigns (soil and vegetation) were performed during a one-year period. Each sample was dried at 105°C, ground, and homogenized. Approximately 100g of samples were hermetically closed in plastic beakers and stored for about 40 days to reach radioactive equilibrium with the radon daughter. The plant and soil samples were analyzed by gamma-spectrometry using CANBERRA HPGe detector with carbon epoxy window, with a resolution of 1,8 keV at <sup>60</sup>Co 1332,5 keV line and approximately 50% relative efficiency, peak (59,5keV) efficiency 6,62%. Efficiencies of the detector at each photon energy are calculated using the specific software Canberra Genie 2000, ISOCS. For both types of samples the total acquisition time was 200000seconds. Finally, were compared to results obtained by gamma spectrometric measurements with those obtained by ICPMS at ITU Karlsruhe.

### References

[1] F. Vera Tome et. al., Journal of Environmental Radioactivity, 65 (2), 161-175, (2003).

- [2] Mirjana Stojanović et. al., *Water, Air and Soil Pollution*, 200 (1-4), 101-108, (2009).  
 [3] S.B. Chen et. al., *Journal of Environmental Radioactivity*, 82(2), 223-236, (2005).  
 [4] IAEA, *Guide Book. Technical Report*, 295, (1989).  
 [5] A. Martinez-Aguirre et. al., *The Science of the Total Environment*, 173, 203-209, (1995).

#### Introductions to Posters / 34

## 234U/238U disequilibrium studies in soil and vegetation samples from tailing dumps

**Authors:** Laura Aldave de las Heras<sup>1</sup>; Mihaela Gladiola Bragea<sup>2</sup>

**Co-authors:** Carmen Cristache<sup>3</sup>; Ramon Carlos Marquez<sup>1</sup>

<sup>1</sup> *European Commission, Joint Research Centre, Institute for Transuranium Elements, P.O. Box 2340, 76125, Karlsruhe, Germany*

<sup>2</sup> *Institute of Public Health Timisoara*

<sup>3</sup> *Horia Hulubei National Institute for Physics and Nuclear Engineering, P.O. Box MG-6, 077125 Magurele (Ilfov), Romania*

**Corresponding Author:** mbragea@yahoo.com

A study is presented on the disequilibrium of uranium isotopes (<sup>234</sup>U and <sup>238</sup>U) in soils and vegetation samples collected near an uranium tailing dump. Factors affecting uptake of uranium by plants, including relationships between these radionuclides in soils and in plants, and the temporal changes of uranium concentrations in different plant species are discussed. The <sup>234</sup>U/<sup>238</sup>U atom ratio can provide information regarding disequilibrium in plants.

#### Summary:

The existence of radioactive disequilibria among nuclides in the decay series is an indication of recent fractionation events, usually related to gain or loss of the more mobile nuclides. Plant uptake is the first step in the major pathways of the trophic chain leading to man. Understanding the processes that govern the uptake of radionuclides in plants is very important in environmental control and surveillance. If plant uptake and accumulation are sufficiently high, plants can be used in cleaning up soils, sediments, and waters contaminated by low and moderate levels of radionuclides [1]. The assimilation of uranium was measured by the determination of U activity in plants samples and associated substrates from one inactive uranium mine tailing as a transport mechanism of uranium in the environment. Two species of plant samples were collected from 4 points located at different distances from the dump of the waste rock of the mine EM, Caras-Severin Country, Romania. The plants were cut at points about 5 cm above the ground surface in order to avoid direct contamination by soil. The total uranium concentration and the isotopic composition from vegetation and soils samples collected at the same sampling site, were determined by high resolution ICPMS Element 2 after separation and preconcentration of uranium. <sup>234</sup>U/<sup>238</sup>U atom ratios in soil and vegetation samples as a function of distance from the uranium tailing dump. The results obtained for the soil samples show that the <sup>234</sup>U/<sup>238</sup>U atom ratios in all soil samples, are clearly higher than the natural <sup>234</sup>U/<sup>238</sup>U atom ratios, 5,54019E-05. Higher <sup>234</sup>U/<sup>238</sup>U ratios in soil were observed at 100 and 200m from uranium dump, decreasing with further distance from the uranium tailing dump. When aquatic systems are in contact with minerals, selective leaching processes lead to preferential dissolution and transport of <sup>234</sup>U, resulting in enhancement of <sup>234</sup>U/<sup>238</sup>U ratio. The reason underlying the enhancement of the ratio is attributed, as a major cause, to a "recoil induced vulnerability to leaching". The mechanism is view as a creation of defects in the crystal lattice when the parent nuclide (<sup>238</sup>U) recoils during emission of an alpha particle, thus the daughter nuclide (<sup>234</sup>U) is in a microenvironment that is more susceptible to chemical attack than the parent [2]. Electron stripping during the decay process such that <sup>234</sup>U is more likely to be in more soluble U(VI) state, facilitating the solution of this isotope by a surface etching process[3]. In the vegetation samples collected up to 200 m from the uranium tailing dump, half of the samples analysed presented an enhancement of the ratio <sup>234</sup>U/<sup>238</sup>U ratio being always higher in grass than in Tussilago farfara. The mobility of uranium in



plant tissues is limited, as it tends to adsorb on cell wall materials; therefore, concentrations are typically higher in tissues found lower on the plant and are highest on the root surfaces [4]. It was presented correlations between  $^{234}\text{U}/^{238}\text{U}$  ratios in grass and *Tussilago farfara* and in soil where the plants were grown. Although these plants were grown and harvested simultaneously, we can see that both  $^{234}\text{U}$  and  $^{238}\text{U}$  were more easily transferred from soil to roots of grass as compared as compared to transfer of these radionuclides from soil to roots *Tussilago farfara*.

Plant radionuclide concentrations are not so often linearly related to soil radionuclide concentrations. Nonlinearity can complicate the measurement of bioavailability, because each plant and soil combination may have a unique curvilinear relationship. The study of temporal variations of  $^{234}\text{U}$  and  $^{238}\text{U}$  in plant showed that short-term dynamics of radionuclide plant concentrations are rather significant and species-specific.

#### References

- [1] P. Blanco Rodríguez et. al., *Science of The Total Environment*, 361(1-3), 1-7 (2006)
- [2] K. Kisogi et. al., *Science*, 173, 47-48, (1971).
- [3] Jurado Vargas et. al., *Nuclear Geophysics*, 9, 567-578, (1995).
- [4] L. S. Morton et. al., *Journal of Environmental Quality* 31, 155-162 (2002).

We acknowledge the “Actinide User Laboratory” program provided by the European Commission, DG-JRC, Institute for Transuranium Elements (ITU) and the financial support from the European Community-Access to Research Infrastructures action of the Improving Human Potential Programme, DG-RTD, Contract No. RITA-CT-2006-026176.

#### Chemistry I / 35

## Uranyl behaviour at the gibbsite-water interface: a Car Parrinello molecular dynamics study

**Author:** Sébastien Lectez<sup>1</sup>

**Co-authors:** Eric Simoni<sup>1</sup>; Jérôme Roques<sup>1</sup>; Mathieu Salanne<sup>1</sup>

<sup>1</sup> CNRS

**Corresponding Author:** lectez@ipno.in2p3.fr

In order to understand the various mechanisms involved in the retention of the radionuclides on mineral surfaces, molecular simulations appear as a complementary tool to experiments. In this work, we propose to study the sorption of the solvated uranyl cation  $\text{UO}_2^{2+}$  on an abundant mineral surface, the gibbsite ( $\text{Al}(\text{OH})_3$ ). The study of such complex systems may involve finite temperature simulations with a realistic representation of the interatomic interactions. We have therefore chosen to perform simulations within the Car-Parrinello molecular dynamics method [1], in which the trajectories of the nuclei are obtained by on-the-fly DFT calculations.

As a first step, a system consisting of an uranyl ion in solution was simulated. This step is crucial to understand the nature of the interactions between this ion and water molecules. The structure of the first and the second solvation shell was characterized, in good agreement with previous experimental [2] and theoretical [3],[4] studies.

The second part of our work concerns the hydration of the (001) gibbsite face. First, we optimized the bulk crystallographic parameters in order to build a (001) gibbsite face model. Calculations display very small relaxation of the surface atomic positions relative to the bulk atomic ones. Then, we simulated a system consisting of the solvent and the gibbsite face. Two different adsorption modes were identified for first layer water molecules on the (001) face, both involving hydrogen bonds with similar energies. These results are in good agreement with experimental findings [5].

In the last part, the full system including the solvated uranyl ion and the hydrated gibbsite (001) face was investigated. We simulated two adsorption mechanisms: the inner sphere and the outer sphere mechanism. Both states are stable, and the transition from one to another one involves the crossing

of an energy barrier. We determined this activation energy using the umbrella sampling method, which allows us to predict the most stable adsorption mechanism.

#### References

- [1] CPMD V3.5, J. Hutter et al., Copyright IBM Zurich Research Laboratory and MPI für Festkörperforschung, (1995 – 2001).
- [2] M. Aaberg et al., *Inorganic Chemistry* 22, 3986 (1983).
- [3] P. Nichols et al., *The journal of chemical physics* 128, 124507 (2008).
- [4] M. Buhl et al., *Journal of the American Chemical Society* 128, 6357 (2006).
- [5] E. Veilly et al., *the journal of chemical physics* 129, 244704 (2008).

WAT-II / 36

## Investigation of Uranium Materials for a Two-Step Target

**Author:** Eugene Spejewski<sup>1</sup>

**Co-authors:** Carola Jost<sup>2</sup>; Dan Stracener<sup>3</sup>; Jon Batchelder<sup>1</sup>; Norm Hubele<sup>4</sup>; Ron Goans<sup>5</sup>; Will Talbert<sup>6</sup>

<sup>1</sup> Oak Ridge Associated Universities

<sup>2</sup> Johannes Gutenberg-Universität Mainz

<sup>3</sup> Oak Ridge National Laboratory

<sup>4</sup> Refrac Systems

<sup>5</sup> University of Tennessee

<sup>6</sup> TechSource

**Corresponding Author:** spejewskieh@ornl.gov

Yield determinations of various uranium targets which could be used in the presented concept of a two-stage target.

Introductions to Posters / 37

## Isothermal section of the U-Fe-Ge ternary system at 900°C

**Author:** Margarida Henriques<sup>1</sup>

**Co-authors:** Adrien Lignie<sup>2</sup>; Alberto C. Ferro<sup>3</sup>; António P. Gonçalves<sup>1</sup>; David Berthebaud<sup>2</sup>; Henri Noel<sup>2</sup>; Olivier Tougait<sup>2</sup>

<sup>1</sup> Departamento de Química, Instituto Tecnológico e Nuclear/CFMC-UL, 2863-953 Sacavém, Portugal

<sup>2</sup> Sciences Chimiques de Rennes, Laboratoire de Chimie du Solide et Matériaux, UMR CNRS 6226, Université de Rennes 1, Rennes, France

<sup>3</sup> Departamento Engenharia Materiais, Instituto Superior Técnico, Av. Rovisco Pais, 1049-001 Lisboa, Portugal

**Corresponding Author:** mish@itn.pt

Investigations on uranium-based ternary intermetallics continue to reveal new phases, with specific structures and rich variety of ground-state properties. In the U-Fe-Ge system the previously reported ternary intermetallic compounds were UFeGe (P21/m, type UFeGe below 500K, and Pnma, type TiNiSi above 500K) [1], UFe<sub>2</sub>Ge<sub>2</sub> (I4/mmm, type ThCr<sub>2</sub>Si<sub>2</sub>) [2], UFe<sub>6</sub>Ge<sub>6</sub> (P6/mmm, type YbCo<sub>6</sub>Ge<sub>6</sub>) [3], and the solid solution U<sub>2</sub>Fe<sub>17-x</sub>Ge<sub>x</sub> with 2 < x < 3 (P63/mmc, type Th<sub>2</sub>Ni<sub>17</sub>) [4], in addition to the recently reported U<sub>2</sub>Fe<sub>3</sub>Ge compound (P63/mmc, type MgZn<sub>2</sub>) [5, 6]. Following the previous work made on the U-Fe-Ge system [7], the aim of the present study is to complete the experimental investigation of the 900°C isothermal section of the U-Fe-Ge phase diagram and the characterization of the new intermetallic compounds. The samples were prepared by direct melting the calculated

amounts of U, Fe and Ge elements (purity >99.9 mass%), in an arc-melting furnace and under high purity argon atmosphere, followed by annealing at 900°C for one week inside evacuated quartz ampoules. The microstructure of all samples was analysed by SEM-EDS and the crystalline structure was characterized by powder and single-crystal X-ray diffraction.

The existence and composition of all the binary phases previously reported at 900°C were confirmed and their crystal data are in agreement with literature. The binary compound UFe<sub>2</sub> is the only one existing in the U-Fe system at the studied temperature, and in this ternary system, there is a substitution of iron by germanium in an amount up to 6.7 at%, as solid solution UFe<sub>2-x</sub>Ge<sub>x</sub>. All the other binary phases have negligible solubility extensions into the ternary system at this temperature. The isothermal section was found to be very rich: there are 13 stable phases at 900°C. Among these, there are nine new intermetallic compounds: U<sub>3</sub>Fe<sub>4-x</sub>Ge<sub>3</sub>, UFe<sub>1-x</sub>Ge<sub>2</sub>, U<sub>3</sub>Fe<sub>2</sub>Ge<sub>7</sub>, U<sub>9</sub>Fe<sub>7</sub>Ge<sub>24</sub>, U<sub>2</sub>Fe<sub>3</sub>Ge, U<sub>6</sub>Fe<sub>16</sub>Ge<sub>7</sub>, U<sub>3</sub>Fe<sub>4</sub>Ge<sub>4</sub>, UFe<sub>4</sub>Ge<sub>2</sub> and U<sub>6</sub>Fe<sub>22</sub>Ge<sub>13</sub>. Within these new phases, three are new original structural types: U<sub>3</sub>Fe<sub>4-x</sub>Ge<sub>3</sub> and U<sub>9</sub>Fe<sub>7</sub>Ge<sub>24</sub> (tetragonal system), and U<sub>6</sub>Fe<sub>22</sub>Ge<sub>13</sub> (orthorhombic system). Within this section there are also two solid solutions UFe<sub>6+x</sub>Ge<sub>6-x</sub> ( $x < 0.7$ ), which crystallizes in the YCo<sub>6</sub>Ge<sub>6</sub> structure type and U<sub>2</sub>Fe<sub>17-x</sub>Ge<sub>x</sub> (with  $2 < x < 3.7$ ), crystallizing in the Th<sub>2</sub>Ni<sub>17</sub>-type structure [7].

## Introductions to Posters / 38

### High-field metamagnetism in UCo<sub>2</sub>Si<sub>2</sub>

**Author:** Yurii Skourski<sup>1</sup>

**Co-authors:** Alexander Andreev<sup>2</sup>; J Wosnitza<sup>1</sup>

<sup>1</sup> *Hochfeld-Magnetlabor Dresden, FZ Dresden-Rossendorf, D-01314 Dresden, Germany*

<sup>2</sup> *Institute of Physics of Academy of Sciences, Na Slovance 2, 18221 Prague, Czech Republic*

**Corresponding Author:** i.scurschii@fzd.de

UCo<sub>2</sub>Si<sub>2</sub> belongs to a wide group of UT<sub>2</sub>X<sub>2</sub> compounds, where T is a late d metal and X is Si or Ge. They exhibit a large variety of magnetic states starting from antiferromagnetic (AF) ordering for UCr<sub>2</sub>Si<sub>2</sub>, ferrimagnetic (UNi<sub>2</sub>Si<sub>2</sub>) and ferromagnetic (F) structures (UCu<sub>2</sub>Si<sub>2</sub>) through Pauli paramagnets (UFe<sub>2</sub>Si<sub>2</sub>) to compounds, which become superconducting inside an AF state (URu<sub>2</sub>Si<sub>2</sub>) [1-3]. UCo<sub>2</sub>Si<sub>2</sub> has a tetragonal ThCr<sub>2</sub>Si<sub>2</sub> crystal structure and orders AF below T<sub>N</sub> = 83-85 K. The magnetic structure (from powder neutron diffraction) consists of F basal-plane layers of U moments of  $\mu_U = 1.42 \mu_B$  oriented parallel to the c axis, which are coupled in a simple sequence + $\uparrow$ + $\uparrow$  (AF type-I structure) in the same direction [2]. Magnetic moment is carried only by U atoms.

UNi<sub>2</sub>Si<sub>2</sub> exhibits in addition to the AF type I structure, a ferrimagnetic and an incommensurate AF phase. In the ground state, it exhibits ++ $\uparrow$  sequence with longitudinally modulated amplitude of the magnetic moment resulting in a spontaneous moment of  $0.53 \mu_B$ , 1/3 of  $\mu_U$  [4]. The ++ $\uparrow$  phase is also observed at high magnetic fields in UPd<sub>2</sub>Si<sub>2</sub> (with an AF type-I structure in zero field) [5]. It was interesting to check whether UCo<sub>2</sub>Si<sub>2</sub> exhibits this phase at high magnetic fields as well. In this work we indeed observed such transition.

The investigated single crystal was grown by Czochralski method in a tri-arc furnace. The x-ray powder-diffraction analysis confirmed the tetragonal body-centered ThCr<sub>2</sub>Si<sub>2</sub>-type crystal structure with lattice parameters  $a = 392.1$  pm, and  $c = 963.9$  pm in agreement with literature. The x-ray Laue patterns showed the high quality of the crystal. The magnetization curves were measured in pulsed fields up to 60 T applied along the c and a axes using a non-destructive pulsed magnet with pulse duration of 25 ms. The magnetization signal was detected by integrating the voltage induced in a pick-up coil surrounding the sample. The absolute values of the magnetization were calibrated from steady-field measurements up to 14 Tesla.

For the fields applied along the c axis, the metamagnetic transition is observed at the critical field  $\mu_0 H_{cr} = 45$  T (Fig. 1). It is very sharp but has a small hysteresis ( $\mu_0 H_{cr} = 0.16$  T). The analogous transition in UPd<sub>2</sub>Si<sub>2</sub> shows huge hysteresis of more than 15 T [5]. The transition in UCo<sub>2</sub>Si<sub>2</sub> is characterized by a magnetization jump of  $\Delta M = 0.52 \mu_B$ .  $\Delta M$  roughly corresponds to 1/3 of  $\mu_U = 1.42 \mu_B$  [2]. Therefore, we can suppose that the high-field state is ferrimagnetic with the ++ $\uparrow$  arrangement along the c direction. At much higher fields another transition to a fully polarized state can be expected. The magnetization curve measured along the a axis shows no transition and is linear up

to the highest fields. The  $a$ -axis susceptibility of  $3.7 \times 10^{-3}$  B/T per U atom is a typical value for the hard-axis magnetization of U intermetallic compounds independent of crystal structure and type of magnetic ground state and reflects mostly the Pauli paramagnetism of the conduction electrons [1]. The transition for  $H \parallel c$  is still very sharp at 20 K. At higher temperatures, it becomes considerably wider and might lose the first-order character above 80 K (Fig. 2). The transition field  $H_{cr}$  determined as maximum in the derivative  $dM/dH$  (Fig. 3) decreases with increasing temperature. At 80 K the small maximum at 21 T in  $dM/dH$  still indicates the metamagnetic transition.  $M$ ,  $H_{cr}$ , and  $H_{cr}$  decrease monotonously with increasing temperature and vanish at  $T_N$ . In the H-T phase diagram of  $UCo_2Si_2$  in fields applied along the  $c$  axis (Fig. 4), the diamonds correspond to  $T_N(H)$  taken from Ref. 3.

Fig. 1. Magnetization curves measured along the principal axes at 1.4 K. Fig. 2. Magnetization curves measured along the  $c$  axis at different temperatures.

Fig. 3. Field dependence of the differential susceptibility  $dM/dH$  measured along the  $c$  axis at different temperatures.

Fig. 4. Temperature dependence of the magnetization gain  $M$  at the transition, the width of hysteresis  $H_{cr}$  and H-T phase diagram of  $UCo_2Si_2$  in fields applied along the  $c$  axis.

This work is a part of the research program AVOZ 10100520 financed by the Academy of Sciences of the Czech Republic and was supported by grant 202/09/0339 of Czech Science Foundation and by EuroMagNET under the EU contract 228043.

#### References

- [1] V. Sechovský and L. Havela, in Handbook of Magnetic Materials, edited by K.H.J. Buschow (North Holland, Amsterdam, 1998), Vol. 11, p. 1 and references therein.
- [2] L. Chelmicki et al., J. Phys. Chem. Solids 46 (1985) 529.
- [3] M. Mihalik et al., J. Phys. Soc. Japan 76 (2007) 54.
- [4] L. Rebelsky et al., Physica B 180-181 (1992) 43.
- [5] T. Honma et al., J. Phys. Soc. Japan 67 (1998) 1017.

#### Introductions to Posters / 39

## Crystallographic study of new phases from the U–Zn–Al ternary system

**Author:** Yuriy Verbovyskyy<sup>1</sup>

<sup>1</sup> *Instituto Tecnológico e Nuclear*

**Corresponding Author:** yuryvv@bigmir.net

Crystallographic study of new phases from the U–Zn–Al ternary system

Yu.V. Verbovyskyy, A.P. Gonçalves

Departamento de Química, Instituto Tecnológico e Nuclear/CFMC–UL, 2863–953 Sacavém, Portugal  
yuryvv@bigmir.net

Uranium based intermetallic compounds have been intensively studied due to their unusual ground states and behaviours (as intermediate valence states, heavy fermion behaviours, unconventional superconductivity, etc.). The binary U–Zn system is characterised by the existence of two compounds,  $UZn_{12-x}$  (high-temperature form of  $SmZn_{12}$ ) and  $U_2Zn_{17}$  (crystallizing in two polymorphic modifications, with  $Th_2Zn_{17}$  and  $Th_2Ni_{17}$  structure types, respectively), which show coexistence of magnetism and heavy fermion behaviour [1,2]. Albeit this, the study of U–Zn–X (X = p element) ternary systems is still scarce. This work is a part of our systematic investigation of uranium – d- and p-metal alloy systems and consists on the exploration of the U–Zn–Al phase diagram and identification of the ternary compounds and solubility ranges.

The samples were synthesized at 950°C from the pure elements, inside quartz ampoules under vacuum. No reaction with the quartz ampoules was observed. The obtained products were characterized by using X-ray powder diffraction techniques. Needle-shape high quality crystals were selected

from crushed samples with nominal  $\text{U}_{10}\text{Zn}_{60}\text{Al}_{30}$  composition and used in the X-ray diffraction measurements. The experiments were made at room temperature by using a four-circle Nonius CAD4 diffractometer with graphite monochromatized  $\text{Mo K}\alpha$ -radiation and a scintillation counter with pulse height discrimination. Scans were taken in the  $\omega/2\theta$  mode. Empirical absorption corrections were applied on the basis of  $\Psi$ -scan data. The crystal structure was refined using Shelxl-97 [3] (full-matrix least-squares on F2). The unit cell parameters were obtained by least-squares refinement of the  $2\theta$  values of 25 intense and well-centered reflections from various parts of the reciprocal space ( $16^\circ < 2\theta < 36^\circ$ ).

The X-ray powder diffraction data of the as-prepared  $\text{U}_{10}\text{Zn}_{60}\text{Al}_{30}$  sample shows the presence of three phases:  $\text{Zn}_{1-x}\text{Al}_x$  (Mg-type), binary  $\text{UAl}_3$  (AuCu<sub>3</sub>-type) and hexagonal phase  $\text{U}_x(\text{Zn}_{1-y}\text{Al}_y)_z$ , with cell dimensional:  $a = 9.047(1) \text{ \AA}$ ,  $c = 8.858(1) \text{ \AA}$ ,  $V = 627.9(1) \text{ \AA}^3$ . The cell dimensions fitting, from the 25 reflections and performed for several single crystals, gave always similar results:  $a \sim 9.03 \text{ \AA}$ ,  $c \sim 8.82 \text{ \AA}$ ,  $V \sim 622 \text{ \AA}^3$ . After testing various models for well-known structures of binary R-Zn and ternary R-Zn-X compounds (R = rare earth), our attention was stopped on the high-temperature form of  $\text{SmZn}_{12}$  type structure (space group P6/mmm). In a first stage this structure type was adopted in the  $\text{U}_x(\text{Zn}_{1-y}\text{Al}_y)_z$  structural refinement from the single crystal X-ray diffraction data and residuals  $R_1 = 0.0642$ ,  $R_w = 0.1154$  (405 F2 values, 41 variables) were obtained. The composition of this hexagonal phase was also refined, being obtained  $\text{U}_{1.12}\text{Zn}_{9.51}\text{Al}_{1.71}$  ( $=\text{U}_9\text{Zn}_{77}\text{Al}_{14}$ ). However, quite high residual factors still remain, which could indicate that the structure of the above mentioned phase was not exactly of the  $\text{SmZn}_{12}$  type, but some derived from it. In a second step direct methods were used and the  $\text{U}_x(\text{Zn}_{1-y}\text{Al}_y)_z$  crystal structure was determined and refined.

#### Acknowledgments

This work was partially supported by FCT, Portugal, under the contract No. PTDC/QUI/65369/2006 and No. SFRH/BPD/34840/2007.

#### References

- [1] P. Chiotti and J.T. Mason. *J. Less-Common Metals* 40 (1975) 39.
- [2] H.R. Ott, H. Rudigier, P. Delsing and Z. Fisk. *Phys. Rev. Lett.* 52 (1984) 1551.
- [3] G.M. Sheldrick. *SHELX97- A Program Package for the Solution and Refinement of Crystal Structures* Universität Göttingen, Germany, 1997.

## Strongly Correlated Systems II / 40

### Magnetic ordering in the heavy-fermion compound $\text{UZn}_{12}$

**Author:** António Pereira Gonçalves<sup>1</sup>

<sup>1</sup> *Instituto Tecnológico e Nuclear*

**Corresponding Author:** [apg@itn.pt](mailto:apg@itn.pt)

Magnetic ordering in the heavy-fermion compound  $\text{UZn}_{12}$

A.P. Gonçalves<sup>1,\*</sup>, D. Gnida<sup>2</sup>, P. Estrela<sup>3,4</sup>, A. de Visser<sup>4</sup>, E.B. Lopes<sup>1</sup>, I. Catarino<sup>5</sup>, G. Bonfait<sup>5</sup>, M. Godinho<sup>6</sup>, M. Almeida<sup>1</sup>, D. Kaczorowski<sup>2</sup>

<sup>1</sup> Dep. Química, Instituto Tecnológico e Nuclear, P-2686-953 Sacavém, Portugal.

<sup>2</sup> Institute of Low Temperature and Structure Research, Polish Academy of Sciences, P.O.Box 1410, 50-950 Wrocław, Poland

<sup>3</sup> Dep. Electronic & Electrical Engineering, University of Bath, Bath, BA2 7AY, UK

<sup>4</sup> Van der Waals-Zeeman Institute, Univ. Amsterdam, Valckenierstraat 65, 1018 XE Amsterdam, The Netherlands.

<sup>5</sup> Dep. Física, FCT-UNL, 2829-516 Monte da Caparica, Portugal.

<sup>6</sup> Dep. Física, FC-UL, Campo Grande ed. C1, P-1749-016 Lisboa, Portugal.

U-based intermetallic compounds continue attracting much attention due to a wide spectrum of their unusual physical properties. Some of them belong to the class of the so-called heavy-fermion systems, and a few of these systems order magnetically at low temperatures, usually with antiferromagnetic structures.

The binary U-Zn phase diagram contains two intermetallic compounds, U<sub>2</sub>Zn<sub>17</sub> and UZn<sub>12</sub>. The low temperature polymorph of U<sub>2</sub>Zn<sub>17</sub> (Th<sub>2</sub>Zn<sub>17</sub>-type) has been deeply studied. The compound shows antiferromagnetic ordering below  $T_N = 9.8$  K, with a sizeable magnetic anisotropy both in the antiferromagnetic and paramagnetic regions [1]. Its Sommerfeld coefficient is equal to 535 mJ/(mol K<sup>2</sup>) [2], indicating a heavy-fermion character of the electronic ground state. The other phase, UZn<sub>12</sub>, crystallizes in the hexagonal high-temperature form of SmZn<sub>12</sub> (P6/mmm) [3]. Single-crystal X-ray data revealed some disorder in the crystal lattice, which leads to compositions deficient in zinc, ranging from UZn<sub>9.4</sub> to UZn<sub>11.5</sub> [4]. Specific heat measurements, performed on polycrystalline samples, revealed a heavy-fermion behaviour of this compound, with  $\gamma(0) = 850\text{--}900$  mJ/(mol K<sup>2</sup>) [5,6]. Neither magnetic nor superconducting phase transitions were observed down to 0.4 K [5,6].

The present work reports on the growth of UZn<sub>12</sub> single crystals, and their study by means of X-ray diffraction, magnetisation, specific heat, and electrical resistivity measurements. These experiments have been supplemented by muon spin relaxation spectroscopy, carried out on polycrystalline sample from the same batch.

Single crystals of UZn<sub>12</sub> with typical dimensions 1.5x1.5x0.2 mm<sup>3</sup> were grown by the high-temperature solution growth method, using zinc as solvent. Single crystal X-ray diffraction studies confirmed the SmZn<sub>12</sub>-type structure with the refined composition U<sub>1.01(1)</sub>Zn<sub>11.7(1)</sub> that is much closer to the ideal one than those reported in the literature [4]. The U atoms are mainly located at the 1a and 2d sites, with the U-U shortest distances (2d-2d) of  $\sim 5.164$  Å. However,  $\sim 4\%$  of the U atoms were also found at the 2c site due to a partial substitution of the 4h Zn pairs.

At odds with the literature data [5,6], bulk magnetization measurements of single-crystalline UZn<sub>12</sub> revealed an antiferromagnetic-type anomaly at 5.0(2) K. This singularity was observed for both characteristic directions in the hexagonal unit cell, but its magnitude was much less pronounced for B || c-axis, hence suggesting that the magnetic moments are confined within the a-b plane. The presence of long-range magnetic order below 5 K was confirmed by muon spin relaxation experiments.

The specific heat of UZn<sub>12</sub> measured in zero magnetic field exhibits a clear  $\lambda$ -type anomaly near  $T_N = 5$  K. Upon applying magnetic fields, directed with the a-b plane, the peak in C(T) shifts to lower temperatures, as expected for antiferromagnets. From the analysis of the specific heat data between 8 and 13 K, the electronic specific heat coefficient  $\gamma_p \approx 340$  mJ/(mol K<sup>2</sup>) is obtained. From the data measured below 3.7 K, the  $\gamma(0)$  value as large as 800 mJ/(mol K<sup>2</sup>) can be derived. The strongly enhanced electronic contribution to the specific heat corroborates the previously formulated hypothesis [5,6] that UZn<sub>12</sub> can be classified as a heavy-fermion system.

The heavy-fermion character of UZn<sub>12</sub> manifests clearly in the overall shape of temperature-dependent electrical resistivity that is dominated by a single-ion Kondo effect at high temperatures and coherent Kondo scattering at low temperatures. From room temperature down to about 150 K, the resistivity changes with temperature in a logarithmic manner. At about 15 K, a maximum in  $\rho(T)$  is seen, which marks a crossover from incoherent to coherent Kondo regime. Below this temperature the resistivity decreases with decreasing temperature down to about 80  $\mu\Omega\text{cm}$  at 2 K. This rather large value indicates significant residual scattering, mainly caused by the inherent atomic disorder, evidenced in the X-ray studies, but probably also due to significant disorder in the spin system that persists down to the lowest temperatures. Remarkably hardly any singularity in  $\rho(T)$  occurs at the antiferromagnetic phase transition at  $T_N = 5$  K. It seems likely that the expected change at  $T_N$  in the magnetic contribution to the resistivity is obscured by the much more effective scattering conduction electrons on structural and magnetic defects.

In conclusion, UZn<sub>12</sub> is a heavy-fermion system with antiferromagnetic ordering below 5 K. The obtained results point to a fundamental role of structural disorder on the onset of magnetism in this compound.

#### Acknowledgments

This work was partially supported by the Executive Programme of Scientific and Technological Cooperation between Portugal and Poland, for the years 2009-2010, and by FCT, Portugal, under the contract nr. PTDC/QUI/65369/2006.

#### References

- 1- J.O. Willis, Z. Fisk, R.M. Aikin, M.W. McElfresh, J.D. Thompson, E. Zirngiebl, J.A. O'Rourke, J.L. Smith, J. Appl. Phys., 61 (1987) 4373.
- 2- H.R. Ott, H. Rudigier, P. Delsing, Z. Fisk, Phys. Rev. Lett., 52 (1984) 1551.
- 3- J.T. Mason, P. Chiotti, Acta Cryst. B27 (1971) 1789.

- 4- P. Chiotti, J.T. Mason, J. Less-Common Metals 40 (1975) 39  
 5- Y. Nakazawa, M. Ishikawa, S. Noguchi and K. Okuda, Physica B 186-188 (1993) 711.  
 6- Y. Nakazawa, M. Ishikawa, S. Noguchi and K. Okuda, J. Phys. Soc. Jpn. 62 (1993) 3003.

## Introductions to Posters / 41

### Considerations on the U-Fe-B ternary system

**Author:** António Pereira Gonçalves<sup>1</sup>

<sup>1</sup> *Instituto Tecnológico e Nuclear*

**Corresponding Author:** apg@itn.pt

Considerations on the U-Fe-B ternary system

M. Dias<sup>1,2</sup>, I.C. Santos<sup>1</sup>, P.A. Carvalho<sup>2</sup>, M.Bohn<sup>3</sup>, O. Tougait<sup>4</sup>,  
 H. Noël<sup>4</sup>, A.P. Gonçalves<sup>1</sup>

1Dep. Química, Instituto Tecnológico e Nuclear/CFMC-UL, P-2686-953 Sacavém, Portugal  
 2Dep. Eng. Materiais, Instituto Superior Técnico, Av Rovisco Pais, 1049-001 Lisboa, Portugal  
 3Departement DRO/Geosciences Marines, Ifremer Centre de Brest, B.P. 70-29280 Plouzane, France  
 4Laboratoire de Chimie du Solide et Inorganique Moléculaire, UMR CNRS 6511, Université de Rennes  
 1, Avenue de Général Leclerc, 35042 Rennes, France

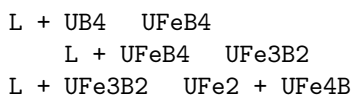
Uranium based intermetallic compounds frequently show unusual ground states and behaviours, such as unconventional superconductivity, coexistence of magnetic order and superconductivity, heavy fermion behaviour, etc. Ternary intermetallic borides of AM<sub>x</sub>B<sub>y</sub> type (A = actinide or rare earth; M = d-transition metal) have also attracted considerable interest due to their large diversity of physical characteristics, which extend from permanent magnetism with high coercive fields (like in SmCo<sub>4</sub>B) to unconventional magnetic ordering (as seen in UNi<sub>4</sub>B). However, the study of the U-Fe-B ternary phase diagram was far from being complete. Partial results on the isothermal section at 800°C for this system were first reported, with the identification of two compounds, UFe<sub>4</sub>B and UFe<sub>3</sub>B<sub>2</sub> [1,2]. In this contribution we will present an overview of our recent work on the U-Fe-B ternary system, including the study of its isothermal section at 950°C, the liquidus projection and selected vertical section.

Over 70 alloys, with general xU:yFe:zB compositions, were prepared by arc-melting the desired amounts of the elements, the melting process being repeated at least three times in order to ensure homogeneity. No losses higher than 1 wt.% were observed. The high cooling rate of the solidification process enabled to follow the solidification path of the alloys under non-equilibrium conditions. Subsequent heat treatments at 950 °C allowed inferring the transitions leading to equilibrium. The as-cast and annealed alloys were characterized by powder X-ray diffraction (PXRD), scanning electron microscopy (SEM), complemented with Energy Dispersive Spectroscopy (EDS), electron microprobe micro-analysis (EPMA), differential thermal analysis (DTA) and Electron Backscatter Diffraction (EBSD). Single crystal X-ray diffraction studies were also performed for some of the ternary compounds.

The U-Fe-B ternary system is considerably richer than what was reported before. A total of five ternary compounds were identified at 950°C: in addition to the previously reported UFe<sub>4</sub>B and UFe<sub>3</sub>B<sub>2</sub>, three new compounds, UFe<sub>4</sub>B, U<sub>2</sub>Fe<sub>21</sub>B<sub>6</sub> and UFe<sub>2</sub>B<sub>6</sub> were found to be stable at this temperature. However, all these ternary compounds are formed by peritectic reactions, being difficult to obtain as single phase samples. Moreover, only for the UFe<sub>4</sub>B, UFe<sub>3</sub>B<sub>2</sub> and UFe<sub>2</sub>B<sub>6</sub> compounds it was possible to get small single crystals suitable for X-ray diffraction studies. They have confirmed that UFe<sub>4</sub>B and UFe<sub>3</sub>B<sub>2</sub> crystallize in the YCr<sub>4</sub>B<sub>4</sub> and CeCo<sub>3</sub>B<sub>2</sub> -type structures, respectively, and indicated that UFe<sub>2</sub>B<sub>6</sub> is isostructural with the CeCr<sub>2</sub>B<sub>6</sub>-type [3]. Moreover, in the case of the UFe<sub>4</sub>B compound it was found a cooperative (concomittant ?) growth of the YCr<sub>4</sub>B<sub>4</sub> and ThMo<sub>4</sub>B<sub>4</sub> type structures. For the other compounds, only PXRD measurements could be done, which indicate that UFe<sub>4</sub>B crystallizes in a structure type related to the CeCo<sub>4</sub>B-type and that U<sub>2</sub>Fe<sub>21</sub>B<sub>6</sub> most probably crystallizes in the Cr<sub>23</sub>C<sub>6</sub>-type. In order to get more information on the crystal structures of these

last two compounds, EBSD studies were performed. They show that U<sub>2</sub>Fe<sub>21</sub>B<sub>6</sub> really crystallizes in the Cr<sub>23</sub>C<sub>6</sub>-type structure and that the pattern of UFe<sub>4</sub>B is better explained by the Lu<sub>5</sub>Ni<sub>19</sub>B<sub>6</sub>-type simulation.

A cascade of peritectic reactions was found to exist along the U:(Fe,B)=1:5 line [4]:



The solidification paths show that the formation temperatures of the compounds decrease in the above order. Solidification ends with the ternary eutectic of UFe<sub>2</sub> + UFe<sub>4</sub>B +  $\alpha$ -Fe at 980 °C. The liquidus surface of the U-Fe-B ternary system is complex, with the presence of at least eighteen invariant points. The UFe<sub>4</sub>B and UFe<sub>3</sub>B<sub>2</sub> have large primary crystallization surfaces, but for the other three compounds they are small and are far from their nominal composition. All this information represents fundamental knowledge for the synthesis of pure compounds, necessary for the physical properties characterization.

#### Acknowledgments

This work was partially supported by FCT, Portugal, under the contract No. PTDC/QUI/65369/2006 and by the exchange Program FCT/CNRS 2009-2010.

#### References

- [1] Valyovka, I.P., Kuzma, Yu.B., New uranium borides with the structure of YCrB<sub>4</sub> type, Dop. Akad. Nauk Ukr. RSR, A: Fiz.-Tekhn. Mat. Nauki (1975) p-652.
- [2] Valyovka, I.P., Kuzma, Yu.B., New ternary borides with structures of CeCo<sub>3</sub>B<sub>2</sub> and CeCo<sub>4</sub>B type, Dop. Akad. Nauk Ukr. RSR, A: Fiz.-Tekhn. Mat. Nauki (1974) p-1029.
- [3] Dias, M., Carvalho, P.A., Pereira, L.C.J., Santos, I.C., Gonçalves, A.P., Studies on the new UFe<sub>2</sub>B<sub>6</sub> phase, J. Alloys Compd., in press.
- [4] Dias, M., Carvalho, P.A., Dias, A.P., Bohn, M., Franco, N., Tougait, O., Noël, H., Gonçalves, A.P., Cascade of peritectic reactions in the B-Fe-U system, J. Phase Equilib. Diff., in press.

## Introductions to Posters / 42

### Long-term behavior of thorium-plutonium phosphate-diphosphate solid solutions

**Author:** NICOLAS DACHEUX<sup>1</sup>

**Co-authors:** CLAIRE TAMAIN<sup>2</sup>; JEAN-CHRISTOPHE GRIVEAU<sup>3</sup>; NICOLAS CLAVIER<sup>1</sup>; THIERRY WISS<sup>3</sup>

<sup>1</sup> ICSM/LIME

<sup>2</sup> IPNO

<sup>3</sup> EC-JRC-ITU

Considering several properties of interest, Thorium Phosphate-Diphosphate Th<sub>4</sub>P<sub>6</sub>O<sub>23</sub> (namely beta-TPD) was considered as a promising matrix for the specific immobilization of actinides. Among its interesting properties, one can note its capability to form solid solutions with high actinides mole loadings, its good sintering capability and its high resistance to aqueous corrosion or to radiation damages. Since water is the main vector for radionuclide migration from a deep disposal repository, the long-term behavior of beta-TPD and associated solid solutions with tetravalent plutonium was examined. The evolution of raw and leached Th<sub>4</sub>-xPuxP<sub>6</sub>O<sub>23</sub> samples were examined for several years in order to show the effects of internal irradiation on the beta-TPD crystal structure and on the physico-chemical properties of interest such as the chemical durability of the samples.

## Strongly Correlated Systems I / 43



## Electrical transport properties of single crystalline U<sub>2</sub>Cu<sub>4</sub>As<sub>5</sub>

**Author:** Daniel Gnida<sup>1</sup>

<sup>1</sup> *Institute of Low Temperature and Structure Research, Polish Academy of Sciences*

**Corresponding Author:** d.gnida@int.pan.wroc.pl

The ternary uranium arsenide U<sub>2</sub>Cu<sub>4</sub>As<sub>5</sub> crystallizes with a body-centred tetragonal structure of its own type (space group I4/mmm, lattice parameters: a = 3.990 Å, b = 24.299 Å) [1]. Magnetic susceptibility measurements revealed that the compound orders antiferromagnetically at TN = 189 K [1]. The onset of the ordered state is accompanied by a rapid drop in the electrical resistivity [1]. Here, we report on the results of our recent specific heat, electrical resistivity, magnetoresistivity and Hall coefficient measurements, performed in wide ranges of temperature and magnetic field on high-quality single crystals of U<sub>2</sub>Cu<sub>4</sub>As<sub>5</sub> grown by chemical vapour transport method.

**Strongly Correlated Systems I / 44**

## Ferromagnetic ordering in novel ternary germanides: URu<sub>1-x</sub>Ge<sub>2</sub> and U<sub>34</sub>Ru<sub>4-x</sub>Ge<sub>33</sub>

**Author:** Mathieu Pasturel<sup>1</sup>

**Co-authors:** Adam Pikul<sup>2</sup>; Dariusz Kaczorowski<sup>2</sup>; Henri Noël<sup>3</sup>; Olivier Tougait<sup>3</sup>

<sup>1</sup> *Sciences Chimiques de Rennes*

<sup>2</sup> *INTiBS-PAN*

<sup>3</sup> *SCR/CSM*

**Corresponding Author:** mathieu.pasturel@univ-rennes1.fr

Several binary or ternary uranium based germanides have been reported to exhibit superconductivity at low temperatures, that emerges either from paramagnetic state (e.g. U<sub>7</sub>Ge, U<sub>5</sub>Ge<sub>3</sub> [1]) or from ferromagnetically ordered state, in ambient pressure conditions (e.g. URhGe [2], UCoGe [3]) or under applied hydrostatic pressure (e.g. UGe<sub>2</sub> [4]). In the search for other germanides with interesting physical properties, we have recently focused on the ternary system U-Ru-Ge. So far, crystal structures and physical properties of four phases from this system have been reported, namely for: U<sub>4</sub>Ru<sub>7</sub>Ge<sub>6</sub> [5], U<sub>3</sub>Ru<sub>4</sub>Ge<sub>13</sub> [6], URuGe [7] and U<sub>2</sub>Ru<sub>3</sub>Ge [8].

In the present contribution we report on our discovery of two novel compounds: URu<sub>1-x</sub>Ge<sub>2</sub> and U<sub>34</sub>Ru<sub>4-x</sub>Ge<sub>33</sub>. The crystal structures of both phases have been determined by means of single crystal X-ray diffraction. The former phase crystallizes with a monoclinic unit cell of lattice parameters a = 4.098(1) Å, b = 15.936(2) Å, c = 4.045(1) Å and β = 90.09(1)°, which is a derivative of the orthorhombic CeNi<sub>1-x</sub>Si<sub>2</sub> type structure. The other compound adopts a tetragonal structure of the U<sub>34</sub>Fe<sub>4-x</sub>Ge<sub>33</sub> type [a = 10.8933(1) Å and c = 25.3401(3) Å], which may be derived from the binary USi-type unit cell.

The physical properties of both compounds have been studied by means of dc- and ac-magnetization, electrical resistivity and specific heat measurements. Both germanides have been found to order ferromagnetically at T<sub>c</sub> = 62(1) K and 38.5(5) K, for URu<sub>1-x</sub>Ge<sub>2</sub> and U<sub>34</sub>Fe<sub>4-x</sub>Ge<sub>33</sub>, respectively. The obtained results will be comprehensively discussed at the conference with respect to some characteristic structural features, and in comparison to the physical properties of related compounds.

### References

- [1] Y. Onuki et al., J. Phys. Soc. Jpn., 61, 293 (1992).
- [2] D. Aoki et al., Nature, 413, 613 (2001).
- [3] N.T. Huy et al., Phys. Rev. Lett., 99, 067006 (2007).
- [4] S.S. Saxena et al., Nature, 406, 587 (2000).
- [5] B. Lloret et al., J. Magn. Magn. Mater., 67, 232 (1987).
- [6] B. Lloret et al., J. Phys., 49 C8, 487 (1988).

[7] R. Troc et al., J. Magn. Mater., 73, 389 (1988).

[8] A. Vernière et al., J. Alloys Compd., 209, 251 (1994).

WAT-II / 45

## Synthesis and first tests at CERN-ISOLDE of UCx targets produced with carbon nanotubes

**Authors:** Lisa Biasetto<sup>1</sup>; Thierry Stora<sup>2</sup>

**Co-authors:** Gianfranco Prete<sup>3</sup>; Matia Manzolaro<sup>3</sup>; Pier-Luigi Zanonato<sup>4</sup>; Richard Catherall<sup>2</sup>; S Carturan<sup>3</sup>; alberto Andrighetto<sup>3</sup>

<sup>1</sup> LNL-INFN & University of Padova

<sup>2</sup> CERN

<sup>3</sup> LNL-INFN

<sup>4</sup> University of Padova

**Corresponding Author:** thierry.stora@cern.ch

The first online mass separated isotope (ISOL) beam was produced 60 years ago at the Niels Bohr Institute in Copenhagen. Krypton beams were obtained by fission reactions in a large and heated UO<sub>2</sub> target positioned at proximity of a neutron converter [1]. Since then a large variety of other targets and primary drivers have been developed and used in several facilities throughout the world. At CERN-ISOLDE for example, actinide targets (ThnatCx, ThnatO<sub>2</sub>, UdepCx with diverse microstructures) have been developed for over thirty years and represent today more than 60% delivered beam time.

We report here the synthesis and first online tests of UCx targets made by carbothermic reduction of UO<sub>2</sub> powders pressed with carbon nanotubes. This program took place within the SPES project and EURISOL-DS, in which carbide target materials are developed to meet the stringent requirements of both facilities in terms of mechanical, heat and isotope production characteristics [2,3]. The resulting material is compared with the standard ISOLDE UCx production target. We will provide in particular some details on the synthesis, properties and first radioactive ion beam yields obtained with these new targets.

Fig. 1. Left: SEM picture of UCx synthesized for SPES and compared to standard ISOLDE UCx target  
Right : UCx target pellet synthesized with carbon nanotubes

### References

[1] O. Kofoed-Hansen, K.O. Nielsen, Kgl. Danske Videnskab. Selskab, Mat.-fys. Medd., 26(7), (1951).

[2] A. Andrighetto, S. Cevolani, C. Petrovich, M. Santana, Eur. Phys J. A 30, (2006) 591.

[3] Final Report of the EURISOL Design Study, J. C. Cornell Ed., Nov. 2009 and references therein.

Strongly Correlated Systems I / 46

## Low temperature properties of AnFe<sub>2</sub>Si<sub>2</sub> systems (An = Th, Np, Pu)

**Author:** jean-christophe griveau<sup>1</sup>

**Co-authors:** Daniel Bouexiere<sup>2</sup>; Dariusz Kaczorowski<sup>3</sup>; Franck Wastin<sup>2</sup>; Jean Rebizant<sup>4</sup>; Jiri Prchal<sup>5</sup>; Krzysztof Gofryk<sup>6</sup>; Ladia Havela<sup>5</sup>; Rachel Eloirdi<sup>2</sup>; Régis Jardin<sup>2</sup>; Éric Colineau<sup>2</sup>

<sup>1</sup> ITU JRC EC

<sup>2</sup> *European Commission, Joint Research Centre, Institute for Transuranium Elements, Postfach 2340, Karlsruhe 76125, Germany*

<sup>3</sup> *Institute of Low Temperature and Structure Research, Polish Academy of Sciences, P. O. Box 1410, 50-950 Wrocław 2, Poland*

<sup>4</sup> *European Commission, Joint Research*

<sup>5</sup> *Charles University, Faculty of Mathematics and Physics, Department of Condensed Matter Physics, Ke Karlovu 5, 121 16 Prague 2, The Czech Republic*

<sup>6</sup> *Los Alamos National Laboratory, P.O. Box 1663, MS K764, Los Alamos, NM 87545, USA*

**Corresponding Author:** jean-christophe.griveau@ec.europa.eu

The ThCr<sub>2</sub>Si<sub>2</sub> (body centered I/4mmm) structure has long been typical of systems presenting striking physical properties. Two compounds presenting this structure, namely CeCu<sub>2</sub>Si<sub>2</sub>[1] and URu<sub>2</sub>Si<sub>2</sub>[2] are unconventional superconductors, and the nature of the coupling mechanism is still under debate 30 years after their discovery. Here we have focused on Transuranium systems (TU) with this structure and selected compounds with Fe as transition metal. The interplay between the hybridization and magnetism of 3d electrons from Fe and the 5f electrons from Actinides is in the background of exotic phenomena.

Low temperature properties have been examined (or re-examined) for ThFe<sub>2</sub>Si<sub>2</sub>, NpFe<sub>2</sub>Si<sub>2</sub> and PuFe<sub>2</sub>Si<sub>2</sub>. Polycrystals of each system have been produced by arc melting stoichiometric amounts of the pure metals components in argon atmosphere. X-ray-diffraction patterns were collected indicating that ThFe<sub>2</sub>Si<sub>2</sub> and NpFe<sub>2</sub>Si<sub>2</sub> samples are single phase, while PuFe<sub>2</sub>Si<sub>2</sub> presents a small amount (<5%) of an extra phase. All the majority phases present the ThCr<sub>2</sub>Si<sub>2</sub> structure and the lattice parameters are very close to those previously reported in literature.

Magnetization has been performed in a MPMS-7 down to 2 K and in magnetic fields up to 7 T. Previous studies indicated that ThFe<sub>2</sub>Si<sub>2</sub> and PuFe<sub>2</sub>Si<sub>2</sub>, order antiferromagnetically (TN ~ 100 K) [3] and ferromagnetically (TC ~ 35 K) [4], respectively. Starting from very pure thorium metal for the preparation of ThFe<sub>2</sub>Si<sub>2</sub> and after a thermal treatment for PuFe<sub>2</sub>Si<sub>2</sub>, it appears that both are actually paramagnetic. Nevertheless, we confirm the occurrence of antiferromagnetism in NpFe<sub>2</sub>Si<sub>2</sub> as previously reported [5], but we determine a Néel temperature TN=90 K slightly higher than the reported value (TN ~ 87 K).

Low temperature specific heat measurements under magnetic fields have been performed in a PPMS-9 down to 1.9 K and up to 9 T. No hint of magnetic order has been observed neither in ThFe<sub>2</sub>Si<sub>2</sub> nor PuFe<sub>2</sub>Si<sub>2</sub> in agreement with our magnetic studies. In the case of NpFe<sub>2</sub>Si<sub>2</sub> a clear peak is visible at TN (Fig. 1). This peak presents a shoulder that may be reminiscent of a possible double magnetic transition. This feature has not been reported before [5,6]. In addition, the specific heat of ThFe<sub>2</sub>Si<sub>2</sub> has been used to estimate the phonon contribution in NpFe<sub>2</sub>Si<sub>2</sub>.

Transport properties measurements ( $\rho$ ,  $d\rho/\rho$ ,  $S$ ) down to 1.8 K have been performed also for NpFe<sub>2</sub>Si<sub>2</sub> and PuFe<sub>2</sub>Si<sub>2</sub>. Electrical resistivity measurements confirm the presence of a clear magnetic transition at 93 K for NpFe<sub>2</sub>Si<sub>2</sub> while no signature of any magnetic transition is noticeable in PuFe<sub>2</sub>Si<sub>2</sub>. The thermo power of NpFe<sub>2</sub>Si<sub>2</sub> is relatively small (~2 mV/K) at room temperature, suggesting a rather localized character of the 5f electrons and it also reverses its sign in the vicinity of TN. This indicates a large impact of the magnetic ordering on the Fermi surface and its possible reconstruction below TN.

Finally, we performed high pressure resistivity measurements on NpFe<sub>2</sub>Si<sub>2</sub> up to 12 GPa. We observed an increase of the Néel temperature up to 130 K. This relatively strong increase indicates that the magnetic order is dominated by antiferromagnetic Np-Np interactions already suggested for this system by Mossbauer studies [5].

## Introductions to Posters / 47

# Techniques elaborated for the R&D on fission targets for SPIRAL2

**Author:** Botoum Hy<sup>1</sup>

**Co-authors:** Ahmet Özgümüş<sup>1</sup>; Brigitte Roussière<sup>1</sup>; Christophe Lau<sup>1</sup>; Evelyne Cottureau<sup>1</sup>; Henri Noël<sup>2</sup>; Maher Cheikh Mhamed<sup>1</sup>; Mathieu Pasturel<sup>2</sup>; Michel Potel<sup>2</sup>; Nicole Barré-Boscher<sup>1</sup>; Olivier Tougait<sup>2</sup>; Saïd Essabaa<sup>1</sup>

<sup>1</sup> IPN Orsay

<sup>2</sup> *Sciences Chimiques de Rennes*

**Corresponding Author:** hy@ipno.in2p3.fr

The SPIRAL2 fission target must fulfill restrictive specifications to ensure an efficient production of neutron-rich isotope beams. The realization of such a target requires a thorough program to develop the appropriate uranium carbide (UCx) material. In particular, the material should provide a high fission yield and allow a fast release of the fissions products. These requirements can only be reached by finding an optimization between the material density and its porosity.

A R&D program has been set up at IPNO and Sciences Chimiques de Rennes to elaborate techniques of synthesis and characterization. First, three different processes for the UCx material synthesis have been selected for investigation: the carbothermal reduction of uranium oxide mixed with graphite [1-3], the carbothermal reduction of uranium oxalate [4-5] and the direct melting of a mixture of metallic uranium and graphite by electrical arc [6].

Each of the three processes requires careful techniques to manufacture and to check the product at the various stages.

To determine the process which best suits the specifications, we first have to understand how the different parameters of the synthesis process affect the material. For this purpose, we are carrying out systematic characterization measurements on the samples: determination of the material composition, measurement of density and porosity, evaluation of grain sizes and measurement of the pore size distribution.

The implementation of the different synthesis processes of the UCx material and the measuring devices for the material characterization will be described in details.

Abstract submitted for a poster presentation.

## Materials I / 48

### Study on the U-Co-Ge ternary system at 973K

**Author:** Arnaud Soudé<sup>1</sup>

**Co-authors:** Dariusz Kaczorowski <sup>2</sup>; Henri Noël <sup>1</sup>; Mathieu Pasturel <sup>1</sup>; Olivier Tougait <sup>1</sup>

<sup>1</sup> *Université Rennes 1*

<sup>2</sup> *INTiBS*

**Corresponding Author:** arnaud.soude@univ-rennes1.fr

The recent discovery of the coexistence of ferromagnetic order and pressure induced superconductivity in UCoGe [1] has boosted up explorative investigations on the crystal-chemistry and low-temperature physical properties of novel intermetallic phases in the U-Co-Ge ternary system. These efforts resulted in the characterization of six intermediate phases, which have hitherto been reported in the literature, namely: UCoGe [2], UCo<sub>2</sub>Ge<sub>2</sub> [3], UCo<sub>6</sub>Ge<sub>6</sub> [4], U<sub>3</sub>Co<sub>2</sub>Ge<sub>7</sub> [5], U<sub>3</sub>Co<sub>4</sub>Ge<sub>7</sub> [6] and U<sub>2</sub>Co<sub>17</sub>yGey with  $1.3 \leq y \leq 3$  [7].

Our systematic study on the U-Co-Ge system was carried out in the whole concentration range of the ternary phase diagram. The syntheses were performed by melting appropriate amounts of the elements in an arc furnace under high-purity argon atmosphere. The samples were annealed at 973 K for 3 weeks in sealed silica tubes, followed by air quenching down to room temperature. The products were characterized by powder X ray diffraction. The microstructure and the chemical compositions were studied on polished surfaces using a scanning electron microscope coupled with an energy dispersive spectrometer (SEM-EDS). The crystal structures were determined from single crystal X-ray diffraction data. DC magnetic measurements were carried out using a SQUID magnetometer. The electrical resistivity was measured employing a standard DC four-point technique.

The assessment of U-Co-Ge isothermal section at 973 K confirmed the formation of the previously reported compounds. However, the crystal structure of UCo<sub>6</sub>Ge<sub>6</sub> was found different from that reported in the literature. In addition, our study revealed the existence of as many as twelve novel

compounds:  $\text{UCo}_3\text{yGe}_y$  with  $0.2 \leq y \leq 0.4$ ,  $\text{UCo}_{4.5}\text{Ge}_{0.5}$ ,  $\text{U}_2\text{Co}_3\text{Ge}$ ,  $\text{U}_3\text{Co}_6\text{Ge}_2$ ,  $\text{U}_3\text{Co}_{12}\text{xGe}_4$  with  $0.0 \leq x \leq 2.0$  [8],  $\text{U}_{15}\text{Co}_{55}\text{Ge}_{30}$ ,  $\text{U}_6\text{Co}_{30}\text{Ge}_{19}$ ,  $\text{U}_3\text{Co}_4\text{xGe}_{33}$  with  $0.0 \leq x \leq 3.0$ ,  $\text{UCo}_{1-y}\text{Ge}_{1+y}$  with  $0.6 \leq y \leq 0.7$ ,  $\text{UCoGe}_2$ ,  $\text{U}_4\text{Co}_{1-y}\text{Ge}_{6-x+y}$  with  $x = 0.6$  and  $0.0 \leq y \leq 0.5$  and  $\text{UCo}_1\text{xGe}_2$  with  $0.22 \leq x \leq 0.45$  [9,10]. In this communication we describe the crystallographic features as well as the magnetic and electrical transport properties of  $\text{U}_4\text{Co}_1\text{yGe}_{6-x+y}$  and  $\text{UCo}_{1-y}\text{Ge}_{1+y}$ .

$\text{UCo}_{1-y}\text{Ge}_{1+y}$  ( $0.6 \leq y \leq 0.7$ ) crystallizes with a unit cell related to the AlB<sub>2</sub> type with the lattice parameters  $a = 4.111(5)$  Å and  $c = 7.641(5)$  Å (fig. 1a). The structure is composed of [U6] trigonal prisms, alternatively centred either by the (Co,Ge) atoms or the Ge atoms. The presence of modulations in the crystal structure makes its refinement difficult. The magnetic measurements revealed a ferromagnetic transition (fig. 2a), at the Curie temperature varying along the homogeneity range ( $38 \text{ K} \leq T_c \leq 48 \text{ K}$ ). In the paramagnetic region, the magnetic susceptibility follows a modified Curie-Weiss law with the effective magnetic moment of  $2.40(1)$   $\mu\text{B}/(\text{U atom})$ . The electrical resistivity of  $\text{UCo}_{1-y}\text{Ge}_{1+y}$  is about  $360 \mu\Omega\text{cm}$  at room temperature and shows rather minor temperature variation (fig. 2b). Below 75 K, it slightly increases with decreasing temperature reaching  $375 \mu\Omega\text{cm}$  at liquid helium temperature. The ferromagnetic phase transition is hardly resolvable from the resistivity curve.

Fig.1: Projections on the (a,b) plane of the crystal structures of a)  $\text{UCo}_{1-y}\text{Ge}_{1+y}$  and b)  $\text{U}_4\text{Co}_1\text{yGe}_{6-x+y}$

$\text{U}_4\text{Co}_1\text{yGe}_{6-x+y}$  ( $x = 0.6$  and  $0.0 \leq y \leq 0.5$ ) adopts the hexagonal  $\text{Er}_4(\text{Ga,Ge})_7$  type structure (space group  $P6_3/m2$ ) with the lattice parameters  $a = 8.016(1)$  Å and  $c = 4.021(1)$  Å. This crystal structure is a derivative of the AlB<sub>2</sub> type. The U atoms form [U6] trigonal prisms. Six over eight of them are occupied by the Ge atoms, one is centred by the Co atom and the eighth prism is empty, due to the proximity of two Ge atoms that are strongly shifted from the center of their prisms (fig. 1b). The compound shows a ferromagnetic transition at  $T_c = 39 \text{ K}$  (fig. 2a). At higher temperatures a modified Curie-Weiss law is observed for the magnetic susceptibility, with the effective magnetic moment of  $2.76(4)$   $\mu\text{B}/(\text{U atom})$ . In the paramagnetic state the resistivity is almost temperature independent being of about  $275 \mu\Omega\text{cm}$  (fig. 2b). The magnetic transition manifests itself as a distinct kink at the resistivity curve, below which the resistivity sharply decreases down to  $175 \mu\Omega\text{cm}$  at 4 K.

Fig.2: Temperature dependencies of (a) the magnetization and (b) the resistivity of  $\text{U}_4\text{Co}_1\text{yGe}_{6-x+y}$  (blue symbols) and  $\text{UCo}_{1-y}\text{Ge}_{1+y}$  (red symbols). The ferromagnetic phase transitions are marked by arrows.

#### References

- [1] N. T. Huy et al., Phys. Rev. Lett. 99 (2007) 067006
- [2] R.Troć, V.H. Tran, J. Magn. Magn. Mater. 73 (1988)389-397
- [3] T. Endstra et al., J. Appl. Phys. 69(8) (1994) 4816-4818
- [4] W. Buchholz, H.U. Schuster, Z. Anorg. Allg. Chem. 482 (1981) 40-48
- [5] S. Bobev et al., J. Solid State Chem. 180 (2007) 2830-2837
- [6] R. Pöttgen et al., J. Solid State Chem. 115 (1995) 247-254
- [7] B. Chevalier et al., J. Alloy Compd. 233 (1996) 174-182
- [8] A. Soudé et al., J. Solid State Chem., submitted
- [9] A.Soudé et al., Book of Abstracts, 38ème Journées des Actinides, Wrocław, Poland, 2008, p.109
- [10] A.Soudé et al., Book of Abstracts, 39ème Journées des Actinides, La Grande Motte, France, 2009, p.57-58

JDA-WAT I / 49

## Development of an actinide target and laser ion-source test-bed at iThemba LABS, South Africa

**Author:** Robert Bark<sup>1</sup>

**Co-author:** Lowrie Conradie <sup>1</sup>

<sup>1</sup> iThemba LABS

**Corresponding Author:** bark@tlabs.ac.za

The main accelerator of iThemba Laboratory for Accelerator Based Sciences is a  $K = 200$  Separated Sector Cyclotron (SSC). Use of the accelerator is shared by groups engaging in nuclear physics research, radiation therapy and radio-isotope production. The long term plan calls for the addition a high-intensity,  $K = 70$  MeV proton accelerator to the laboratory, to both alleviate over-subscription of the SSC and to be used as a primary accelerator for radioactive beam production using the ISOL method. The proposed RIB facility would produce neutron rich species by fissioning uranium. As a first step in this programme, we present a proposal being developed at the laboratory to build a target and laser-ionization demonstrator at the laboratory, utilizing the present 66 MeV proton beam from the SSC. Neutron-rich isotopes produced in this way would be used for materials analysis and beta-decay studies.

JDA-WAT I / 50

## Design concerns for future RIB production facilities at TRIUMF

**Author:** Colin Morton<sup>1</sup>

<sup>1</sup> TRIUMF

**Corresponding Author:** morton@triumf.ca

Since the first Workshop on Actinide Targets in 2006, two such targets have been used successfully for RIB production at TRIUMF's ISAC facility. In a test run in August/September 2008, a uranium oxide target coupled to a surface ionization source was irradiated with  $\sim 300 \mu\text{A}\cdot\text{hrs}$  of 500 MeV protons and RIB yields were measured at the ISAC yield station. In a follow-up run, in December 2009, a similar target coupled to a FEBIAD ion source was irradiated with  $\sim 425 \mu\text{A}\cdot\text{hrs}$  of protons and RIB were delivered to an experimental location. In both runs it was demonstrated that such targets could be used safely within the existing ISAC infrastructure. As a result, TRIUMF now has regulatory permission to proceed with regular irradiations at low proton currents.

Despite the low-current nature of these runs, it was necessary to install new radiation monitoring systems and implement new procedures for the handling of targets and target modules. The experience gained from these runs and from the use of these new systems and procedures (and from ongoing operation with non-actinide targets) is being incorporated into the design specifications for the future ARIEL facility at TRIUMF. ARIEL, the Advanced Radiosotope Laboratory, will have the capability (pending a funding commitment from the Canadian government) of producing RIB via  $\sim 500$ -MeV proton-induced reactions as at ISAC and via photofission using a new 50 MeV, 100+ kW electron-linac driver. Two new target stations will be built to accommodate RIB production and coupled into the existing ISAC beamline and accelerator complex. The impact of TRIUMF's actinide target program on the design of the target stations and their related infrastructure will be discussed.

Materials I / 51

## Recent progress in the synthesis and characterization of uranium carbide compounds

**Author:** Olivier TOUGAIT<sup>1</sup>

**Co-authors:** Ahmet Özgümüs<sup>2</sup>; Christophe Lau<sup>3</sup>; Evelyne Cottureau<sup>4</sup>; Henri Noël<sup>4</sup>; Maher Cheikh Mhamed<sup>4</sup>; Mathieu Pasturel<sup>4</sup>; Michel Potel<sup>4</sup>; Nicole Barré-Boscher<sup>4</sup>; Said Essabaa<sup>4</sup>

<sup>1</sup> Université de Rennes1

<sup>2</sup> Université Paris XI, IPN-O

<sup>3</sup> CNRS, IPN-O

<sup>4</sup> CNRS**Corresponding Author:** tougait@univ-rennes1.fr

The binary uranium-carbon phase-diagram comprises three intermediate phases (UC, U<sub>2</sub>C<sub>3</sub> and UC<sub>2</sub>) showing high melting / decomposition points, high thermal conductivity, lack of phase-transformations at temperatures of practical relevance, and good stability under irradiations, which allow their use under extreme conditions. An enormous amount of work has been directed to those binary compounds as nuclear fuels for fast reactors operating at high temperatures or targets for high energy spallation or fission sources at ISOL facilities of new generation.

Both projects claim a significant gain of the efficiency of the future systems compared with the systems available to date, for this the two most important are the need to increase the life-time of the fuel or of the target and the need to use them at high temperatures (800-1000°C for GFR-He, compared to 300-450°C for current nuclear plants). The first reason is to limit the serious problem arisen for the replacement of the highly radioactive materials, the amount of nuclear wastes and to burn the minor actinides in the case of fuel. The increase of the working temperatures is directly linked to the efficiency of the fuel or of the target, but also it allows co-generation, in the case of Gen-IV nuclear plants.

For a decade, the research activities of our research group focused on the study of uranium, carbides, covering various aspects, such as the synthesis, the phase relations in the U – C binary phase-diagram, the microstructural characterization of the powders, and finally the sintering of these powders. In this presentation, a general description of these experimental tasks will be given. New results will be exposed and compared with literature data. The conclusion will focus on the most significant advances for the preparation of high purity powders of uranium carbides, by means of controlled key-parameters, that were identified as, U to C atomic ratios, temperature, partial pressure of the reaction chamber, time of the dwell.

### Strongly Correlated Systems III / 52

## Crystal structure and physical properties of NpRh<sub>2</sub>Sn, a new Np-based ternary compound

**Author:** T. Klimczuk<sup>None</sup>

Crystal structure and physical properties of NpRh<sub>2</sub>Sn,  
a new Np-based ternary compound

T. Klimczuk,<sup>1,2</sup> J.-C. Griveau,<sup>1</sup> R. Eloirdi,<sup>1</sup> E. Colineau<sup>1</sup>, and R. Caciuffo<sup>1</sup>

<sup>1</sup> European Commission, Joint Research Center, Institute for Transuranium Elements, Postfach 2340, Karlsruhe, D-76125 Germany, e-mail: Tomasz.Klimczuk@ec.europa.eu

<sup>2</sup> Faculty of Applied Physics and Mathematics, Gdansk University of Technology, Narutowicza 11/12, 80-233 Gdansk, Poland

The large family of the ternary actinide compounds AnT<sub>2</sub>M, where An is an actinide element, T is a transition element, and M is a metalloid, forms mainly in the orthorhombic crystal structure (Pnma, s.g. 62). The uranium based alloys (UT<sub>2</sub>M) have attracted considerable attention due to a wide range of physical properties, which originates from the sensitive nature of the uranium 5f-electrons. Very few compounds with An other than uranium have been reported, and most of them contain palladium as the transition element.

Here, we will present the crystal structure and physical properties of a new intermetallic NpRh<sub>2</sub>Sn compound, which is the first member of the AnRh<sub>2</sub>M family.

A sample with nominal stoichiometry NpRh<sub>2</sub>Sn was prepared by arc-melting under argon atmosphere. The as-cast piece was studied by x-ray powder diffraction and the result is presented in Figure 1. The GSAS package was used for Rietveld structure refinement [1,2]. Refined lattice parameters, An-An distance for NpRh<sub>2</sub>Sn, and few other members of AnT<sub>2</sub>M, are summarized in Table 1.

Fig. 1. Room temperature x-ray diffraction pattern of NpRh<sub>2</sub>Sn. (+) represent experimental data, black and red ticks indicate Bragg peak positions for NpRh<sub>2</sub>Sn and NpO<sub>2</sub> respectively. The refine-

ment and difference are shown as solid lines. The crystal structure of NpRh<sub>2</sub>Sn is presented in the inset.

a (Å) b (Å) c (Å) d An-An (Å) TN (K)  $\chi$ CW (K)  
 NpRh<sub>2</sub>Sn 9.7300(6) 4.4278(3) 6.9115(5) 3.984 34 -29  
 NpPd<sub>2</sub>Sn [3] 10.004(3) 4.535(2) 6.961(1) ) 15 -80  
 PuPd<sub>2</sub>Sn [4] 10.053(9) 4.502(4) 7.065(6) 11 -30  
 UPd<sub>2</sub>Sn [5] 9.9415(4) 4.6050(2) 6.8633(3) 4.182 - -100

Table 1. Refined lattice parameters, distance between actinide atoms (dAn-An), Néel temperature (TN), and paramagnetic Curie-Weiss temperature ( $\chi$ CW), for selected members of AnT<sub>2</sub>Sn family. \*) – due to the lack of information about the refined atomic positions for NpPd<sub>2</sub>Sn and PuPd<sub>2</sub>Sn, the dAn-An can not be calculated for these two compounds, but some information can be deduced by comparing b lattice parameter.

In Figure 2 we show the temperature dependence of inverse susceptibility (a) and specific heat (b) of NpRh<sub>2</sub>Sn. The Curie-Weiss fit of the data above 75K (red solid line) gives a Curie-Weiss temperature  $\chi$ CW= -29K, and an effective magnetic moment  $\mu_{\text{eff}}=2.42\mu_B$ . This is close to the expected value  $\mu$ for Np<sup>+3</sup> (2.68 $\mu_B$ ). This measurement indicates an antiferromagnetic anomaly at TN = 34K. At the same temperature region a slight change of slope is observed on the specific heat curve CP(T). Marginal evidence of a specific heat anomaly was reported also for UPd<sub>2</sub>Sn, as discussed in Ref. [5].

Fig. 2. a) The temperature dependence of the inverse magnetic susceptibility ( $\chi^{-1}$ ) and b) specific heat (CP) of NpRh<sub>2</sub>Sn. The straight, red line through the data is the fit by the Curie-Weiss law.

To summarize, we have synthesized and studied a new Np-based ternary NpRh<sub>2</sub>Sn compound. Its properties are similar to NpPd<sub>2</sub>Sn, although a shorter Np-Np distance causes an increase of the Néel temperature. NpRh<sub>2</sub>Sn is a rare representative of heavy-fermion systems amidst Np- inter-metallics.

#### References

- [1] B. H. Toby, J. Appl. Cryst. 34, 210 (2001).
- [2] A. C. Larson and R. B. Von Dreele, Los Alamos National Laboratory Report LAUR, 86 (2000).
- [3] D. Kaczorowski et al., Physica B 359-361, 1102-1104 (2005).
- [4] K. Gofryk et al., Phys. Rev. B 77, 014431 (2008).
- [5] I. Maksimov et al., Phys. Rev. B 67, 104405 (2003).

#### Aknowldegments:

Np metal required for the fabrication of the compound was made available through a loan agreement between Lawrence Livermore National Laboratory and ITU, in the frame of a collaboration involving Lawrence Livermore National Laboratory, Los Alamos National Laboratory, and the US Department of Energy.

T.K. acknowledges the European Commission for financial support.

### Strongly Correlated Systems III / 53

## Synthesis and magnetic properties of a new ferromagnetic Kondo-lattice system Np<sub>2</sub>PdGa<sub>3</sub>

Author: v h tran<sup>None</sup>

Synthesis and magnetic properties  
 of a new ferromagnetic Kondo-lattice system Np<sub>2</sub>PdGa<sub>3</sub>

Blank line (12 points)

V. H. Tran,1 J. -C. Griveau,2 R. Eloirdi,2 W. Miiller, 1 E. Colineau,2

Blank line (12 points)

1 Institute of Low Temperature and Structure Research,  
 Polish Academy of Sciences, P. O. Box 1410, 50-950 Wrocław, Poland

2European Commission, Joint Research Centre, Institute for Transuranium Elements,  
 Postfach 2340, D-76125 Karlsruhe, Germany

Blank line (12 points)



A number of intermetallic of the stoichiometric compounds  $U_2TM_3$ , where  $T = 3d, 4d$  and  $5d$  electron transition metals and  $M = Si$  or  $Ga$  have been discovered [1-3]. Generally, these compounds adopt two well known types of crystal structures, i.e., the hexagonal  $AlB_2$ - or orthorhombic  $CeCu_2$ -type, respectively. Most of the compounds which crystallize in the hexagonal  $AlB_2$ -type are those containing  $M = Si$  and showing spin-glass or ferromagnetic cluster glass behavior [1,4]. On the other hand, the compounds with  $M = Ga$  favor the  $CeCu_2$ -type and exhibit various types of magnetic ordering including the spin fluctuation, ferromagnetic and antiferromagnetic order at low temperatures [3,5]. Amongst  $U_2TGa_3$ , the magnetism of the Pd- and Pt-based compounds appears to be an enormously complex subject owing to a competition between the Kondo effect and randomness for long range antiferromagnetism. Therefore, in order to make a systematic study, an investigation of systems being isostoichiometric and/or isostructural to  $U_2(Pd,Pt)Ga_3$  would be useful. In this contribution, we present the synthesis and crystallographic characterization, and as well magnetic properties for a new Np-based  $Np_2PdGa_3$  compound.

Fig. 1 X-ray powder diffraction pattern of  $Np_2PdGa_3$ . The observed (open circles), calculated (solid line), positions of Bragg reflections (vertical lines) and the difference between observed and calculated data (bottom). Inset: Crystal structure of  $Np_2PdGa_3$ . Large balls represent the Np atoms and small ones the Pd or Ga atoms. Note that the nearest Np neighbors form zigzag chains parallel to the  $b$  axis (thick line) and the next-nearest Np neighbors are connected by zigzag chains along the  $a$  axis (thin line).

The X-ray diffraction data collected in the range  $20 - 100$  deg, shown in Fig. 1, revealed that the majority phase ( $> 95$  mass. %) has the orthorhombic  $CeCu_2$ -type structure. We were able to identify  $NpO_2$ ,  $Np_3Pd_3Ga_8$  and  $NpC$  to be the main impurities are denoted by arrows in the diffraction pattern. The observed Bragg reflections for  $Np_2PdGa_3$  could be indexed with lattice parameters  $a = 0.4445(2)$  nm,  $b = 0.7089(3)$  nm and  $c = 0.7691(3)$  nm. Taking into account the size of  $An^{3+}$  and  $An^{4+}$  ions and comparing the lattice parameters of  $U_2PdGa_3$  and  $Np_2PdGa_3$  one suspects the  $3+$  valence of the magnetic Np ions.

The measurements of magnetization specific heat, electrical resistivity, magnetoresistance and Hall effect for  $Np_2PdGa_3$  indicated a ferromagnetic ordering below  $62.5(5)$  K. The analysis of magnetic susceptibility (Fig. 2) and specific heat (Fig. 3) consistently suggests a CEF splitting with doublet-doublet-doublet scheme and  $\Delta_{CEF} \sim 60$  K and  $180$  K.

Fig. 2 Temperature dependence of magnetic susceptibility of  $Np_2PdGa_3$  and  $Lu_2PdGa_3$ . The solid line is the CEF fit

Fig. 3 Temperature dependence of the contribution of 5f-electron specific heat and 5f-electron entropy of  $Np_2PdGa_3$ .

The lines are calculated CEF, Kondo and magnon contributions to the specific heat.

The enhanced Sommerfeld ratio at low temperature ( $C_{5f}/T = 120$  mJ/K<sup>2</sup>mol.Np at 2 K) and  $\ln T$  dependence of the resistivity can be interpreted due to the Kondo effect with  $T_K \sim 35$  K (see dash-dotted line). The Hall coefficient exhibits a behavior for localized moment ferromagnets with low carrier concentration ( $0.17$  carrier/f.u) and with enhanced effective mass ( $\sim 144 m_0$ ).

The presented data seem to be consistent with the underscreened Kondo lattice model recently developed by Perkins et. al [6]. We argue thus that  $Np_2PdGa_3$  is a new ferromagnetic Kondo lattice with  $T_K < T_{RKKY} \sim \Delta_{CEF}$ . Among Np-based compounds, ferromagnetic Kondo behavior was previously found for  $NpNiSi_2$  [7].

#### References

- [1] D. Kaczorowski and H. Noel, *J. Phys.: Condens. Matter* 5, 9185 (1993).
- [2] B. Chevalier, R. Pottgen, B. Darriet, P. Gravereau, and J. Etourneau, *J. Alloys Compd.* 233 (1996) 150.
- [3] V. H. Tran, *J. Phys.: Condens. Matter* 8, 6267 (1996).
- [4] D. X. Li, S. Nimori, Y. Shiokawa, Y. Haga, E. Yamamoto, Y. Onuki, *Phys. Rev. B* 68, 172405 (2003).
- [5] V. H. Tran, F. Steglich, G. Andre, *Phys. Rev. B* 65, 134401 (2002).
- [6] N. B. Perkins, M. D. Nunez-Regueiro, B. Coqblin, and J. R. Iglesias, *Phys. Rev. B* 76, 125101 (2007).
- [7] E. Colineau, F. Wastin, J. P. Sanchez, and J. Rebizant, *J. Phys.: Condens. Matter* 20, 075207 (2008).

## Theory and Spectroscopy II / 54

**Electronic structure and magnetic properties of UNi<sub>1/2</sub>Sb<sub>2</sub> compound**Author: m. werwinski<sup>None</sup>Electronic structure and magnetic properties of UNi<sub>1/2</sub>Sb<sub>2</sub> compound

Blank line (12 points)

M. Werwiński, A. Szajek

Blank line (12 points)

Institute of Molecular Physics, Polish Academy of Sciences.

ul. M. Smoluchowskiego 17. 60-179 Poznań. Poland, e-mail: werwinski@ifmpan.poznan.pl

Blank line (12 points)

The UNi<sub>1/2</sub>Sb<sub>2</sub> compound crystallizes in the tetragonal HfCuSi<sub>2</sub> type structure with space group P4/nmm [1]. The single crystals studied order antiferromagnetically below 161 K, with the effective magnetic moment 3.17  $\mu_B$  [1].

We present results of ab-initio band structure calculations based on full potential - linearized augmented plane wave (FP-LAPW) implemented in WIEN2k code [2]. Calculations based on experimental lattice constants and Wyckoff positions [1]. The spin polarized calculations were done for parallel and antiparallel magnetic moments arrangements. For antiferromagnetic calculation we prepared double supercell, the Wyckoff positions of uranium atoms were splitted into two nonequivalent sorts: U1 and U2. The antiferromagnetic solution was not assumed in advance. The starting magnetic moments on uranium atoms had opposite signs because of initial splitting. The system reached, iteration by iteration, selfconsistent solution, which was antiferromagnetic state. Starting from the local (spin) density approximation (L(S)DA) we verified either the orbital polarization (OP) correction or the LSDA+U approach with Coulomb repulsion energies U from 0 to 3 eV for the uranium 5f-electrons.

Calculated magnetic moments confirm antiferromagnetic ground state and collinear magnetic sequences. Total LSDA magnetic moment on uranium atom amount to 0.88  $\mu_B$ .

Fig. 1 Crystallographic structure and DOS plots for UNi<sub>1/2</sub>Sb<sub>2</sub> compound.

## References

[1] Z. Bukowski et al. *Intermetallics* 12, 1381 (2004).

[2] P. Blaha et al., WIEN2k\_7.3, An Augmented Plane Wave + Local Orbitals Program for Calculating Crystal Properties, Karlheinz Schwarz, Techn. Universität Wien, Austria, 2007.

55

**Transport and thermodynamic properties of UFe<sub>2</sub>Zn<sub>20</sub>**Author: P Swatek<sup>None</sup>Transport and thermodynamic properties of UFe<sub>2</sub>Zn<sub>20</sub>

Przemysław Swatek and Dariusz Kaczorowski

Institute of Low Temperature and Structure Research, Polish Academy of Sciences,

P.O. Box 1410, 50-950 Wrocław, Poland

e-mail: P.Swatek@int.pan.wroc.pl

Ternary rare-earth-based intermetallic compounds RT<sub>2</sub>M<sub>20</sub> (R = Ce, Gd, Yb; T = d-electron transition metal). Similar compounds with uranium and zinc were reported to form with T = Fe, Co, Ru, Rh, Ir [6–9]. The single crystals of UFe<sub>2</sub>Zn<sub>20</sub> were grown in Zn flux. The obtained crystals were well-developed cubes. The specific heat of UFe<sub>2</sub>Zn<sub>20</sub> was measured with the AC current flowing through the sample. The temperature variation of the specific heat of UFe<sub>2</sub>Zn<sub>20</sub> is shown in Fig. 1. In agreement with the Fig. 2 displays the temperature dependence of the electrical resistivity of UFe<sub>2</sub>Zn<sub>20</sub>. At room temperature the resistivity is about 100 mΩ cm. To summarize hitherto findings, UFe<sub>2</sub>Zn<sub>20</sub> seems to be a novel paramagnetic moderately-enhanced heavy

Fig. 1. Temperature dependence of the specific heat of single-crystalline UFe<sub>2</sub>Zn<sub>20</sub>. The inset shows the heat capacity data in the form  $C/T$  vs.  $T^2$ . The dashed line emphasizes the linear dependence.

Fig. 2. Temperature variation of the electrical resistivity of single-crystalline UFe<sub>2</sub>Zn<sub>20</sub> (note semilogarithmic scale). The solid and dashed curves mark the Fermi-liquid- and Kondo-like behaviors at low and ambient temperatures, respectively.

#### References

- [1] S. Niemann et al., J. Solid State Chem. 114, 337 (1995).
- [2] O. Moze et al., J. Alloys Compd. 268, 39 (1998).
- [3] N. Gross et al., J. Solid State Chem. 161, 228 (2001).
- [4] S. Jia et al., Phys. Rev. B 77, 104408 (2008).
- [5] S. Jia et al., Phys. Rev. B 80, 104403 (2009).
- [6] A. P. Goncalves et al., J. Alloys Compd. 271-273, 456 (1998).
- [7] E. D. Bauer et al., Phys. Rev. B 74, 155118 (2006).
- [8] E. D. Bauer et al., J. Magn. Magn. Mater. 449-451, 310 (2007).
- [9] E. D. Bauer et al., Phys. Rev. B 78, 115120 (2008).

## Theory and Spectroscopy I / 56

### X-ray absorption and emission spectroscopic study at O K-edges of light actinide oxides

Author: s m butorin<sup>None</sup>

X-ray absorption and emission spectroscopic study at O K-edges of light actinide oxides

S. M. Butorin,<sup>1</sup> A. Modin<sup>1</sup>, Y. Yun<sup>1</sup>, M.-T. Suzuki<sup>1</sup>, J. Vegelius<sup>1</sup>, L. Werme<sup>1</sup>,  
D. K. Shuh<sup>2</sup>, P. M. Oppeneer<sup>1</sup>, J. Nordgren<sup>1</sup>,

<sup>1</sup> Department of Physics and Astronomy, Uppsala University, Box 516, S-751 20 Uppsala, Sweden,  
e-mail: sergei.butorin@fysik.uu.se

<sup>2</sup> Lawrence Berkeley National Laboratory, Chemical Sciences Division, Mail Stop 6R2100, One Cyclotron Road, Berkeley, CA 94720, USA

Here we present soft X-ray emission and X-ray absorption spectroscopic data recorded at O K edges of UO<sub>2</sub>, NpO<sub>2</sub> and PuO<sub>2</sub>. Interpretation of the experimental data is supported by first-principle calculations in framework of LDA+U and GGA+U formalisms (see Fig. 1). A discussion regarding the origin of different structures in the X-ray emission and X-ray absorption spectra is included. The effect of varying intra-atomic Coulomb interaction  $U$  for the f-electrons is investigated. Our data indicate that O-K X-ray absorption and X-ray emission spectroscopies can successfully be used to study correlation effects in compounds of light actinides.

For single-crystal Pu(<sup>239</sup> isotope)O<sub>2</sub>, the measured O 1s X-ray absorption spectra show significant difference in intensity for the first two peaks between different areas/spots on the single crystal surface. From theoretical results, the first peak can be attributed to O 2p-Pu 5f hybridization, while the second peak is due to hybridization with Pu d-states. The observed difference in the O 1s X-ray absorption spectra was studied by simulating a number of defect structures of PuO<sub>2</sub> as well as existence of Pu(V) sites. The results indicates the presence of higher oxidation states than Pu(IV) in some surface areas of the single crystal. The results also suggest that plutonium oxide with a Pu fraction in a higher oxidation state than Pu(IV) consists of inequivalent sites with Pu(IV)O<sub>2</sub> and Pu(V)O<sub>2</sub> rather than is being a system where the Pu oxidation state is constantly fluctuating between Pu(IV) and Pu(V).

Oral presentation.

Fig.1 Comparison of experimentally recorded (in red) and LDA+U calculated (in blue) O K $\alpha$  X-ray emission and O 1s X-ray absorption spectra of UO<sub>2</sub>, NpO<sub>2</sub> and PuO<sub>2</sub>.

## Strongly Correlated Systems I / 57

**Kondo effect in the presence of ferromagnetism in  $U_{1-x}Th_xNiSi_2$** Author: a p pikul<sup>None</sup>Kondo effect in the presence of ferromagnetism in  $U_{1-x}Th_xNiSi_2$   
(ORAL)

Adam P. Pikul and Dariusz Kaczorowski

W. Trzebiatowski Institute of Low Temperature and Structure Research, Polish Academy of Sciences,  
P Nr 1410, 50–950 Wrocław 2, Poland; e-mail: A.Pikul@int.pan.wroc.pl

The compound  $UNiSi_2$  crystallizes with an orthorhombic structure of the  $CeNiSi_2$ -type and exhibits a ferromagnetic ordering of localized magnetic moments of uranium ( $\sim 1.2 \mu_B$ ) at the Curie temperature  $T_C = 95$  K [1]. Our recent experiments carried out on high-quality single crystalline specimens revealed that the ferromagnetic ordering occurs in the system in the presence of the Kondo effect, which dominates the electrical resistivity of  $UNiSi_2$  in the paramagnetic region [2]. In turn, investigation of a solid solution  $UNi_{1-x}Co_xSi_2$  ( $0 \leq x \leq 1$ ) indicated a very robust nature of the ferromagnetism observed in the parent compound, and its persistence up to the very vicinity of  $x = 1$  [3]. Also partial substitution of silicon by germanium in  $UCoSi_2-xGe_x$  revealed immediate appearing of the ferromagnetic order to be observed already for  $UCoSi_2$  doped with about 1% of germanium [4].

In order to shed more light on the origin of the strong ferromagnetism in  $UNiSi_2$  we have undertaken comprehensive studies of another isostructural solid solution of that system, namely  $U_{1-x}Th_xNiSi_2$ . Here we present some preliminary results of X-ray powder diffraction, magnetic susceptibility, electrical resistivity and specific heat measurements carried out in wide temperature and magnetic field ranges using polycrystalline specimens of the latter system.

Since the partial substitution of uranium by 15%-larger thorium expands the unit cell of the parent compound (cf. Fig. 1), the Kondo effect in the system is supposed to become weaker than the RKKY interactions for a certain Th-content [5], and thus the ferromagnetic order might be promoted at temperatures higher than in pure  $UNiSi_2$  (95 K). On the other hand, the U/Th substitution gradually dilutes the magnetic sublattice in the  $U_{1-x}Th_xNiSi_2$  system and hence the long range magnetic order in the diluted limit should eventually be suppressed to absolute zero temperature. Indeed, as can be inferred from the temperature variations of magnetization (Fig. 2), electrical resistivity (Fig. 3) and specific heat (Fig. 4), the U/Th substitution results in systematic decrease of the Curie temperature from  $T_C = 95$  K in pure  $UNiSi_2$  down to about 30 K in  $U_{0.2}Th_{0.8}NiSi_2$ . Though in the Th-rich alloys the phase transition is no longer as sharp as in the parent compound  $UNiSi_2$ , the ferromagnetic order remarkably survives in the system down to very diluted limit, hence reflecting a very robust nature of the ferromagnetism in  $U_{1-x}Th_xNiSi_2$ .

In the paramagnetic region, the electrical resistivity of all the samples studied increases logarithmically with decreasing temperature, being characteristic of Kondo systems. The slope of the resistivity curves does not change significantly upon increasing  $x$ , hence indicating that the transport properties are governed by single Kondo impurity effects. Minor modification of the  $\rho(T)$  curves in this region can be ascribed to the reduction of the Kondo temperature being a consequence of the change in the unit cell volume.

The presented results suggest that  $UNiSi_2$  may be another clear example (together with e.g. isostructural  $NpNiSi_2$  [6]) of a ternary system that shows coexistence of ferromagnetic ordering and Kondo interactions, as recently considered by Coqblin and co-workers in terms of underscreened Kondo lattice approach [7]. Further results (in particular for samples with lower uranium content) as well as their extended analysis will be updated at the time of the conference.

Fig.1. Lattice parameters  $a$ ,  $b$  and  $c$  (left axis), and unit cell volume  $V$  (right axis) of  $U_{1-x}Th_xNiSi_2$  as a function of Th content  $x$ .

Fig.2. Temperature dependence of magnetization  $M$  of  $U_{1-x}Th_xNiSi_2$  measured in field cooling regime. The arrows mark the phase transition temperatures.

Fig.3. Temperature variation of the normalized electrical resistivity  $\rho/\rho_{300K}$  of  $U_{1-x}Th_xNiSi_2$ . The arrows mark the Curie temperatures. Fig.4. Specific heat of the compounds  $U_{1-x}Th_xNiSi_2$  as a function of temperature. The arrows mark the phase transition temperatures.

This work was supported by the Polish Ministry of Sciences and Higher Education through the

research grant No. N202 116 32/3270.

#### References

- [1] D. Kaczorowski, Solid State Commun. 99, 949 (1996).
- [2] D. Kaczorowski, A.P. Pikul and D. Gnida, Abstracts of the „39èmes Journées des Actinides”, 28–31 March 2009, La Grande Motte, France.
- [3] D. Kaczorowski and A.P. Pikul, Abstracts of the „37ièmes Journées des Actinides”, 24–27 March 2007, Sesimbra, Portugal.
- [4] A.P. Pikul and D. Kaczorowski, unpublished
- [5] S. Doniach, in Valence Instabilities and Related Narrow Band Phenomena (Plenum Press, New York, 1977).
- [5] E. Colineau, F. Wastin, J.-P. Sanchez, and J. Rebizant, J. Phys.: Condens. Matter 20, 075207 (2008).
- [6] N.B. Perkins, M.D. Núñez-Regueiro, B. Coqblin, and J.R. Iglesias, Phys. Rev. B 76, 1251

JDA-WAT I / 59

## White line of actinide x-ray absorption spectra as a tool for their atomic environment description

**Author:** c degueldre<sup>None</sup>

White line of actinide x-ray absorption spectra as a tool for their atomic environment description

Claude Degueldre,<sup>1</sup> Manuel Pouchon<sup>1</sup>, Goutam Kuri<sup>1</sup>, Camelia Borca<sup>2</sup>, Cedric Cozzo<sup>1</sup>

<sup>1</sup> LNM – NES, Paul Scherrer Institute -5232 Villigen, Switzerland, e-mail: claude.degueldre@psi.ch

<sup>2</sup> SYN Paul Scherrer Institute -5232 Villigen, Switzerland,

From a recent plutonium uranium mixed oxide (MOX) fuel characterization campaign by micro-x-ray absorption fine structure ( $\mu$ -XAFS) spectroscopy the chemical bounds, valences and stoichiometry of Pu and U were determined. Experimental data was gained for non-irradiated as well as for the irradiated (burn-up 60 MW d kg<sup>-1</sup>) fuel material examined in the center of the fuel as well as in its peripheral zone (rim). The MOX fuel undergoes locally crystalline changes during burn-up. In the fuel center, the slightly smaller burn-up ( $\approx$ 1700 dpa) compared to the fuel average limits damage and the rather high temperature (e.g.  $\sim$ 1675 K) allows healing. In the rim zone, the larger burn-up ( $\approx$ 2500 dpa) compared to average increases damage potential, however, the rather low temperature (e.g.  $\sim$ 875 K) reduces the healing action, which increases the defect occurrence and the partial disaggregation of the fuel. In the irradiated sample Pu remained Pu(IV) >95% and no (<5%) Pu(V) or Pu(VI) could be detected while the fuel could undergo slight oxidation in the rim zone. Any slight oxidation may be buffered by the UO<sub>2</sub> matrix while locally fuel cladding interaction might also affect the redox of the fuel [1].

The white line factor ( $\mathcal{W}$ ) may be defined from the characteristics of the near edge structure XANES feature as  $\mathcal{W} = 2 (IM - Im) / (IM + Im)$  with IM the intensity of the white line and Im its intensity from the first minimum behind the white line. Its trend for Pu as a function of the coordination number (CN) is sketched in Fig 1. It is clearly observed that the white line decreases when Pu increases in valence state. This is due to the change of valence state as depicted in the structural pictures e.g. [O<sub>4</sub>AnO<sub>4</sub>]<sup>12-</sup> in AnO<sub>2</sub>(s) but also due to the formation of actinyl feature of [O=An=O]<sup>2+</sup> and the potential of 5 oxygen atoms (e.g. water molecules) in equatorial plane.

The paper discusses also the impact of actinide Th, U, Np and Pu valence and atomic environment with regards to oxygen atoms from solution (hydrated ion) to gel (disordered) and to oxide (ordered) on the white line amplitude and morphology as recorded earlier [2].

This understanding is crucial since no significant edge energy shifts are generally recorded between Np(IV) and Np(V) or Pu(IV) and Pu(V). The discussion emphasises the use of XAFS for the characterization of actinides.

Fig. 1. Pu white line factor for Pu(III), Pu(IV), Pu(V) and Pu(VI) in solution (sol) or gel or oxide (Ox).

#### References

- [1] C. Degueldre et al., J. Nucl. Mater (2011) submitted.
- [2] S. Conradson et al., J. Solid State Chem. 178, 521 (2005).

WAT-II / 60

## Concepts for high power targets of thorium and uranium

Author: i gomes<sup>None</sup>

Concepts for high power targets of thorium and uranium

Itacil Gomes,<sup>1</sup> Jerry Nolen<sup>2</sup>, John Greene<sup>2</sup>

<sup>1</sup> I.C.Gomes Consulting & Investment Inc, Naperville, IL, USA, e-mail: icgomes@icgomes.com

<sup>2</sup> Argonne National Laboratory, Physics Division, Argonne, IL, USA, e-mail: nolen@anl.gov; greene@anl.gov

In recent years the high power Radioactive Beam community has had a renewed interest in actinides targets that has sparked several research activities around the world. In the USA, despite the FRIB (Facility for Radioactive Ion Beams) project not having, in the DOE approved form, an ISOL station, the studies of high power actinide targets continue to be of high priority for the research community. In Europe, with the EURISOL project among others, also there is a great interest in high power actinide targets. The development of thorium and uranium targets that can withstand beam powers of 100-400 kW is of high interest for the community. Targets with fast release characteristics are also of high interest. Currently there is a project funded by DOE to produce thin plates of uranium and thorium to be used in a tilted or multi-foil target. The primary candidate for this kind of targets is compressed powder with some pore former. Several pore formers are under consideration and the literature for HTGR fuel elements has a number of experiments performed with successful pore formation and structural soundness of thin samples.

The production of rare isotopes using a tilted target is an option being pursued for a few years. The two greatest advantages of this approach are: (a) a short path for the produced rare isotope to reach the plate surface for desorption, and (b) a large area to radiation heat transfer to the enclosure. Using a tilted angle of 60 it is possible to have the distance from any production point to the nearest surface roughly 20 times smaller than the thickness of the plate seen by the beam particles. The use of porous material facilitates the release of the produced rare isotopes. The porosity of the plate cannot be high because it has to be structurally sound and have good thermal conductivity.

Another option is to have very thin plates, in the sub-millimeter range, stacked as it is done in ISAC and ISOLDE. This approach facilitates diffusion out of the plates but the heat transfer to the enclosure is limited to the surface area of the cylinder. However, this concept would also profit from having thin plates with controlled porosity to stack them in available target enclosures.

Another area of interest is the production of radioisotopes for medical, industrial, and other applications. Actinide targets are seen as a good option for the production of several isotopes of interest. There are proposed configurations to directly irradiate uranium targets with proton beams to harvest <sup>99</sup>Mo and other radioisotope of interest [1]. The cooling of the plates becomes an important issue in those systems and new approaches are necessary to produce the isotopes while efficiently removing the heat deposited.

In this area of application active cooling of the plates is possible, in contrast with radioactive beam applications, because the produced isotopes, in most of the cases, should be kept inside the material for post-irradiation processing. Foam products that have a complete structure of interconnected pores with pore volume percentage ranging from 85 to 50% are of interest and commercially available. The large internal surface area of metallic, carbide, or oxide foam material presents an attractive feature for heat transfer and cooling (Fig. 1). The large internal surface area per unit volume for heat transfer makes it possible to extract large amounts of heat without a large increase in temperature of the coolant or target material. The application of the foam fabrication technique to actinide targets is one of the goals of this project of actinide target development.

As an alternative to the foam target structure, a stack of thin foils of sub-millimeter thickness tilted

at an angle of about 60 to the beam direction (Fig.2) can be used. The plates can be actively cooled by forced flow of a liquid or gas through sub-millimeter channels that separate the plates. The same advantage of the one-plate tilted can be accomplished with the added advantage of the active cooling to reach high power levels.

Fig. 1. Schematic representation of the Foam Target model with cooling across the porous media.

Fig. 2. A schematic representation of the Tilted Target model with multi-foil and cooling channels; the plates are tilted 60 from the beam direction in this model.

#### References

[1] Y. Jongen, "A cyclotron driven neutron multiplier for the production of  $^{99}\text{Mo}$ ," at the 37th European Cyclotron Progress Meeting, Groningen, The Netherlands, October 29, 2009.

This work was supported by the U.S. Department of Energy, STTR from Office of Nuclear Physics, under Grant No. DE-SC0000750

WAT-II / 61

## Synthesis of $^{244}\text{Bk}$ by $^{11}\text{B} + ^{238}\text{U}$ reaction for spectroscopic investigations

Author: s sodaye<sup>None</sup>

Synthesis of  $^{244}\text{Bk}$  by  $^{11}\text{B} + ^{238}\text{U}$  reaction for spectroscopic investigations

Suparna Sodaye<sup>1\*</sup>, K. Sudarshan<sup>1</sup>, D. Banerjee<sup>2</sup>, R. Tripathi<sup>1</sup>, P. Maheshwari<sup>1</sup>, D. Dutta<sup>1</sup>, R. Guin<sup>2</sup>, R. Palit<sup>3</sup>, and P.K.Pujari<sup>1</sup>

<sup>1</sup> Radiochemistry Division, Bhabha Atomic Research Centre, Mumbai, India

<sup>2</sup> Radiochemistry laboratory, VECC, 1/AF, Bidhan Nagar, Kolkata, India

<sup>3</sup> Tata Institute of Fundamental Research, Homi Bhabha Road, Colaba, Mumbai, India

Study of chemical properties of heavier actinides is challenging due to their short-half lives and production in minute quantities. One of the major factors in producing these actinides in larger quantities is the large fission cross section when compared to the evaporation leading to the formation of actinides. The studies of these actinides make its necessary to have a mass separator or adopt suitable chemical procedures to minimize the unwanted activity.

With the objective of producing and separating berkelium isotopes to ascertain the decay scheme of  $^{244}\text{Bk}$ , uranium metal targets of thickness  $\sim 30$  mg/cm<sup>2</sup> were irradiated with 63.5 MeV  $^{11}\text{B}$  beam at the BARC-TIFR pelletron facility. The energy was optimized using HICOL code to get maximum cross section for  $^{244}\text{Bk}$ . However, even at this energy, the fission cross section is 500 times more than the evaporation. The solvent extraction procedures were optimized to remove major fission product activity and the bulk uranium from the sample [1]. The sample was assayed by gamma-spectrometry using an 30% HPGe and a clover containing 4 segments. The reported gamma-lines of  $^{244}\text{Bk}$  are 217.6  $\pm$  0.3 keV and 891.5  $\pm$  1.0 keV [2]. These were identified in the  $\gamma$ -spectra and their decay profiles were followed. The measured half life from the above gamma-lines was 5.56  $\pm$  1.16 h. The only reported value of half life of  $^{244}\text{Bk}$  is 4.35  $\pm$  0.15 h [3]. Treating each of the segments of the clover as separate detectors, the coincidence spectra were built from the list mode data with a gate on 217.4 keV on other 3 segments of the detector. The gamma-line at 1243.5  $\pm$  1.5 keV was found to be in coincidence with 217.4 keV. There is also a signature of another gamma-line at 2401  $\pm$  2 keV. These gamma-lines have not been reported earlier. The details will be discussed.

#### References

1. Cornelius Keller, The chemistry of transuranium elements (1971) 553.

2. R.B. Firestone and V.S. Shirley, Table of Isotopes, Eighth edition (1999), John Wiley & Sons, New York.

3. I. Ahmad, Ph.D Thesis, University of California, 1962

**Materials I / 62****Solid state physics at ISOLDE: using radioactive ion beams to study materials****Author:** Karl Johnston<sup>1</sup><sup>1</sup> ISOLDE/CERN**Corresponding Author:** karl.johnston@cern.ch

At the radioactive ion beam facility, ISOLDE-CERN, more than 900 isotopes of 70 elements are produced and delivered as radioactive ion beams of high elemental and isotopic purity. At ISOLDE an extensive solid state programme of research has been in place for many years and continues to develop and expand by the year. This activity embraces a wide range of techniques and materials.

Among the techniques used are those which utilize nuclear properties such as Perturbed Angular Correlation (PAC), Emission channeling (EC), Mössbauer spectroscopy and  $\mu$ -NMR. These methods are capable of probing the local environment of the host material and provide important and often unique hyperfine data. In addition to these techniques traditional semiconductor spectroscopies such as Deep level Transient Spectroscopy (DLTS), Photoluminescence (PL) and diffusion gain extra sensitivity and yield chemical information when combined with radioactivity.

The materials studied have changed as research priorities in the world at large have changed. Nowadays the bulk of the semiconductor work is focused on compound materials such as ZnO, GaN and CdTe. In addition Multiferroic materials such as RMnO<sub>3</sub> (R = Tb, Dy) (among others) now account for significant proportion of the beamtimes, along with studies of high T<sub>c</sub> Superconductors. One of the advantages of many of the techniques which utilize radioactive probes – such as PAC – is their flexibility to be applied to a wide variety of materials. This has allowed us to pursue a very active biophysics program in parallel with the more “traditional” solid state work. These experiments use the implanted radioactive ions to study the local environment of proteins, complementing and enhancing similar experiments using NMR and synchrotron radiation.

In this talk I will detail the recent successes of experiments at ISOLDE, and of the unique advantages that radioactive probes can bring. Results from the previous few years will be presented from the main areas of work: semiconductor physics, multiferroic materials and biophysics.

Abstract submission for oral presentation.

**Introductions to Posters / 63****High temperature drop calorimetry for actinide samples****Author:** octavian valu<sup>None</sup>

High temperature drop calorimetry for actinide samples

Octavian S. Vălu<sup>1,2</sup>, Markus Beilmann<sup>2</sup>, Ondrej Beneš<sup>2</sup> and R. J. M. Konings<sup>2</sup>

<sup>1</sup> “Al. I. Cuza” University, Department of Chemistry, 11 – Carol I Blvd., 700506 – Iași, Romania, e-mail: octavian.valu@yahoo.com

<sup>2</sup> European Commission, Joint Research Centre, Institute for Transuranium Elements, Karlsruhe, Germany

Using a Setaram multi-detector high temperature calorimeter (MHTC 96 type) operating in drop mode we try to prove that it is possible to perform drop calorimetric measurements for actinide samples using a very small amount of substance (less than 150 mg).

Therefore, we performed drop calorimetric measurements for CsF samples and compare our results with existing literature data Nist – Janaf [1] and A. C. Macleod [2].

a)

b)



Fig. 1. Results of our experiment and Macleod's work. a) liquid phase; b) solid phase

Using the equations from Figure 1, which are obtained from linear fit of the data, the enthalpy of fusion is calculated as well as the heat capacity for our experiment and Macleod's work. The results of the calculation are shown in Table 1.

Table 1. Enthalpy of fusion and heat capacity of CsF.

Comparing our results with the results of Macleod we can observe that the heat capacity has a very similar value. It is important to mention that in his experiment Macleod used an amount of 10 g of CsF for every drop whereas we used only 150 mg. From here we conclude that it is possible to analyze actinide samples using a relatively small amount of substance obtaining enough accurate results in order to predict the behavior of the Molten Salt Reactor (MSR) fuel.

The principle of the Drop technique is based on measuring the enthalpy increments of a sample, while dropping it from ambient temperature (exactly measured) to the programmed temperature, which is kept at constant value. The crucible design used for the encapsulation was presented in Beneš et al. [3].

Each measurement consists of several drops made in 25 minutes intervals, enough to re-stabilize the temperature and the heat flow signal. From several measurements the temperature function of enthalpy is obtained and from these results the heat capacity is derived according to equation:  $CP = \dots$

Prior to each drop the samples were stored in a sample holder, which is positioned over the detector. The furnace of the calorimeter is programmed to stabilize at desired temperature and to keep it constant during the experiment. After this period the sample is dropped into the calorimeter. At this moment extra heat (monitored as heat flow) is delivered into the detector in order to maintain the pre-set temperature. The amount of heat corresponds to the energy which is necessary to heat up the sample from ambient temperature to the operation temperature. Typical results of one measurement are shown in Figure 2. Before and after every sample, a reference material is dropped to determine the sensitivity of the detector. As reference material we used small pieces (75 – 95 mg) of corundum (Al<sub>2</sub>O<sub>3</sub>) whose heat capacity is known.

Fig. 2. An example of measurement made by Drop calorimeter; the investigated sample is CsF and as reference

Each peak, on the heat flow curve, is analyzed individually by integration with respect to time, using OriginPro 7.5 Software and knowing the sensitivity of the calorimeter the obtained are is converted into enthalpy.

The same technique to measure the high temperature heat capacity has been used by Burriel et al. [1] and Beneš [3].

#### References

- [1] NIST – JANAF, Thermochemical Tables, Fourth Edition, Part II, Journal of Physical and Chemical Reference Data.
- [2] A. C. Macleod, High-temperature Thermodynamic properties of the Alkali-metal Fluorides, J. Chem. Soc. Faraday Trans I, 2026-2035, (1973).
- [3] O. Beneš, R. J. M. Konings, C. Kuentzel, M. Sierig, A. Dockendorf, L. Vlahovic, J. Chem. Thermodyn., 41, 899 – 903, (2009).
- [4] P. D. Desai, Int. J. Therm., 8, 763 – 780, (1987).
- [5] Octavian S. Vălu, Markus Beilmann, O. Beneš, R. J. M. Konings, The high temperature heat capacity of CsF, in publication.

WAT-III / 64

## Dose coefficients for radiation protection at present and future RIB facilities

Author: thomas otto<sup>None</sup>

WAT-III / 65

## **use of actinide targets at the HRIBF**

**Author:** dan stracener<sup>None</sup>

JDA-WAT I / 66

## **Review on UC targets (Invited talk)**

**Author:** jerry nolen<sup>None</sup>

67

## **Invited talk (TBC)**

WAT-III / 68

## **Measurements of neutron capture and fission cross-sections on actinides at n\_TOF**

**Author:** Nicola Colonna<sup>1</sup>

<sup>1</sup> *INFN Bari*

69

## **NTOF 2**

WAT-III / 70

## **Remote and optimized inspection, measurement and handling for radiation areas at CERN.**

WAT-III / 71

## **Summary and Closure**

Materials I / 72

## **Opening of conference**

73

**Fuels & targets talk I TBC**

74

**Fuels & targets talk II (TBC)**

75

**Fuels & targets talk III (TBC)**

76

**Fuels & targets Invited talk (TBC)**

77

**Keith Kershaw: Development of equipment and optimized procedures for remote inspection, measurement and handling in radiation areas at CERN****Author:** Keith Kershaw<sup>None</sup>

The Handling Engineering Group at CERN has undertaken several initiatives to reduce personnel radiation doses incurred during handling and other activities by developing remote handling equipment, optimized handling equipment / procedures as well as remote inspection and measurement devices. The equipment produced and under development will be presented along with some results for radiation dose reductions.

WAT-III / 78

**Plans For the Production Building at the future Radioactive Ion Beam production laboratory SPIRAL 2 at GANIL and handling of the targets****Author:** Mathieu QUICLET<sup>1</sup><sup>1</sup> GANIL

Poster Session / 79

## Details of poster session

1. Magnetic anisotropy of a UFe<sub>5</sub>Al<sub>7</sub> single crystal ANDREEV, Alexander S
2. Field-Induced Phase Transitions in UIrGe Probed by Ultrasound Measurements Dr. YASIN, Shadi
3. High-pressure hydrogen doping into the UTGe compounds. Ms. ADAMSKA, Anna Maria
4. Electrical properties of (Pu,Lu)Pd<sub>3</sub> Dr. LE, Manh Duc
5. On the existence of cerium (IV) orthophosphate, 'Ce<sub>3</sub>(PO<sub>4</sub>)<sub>4</sub>' Mr. BORHAN, Adrian Mr. APE-TRACHIOAIEI, Bogdan
6. Synthesis and characterization of MIVSiO<sub>4</sub> compounds Mr. COSTIN, Dan Tiberiu
7. Synthesis of nanocrystalline oxide fuel Ms. JOVANÍ ABRIL, Raquel
8. Initial electron back-scattered diffraction observations of Ce-La alloy Dr. SCOTT, Thomas
9. Distribution of soil-to-plant transfer factors for the natural uranium isotopes in the vegetation in zones affected by uranium mines Mrs. CRISTACHE, Carmen Ileana
10. <sup>234</sup>U/<sup>238</sup>U disequilibrium studies in soil and vegetation samples from tailing dumps Dr. BRAGEA, Mihaela Gladiola
11. Isothermal section of the U-Fe-Ge ternary system at 900°C Ms. HENRIQUES, Margarida
12. High-field metamagnetism in UCo<sub>2</sub>Si<sub>2</sub> SKOURSKI, Yurii
13. Crystallographic study of new phases from the U-Zn-Al ternary system VERBOVYTSKYI, Yuriy
14. Considerations on the U-Fe-B ternary system Dr. PEREIRA GONÇALVES, António
15. Long-term behavior of thorium-plutonium phosphate-diphosphate solid solutions Prof. DACHEUX, NICOLAS
16. Techniques elaborated for the R&D on fission targets for SPIRAL2 Ms. HY, Botoum
17. High temperature drop calorimetry for actinide samples VALU, octavian
18. Synthesis and Characterization of Carbide Foams for the SPES target Mr. CORRADETTI, Stefano
19. Transport and thermodynamic properties of UFe<sub>2</sub>Zn<sub>20</sub>, Mr P. Swatek